UNIVERSITY OF THESSALY
SCHOOL OF ENGINEERING
DEPARTMENT OF MECHANICAL ENGINEER

Diploma thesis

Electrochemical gas sensors based on solid electrolytes

by

CHLOROS DIMITRIOS

Submitted in partial fulfillment of the requirements for the degree of diploma in Mechanical Engineering at the University of Thessaly

Volos, 2021

ΠΑΝΕΠΙΣΤΗΜΙΟ ΘΕΣΣΑΛΙΑΣ
ΠΟΛΥΤΕΧΝΙΚΗ ΣΧΟΛΗ
ΤΜΗΜΑ ΜΗΧΑΝΟΛΟΓΩΝ ΜΗΧΑΝΙΚΩΝ

Διπλωματική εργασία

Ηλεκτροχημικοί αισθητήρες αερίων με στερεό ηλεκτρολύτη

υπό

ΧΛΩΡΟΣ ΔΗΜΗΤΡΙΟΣ

Υπεβλήθη για την εκπλήρωση μέρους των απαιτήσεων για την απόκτηση του Διπλώματος Μηχανολόγου Μηχανικού

Βόλος, 2021

Εγκρίθηκε από τα Μέλη της Τριμελούς Εξεταστικής Επιτροπής:

1st Examiner: Dr Tsiakaras Panagiotis
(Supervisor) Professor
Department of Mechanical Engineering
School of Engineering
University of Thessaly

2nd Examiner: Dr Charalampous Georgios
Assistant professor
Department of Mechanical Engineering
School of Engineering
University of Thessaly

3rd Examiner: Dr Angeliki Brouzgou
Assistant professor
Department of Energy systems
Faculty of Technology
University of Thessaly

ACKNOWLEDGMENTS

First of all, I would like to express my thanks to my patient and supportive Professor Panagiotis Tsiakaras for his important work as my supervisor and professor. His experience, support, advice, knowledge and commitment were the motivation for me to get through this past-graduate experience. Also, I want to express my gratitude to him for giving me the possibility to stay and work at the Laboratory of Alternative Energy Conversion Systems at the Department of Mechanical Engineering at the University of Thessaly , where i saw the working environment in a real scientific lab and further understood the experiments that take place.

Furthermore, I want to thank Laboratory's Alternative Conversion Systems Research Group, Dr. Angeliki Brouzgou and Dr. Fotini Tzorbatzoglou and Dr. Sotiria Kontou. Their guidance, support and assistance during this time were some of the tools that helped with the elaboration of this thesis. I would also like to thank the members of the examination committee for their advice and time.

Last, I would like to thank my family, my father, Paulos, and my mother, Katerina, for their love, trust and moral and financial support provided through not only the elaboration of this thesis but also throughout my studies at the Department of Mechanical Engineering in the University of Thessaly. I wouldn't be able to elaborate on this thesis or finish my studies without them.

ΕΥΧΑΡΙΣΤΙΕΣ

Θα ήθελα να εκφράσω τις ευχαριστίες μου, αρχικά, στον υπομονετικό και υποστηρικτικό καθηγητή και επόπτη μου καθηγητή Παναγιώτη Τσιακάρα. Η εμπειρία, η υποστήριξη, οι συμβουλές, η γνώση και η αφοσίωση του μου έδιναν κίνητρο, ώστε να μπορέσω να ολοκληρώσω αύτη την προ-πτυχιακή εμπειρία. Επίσης, θα ήθελα να τον ευχαριστήσω που μου έδωσε την ευκαιρία να μείνω και να δουλέψω στο εργαστήριο Εναλλακτικών Συστημάτων Μετατροπής Ενέργειας του τμήματος Μηχανολόγων Μηχανικών του Πανεπιστημίου Θεσσαλίας. Κατά την παραμονή μου στο εργαστήριο, είδα πως είναι το εργασιακό περιβάλλον σε ένα πραγματικό επιστημονικό εργαστήριο και εμβάθυνα στην κατανόηση των διαδικασιών.

Επιπλέον, θα ήθελα να ευχαριστήσω το προσωπικό του εργαστήριου, την Δρ. Αγγελική Μπρούζγου, την Δρ. Φωτεινή Τζορμπατζόγλου και την Δρ. Σωτηρία Κόντου. Η καθοδήγηση, η υποστήριξη και η βοήθεια τους αυτόν τον καιρό ήταν μερικά από τα εργαλεία μου που βοήθησαν στην εκπόνηση της διπλωματικής εργασίας. Θα ήθελα επίσης να ευχαριστήσω τα μέλη της εξεταστικής επιτροπής για τον χρόνο τους και τις συμβουλές τους.

Τέλος, θα ήθελα να ευχαριστήσω την οικογένεια μου, τον πατέρα μου, Παύλο, και την μητέρα μου, Κατερίνα για την αγάπη, την εμπιστοσύνη και την ηθική και οικονομική υποστήριξη που μου έδωσαν σε όλη την διάρκεια των σπουδών μου στο Πανεπιστήμιο Θεσσαλίας. Δεν θα ήταν δυνατή η ολοκλήρωση της διπλωματικής ή των σπουδών χωρίς αυτούς.

ABSTRACT

The rapid growth in science and engineering in the 21st century has provided a remarkable rise in our living standards. Unfortunately, in parallel with this development, problems have also arisen concerning the environment, such as the depletion of ozone in the atmosphere, acid rain, problems in human health and the greenhouse effect. The main source of these problems is related to the continuously increasing need for energy, 85% of which derives from the combustion of mineral fuels, mainly hydrocarbons. From this combustion processes, except energy, the main greenhouse gases - carbon dioxide and steam - are produced. Moreover, due to industrialization, many hazardous gases are realized through industrial processes. So, gas-detecting devices, such as electrochemical gas sensors, that can analyze the composition of a targeted atmosphere in real-time are important for the future. Such devices can help address environmental problems and warn people about the presence of dangerous gases. Furthermore, as the non-renewable energy sources run out, there is a need for energy saving. By analyzing the composition of combustion emissions of automobiles or industries, the combustion processes can be optimized.

The first chapters of this thesis provide basic information about electrochemical processes. At first, the fundamentals of solid-state electrochemistry and the basics of solid electrolytes are examined that are important for the understanding of electrochemical devices. Next, the most important electrochemical and physicochemical techniques for analyzing the tested devices or used materials are presented. Last, the configuration and the principle of operation of future electrochemical devices are discussed.

Next, sensors for the detection of important gases are reviewed. The configuration and principle of operation of a wide variety of electrochemical sensors based on solid electrolytes for the detection of common gases are presented. All of those sensors operate at intermediate or high temperatures. The efficiency of every sensor is examined throughout experimental data and *I-V* curves.

ΠΕΡΙΛΗΨΗ

Η απότομη ανάπτυξη στην επιστήμη και στην τεχνολογία του 21^{ου} πρώτου αιώνα έχει προσφέρει σημαντική αύξηση στον τρόπο ζωής της πλειοψηφίας των ανθρώπων. Δυστυχώς, παράλληλα με αύτη την ανάπτυξη, δημιουργήθηκαν και προβλήματα που αφορούν την ατμόσφαιρα του πλανήτη, όπως η εξάντληση του όζοντος της ατμόσφαιρας, η όξινη βροχή, προβλήματα στην υγεία των ανθρώπων και το φαινόμενο του θερμοκηπίου. Η βασική πηγή αυτών των προβλημάτων σχετίζεται με την ανάγκη για ενέργεια, το 85% της οποίας έρχεται από την καύση ορυκτών καύσιμων, κυρίως υδρογονανθράκων. Ωστόσο έκτος από ενέργεια, απελευθερώνονται και τα βασικά αέρια του θερμοκηπίου, διοξειδίου του άνθρακα και ατμός. Έτσι, συσκευές ανίχνευσης αερίων όπως οι ηλεκτροχημικοί αισθητήρες αερίων που μπορούν να αναλύσουν την σύσταση ενός αερίου σε πραγματικό χρόνο μπορούν να φανούν πολύ χρήσιμες για το μέλλον. Τέτοιες συσκευές μπορούν να συμβάλλουν στην αντιμετώπιση των περιβαλλοντικών προβλημάτων και να προειδοποιήσουν τους ανθρώπους για την παρουσία επικίνδυνων αερίων. Επιπλέον, καθώς οι μη-ανανεώσιμες πηγές ενέργειας εξαντλούνται δημιουργείται η ανάγκη για οικονομία στην ενεργεία. Μέσω της ανάλυσης της σύστασης των καυσαερίων των αυτοκινήτων ή των εργοστασίων μπορεί να βελτιστοποιηθεί η λειτουργία τους.

Στα πρώτα κεφάλαια της διπλωματικής εργασίας δίνονται οι βασικές πληροφορίες για τις ηλεκτροχημικές διεργασίες. Αρχικά, εξετάζονται οι βασικές αρχές της ηλεκτροχημείας στερεάς κατάστασης και τα βασικά για τους στερεούς ηλεκτρολύτες τα οποία είναι απαραίτητα για την κατανόηση των ηλεκτροχημικών συσκευών. Μετά, παρουσιάζονται οι πιο σημαντικές ηλεκτροχημικές και φυσικοχημικές διεργασίες ανάλυσης συσκευών και υλικών. Τέλος, παρουσιάζεται η δομή και ο τρόπος λειτουργίας των μελλοντικών ηλεκτροχημικών συσκευών.

Στην συνεχεία, εξετάζονται αισθητήρες για την ανίχνευση σημαντικών αερίων. Παρουσιάζεται η δομή και ο τρόπος λειτουργίας ενός μεγάλου εύρους αισθητήρων με στερεό ηλεκτρολύτη. Οι αισθητήρες αυτοί χρησιμοποιούνται για περιβάλλοντα υψηλής θερμοκρασίας. Εξετάζεται η αποδοτικότητα των αισθητήρων με βάση τα δεδομένα και τα διαγράμματα ρεύματος-τάσης.

TABLE OF CONTENTS

LIST OF TABLES

LIST OF FIGURES

Chapter I

Introduction

1.1 Utility of electrochemical sensors

The most important concepts in electrochemistry were introduced by Nernst (thermodynamic approach), Kohlrausch (conductivity measurements), Faraday (relation between electricity and quantity of matter) and Volta (classification of redox couples) during the 19^{th} century. However, the first electrochemical sensors were available at the second part of the next century. Nowadays, the need for accurate and automatic control of combustion emissions from automobiles or other industrial processes is increasing, following the rapid development of several countries. The pace of this industrialization has made clear that the industries of advanced and developed countries are expanding year to year. Following this expansion, there is an exponential growth in environmental protection policies, strictly regulating pollution emission standards, and prompting people to continuously explore technologies with low pollution and low energy consumption. Consequently, it is important, for the future, to develop reliable, robust, low-cost and miniaturized sensors for the detection of various gases in aggressive environments. Among other types of gas sensors, electrochemical sensors have some advantages to meet these requirements.

Although there is a great turn of interest in that kind of sensors due to the growing public concern for climate change and an impressive progress in science and engineering, there is still a need for faster, more sensitive and selective electrochemical sensors in order to successfully limit emissions from automotive and industries especially in developed countries. Among the most common dangerous gases realized from combustion are hydrocarbons (HCs), carbon and sulfur monoxide and dioxide (CO_x and SO_x), hydrogen (H_2), hydrogen sulfide (H_2S), ammonia (NH_3) and nitrogen oxides (NO_x). As a result, there is strict legislation related to the acceptable limits of those emissions.

Electrochemical sensors based on solid electrolytes are considered the most promising gas sensing devices for commercial use because they offer excellent sensitivity, simple operation and construction, direct in-situ response and scope for miniaturization. Among the various types of electrochemical sensors, amperometric ones are the most promising type as they offer simplicity and direct response. Moreover, the advance in solid-state ionics and electronics further accelerates the progress in electrochemical solid-state sensors. The most well-known and commercially used sensor mainly in automotives is the λ-sensor based on yttria-stabilized zirconia (YSZ) with platinum (Pt) working electrode (WE). λ-sensors are already employed for about 40 years on gasoline-based vehicles worldwide.

Concluding, the yttria-stabilized zirconia electrolyte has already been proven to be a suitable and effective electrolyte for electrochemical sensors. Zirconium oxide is the first pure oxide doped with a different oxide to form a stable structure and an effective oxygen ion conductor. Calcium was the first tested dopant for stabilizing the pure zirconium oxide to form a stable solid oxide electrolyte, however many more oxides were tested after calcium as zirconium stabilizing agents, such as the favorable yttria, magnesia, scandia and ceria. The ever-growing success of those oxygen-ion conductors based on zirconia has laid the foundation for even more research and studies for the development of other types of electrolytes and sensors to control industrial pollutants.

1.2 Importance of solid electrolytes

Environmental crisis and non-renewable energy sources have firmly confirmed that there is a need for cleaner energy sources to reduce greenhouse gases emissions and renewable energy sources to address the energy crisis. However, there isn't yet an optimal solution. Electrochemical devices for the storage and production of energy and the control of emissions such as lithium-ion batteries, fuel cells and electrochemical gas sensors are considered a promising technology to eliminate greenhouse gas emissions and partially address these problems. The efficiency of such devices mainly depends on the properties and the characteristics of the materials, so it is important to develop innovative materials for these systems.

Electrolytes are one of the most important components of every electrochemical device. Electrolytes conduct electricity by the movement of ions in contrast to metals that conduct electricity by the movement of electrons. Generally, high ion conductivity is observed in liquid electrolytes, such as aqueous solutions of salts and molten salts. However, during the last three decades, there have been developed several solid materials that exhibit significant ionic conductivity and have negligible to zero electronic conductivity. The conductivities of those solid electrolytes are comparable to the conductivities of many liquid electrolytes and considering their physical properties, solid electrolytes are already preferred in many electrochemical devices such as fuel cells, batteries, supercapacitors and electrochemical gas sensors. Nowadays, the studies for the development of solids electrolytes are transforming into an interdisciplinary field concerning chemistry, material science, physics and engineering.

Ion conductivity in solids is usually achieved at elevated temperatures but far lower than their melting point. Generally, the activation energy and ionic conductivity of solid electrolytes vary from 0.1 to 2eV and 10^{-5} to $1 S \cdot cm^{-1}$, respectively. There are many types of solid electrolytes, varying from ceramic and glasses to acids, hydrates, gels and polymers. However, ceramic solid electrolytes such as YSZ are the most preferred electrolytes for aggressive environments as they fulfill all the requirements.

Chapter II

Theoretical background

Abstract

In the second chapter, the basic characteristics and the different types of solid electrolytes are described. An introduction to the electrochemistry fundamentals and basic diffusion theory is being conducted. This introduction is necessary for the understanding of the mechanisms that take place at solid electrolytes and electrochemical devices. Last, the principle of operation and characteristics for different types of electrochemical devices are reported.

2.1 Solid electrolytes

2.1.1 Introduction

Electrolytes are the key to every electrochemical device. Solid electrolytes, also known as superionic, fast or optimized ionic conductors, are the most recent type of electrolyte. Solid electrolytes are solid materials that exhibit high conductivity of anions or cations and low to zero electronic conductivity. The field of ion conductive solids, with or without electronic conductivity, is referred to as solid-state ionics. High-density batteries, high-temperature gas sensors for a wide range of different gases, supercapacitors and high-temperature fuel cells are some of the applications of solid electrolytes, resulting in a great

turn of research and funding for the development of new and more optimized solid electrolytes [1].

2.1.2 History

Conductivity in solids was reported for the first time more than a century ago. Michael Faraday first discovered an electrically conductive solid in 1883. Faraday found that the ionic conductivity of Ag_2S (silver sulfide) is proportional to the temperature, as the temperature increases, so does the conductivity. In addition, similar behavior was reported in other solids such as PbF_2 (lead fluoride). This phenomenon couldn't be explained at the time, as this behavior was different from that of the metallic phase. Hittorf studied ion conductivity in AgS and Cu_2S (silver monosulfide and copper sulfide, respectively) and figured out that there was a different electrolytic conduction mechanism in these materials. Warburg proved that sodium ions could flow through the solid in 1884. This conclusion changed the conclusion of Arrhenius that pure salt and pure water couldn't be conductors like salt dissolved in water [2].

One of the earliest applications of solid (ceramic) electrolytes was Nernst's lamp. In 1897, Nernst discovered that second-class conductors in the shape of a thin rod could exhibit ion conduction with the help of an auxiliary heating appliance and then kept glowing by the presence of an electric current. In the beginning, Nernst reported only lime and magnesia as proper conductors. However, through further research, Nernst concluded that the ionic conductivity in pure oxides increases with an increase in temperature but generally remains considerably low, whereas mixtures based on oxides show much better conductivity. These results come in agreement with the already studied and known behavior of liquid electrolytes. Soon many solid oxide electrolytes with good ionic conductivity at increased temperatures, such as the particularly favorable composition of 85mass% zirconia and 15mass% yttria (YSZ), were identified. Yttria-stabilized zirconia has been proven an excellent oxygen conductor considering, that even after a century, it is still considered an effective electrolyte for high-temperature operation and employed in many electrochemical devices. Given the technology and the knowledge at the time, Nernst couldn't prove that his glowers were ionic conductors. However, he assumed that there are defects in the structure of YSZ caused by yttria additions that provide the necessary charge carrier. Wagner later in

1943 explained the conduction mechanisms in Nernst devices. Wagner proved the existence of vacancies in the structure of YSZ. Now, it is known that platinum contacts had the role of air electrodes and the glowers were oxide-ion conductors. That makes Nernst glower a really important discovery because it is the first finding proving that there is ionic conductivity in solid-state electrolytes and can be as effective as that of a liquid electrolyte [3].

In 1957/1958, Kiukkola and Wagner performed thermodynamic investigations using CaO-stabilized ZrO_2 as solid electrolyte [4], [5]. These works were the first step for many applications around the world in the field of solid-state electrochemistry. In that field, ZrO_2-based solid electrolytes dominated over the other ceramic electrolytes. For example, in 1961, in their work, Weissbart and Ruka described a ZrO_2-based galvanic cell for the detection of oxygen in high-temperature gases named oxygen gauges [6].

After all the popularity that solid electrolytes gained, many more families of materials were identified as ion conductors to different kinds of ions. Some of the most important are β and β'' aluminas, glasses, polymers and mixed conductors that present both ionic and electronic conductivity [7]. Among the newly discovered electrolytes, proton conductors are the most promising technology for future proton conductor-based electrochemical devices. Iwahara et al. first discovered in the 1980s the proton-conducting properties of $LaYO_3$ and $SrZrO_3$. Following these findings, Maiti and Vikar reported that pure $BaCeO_3$ and yttria-doped $BaCeO_3$ are proton conductors at $p_{O2}<10^{-6}$ and temperatures between 600-1000°C. It was not until 1987 when Mitsui et al. proved the proton conduction in $BaCe_{0.95}Yb_{0.05}O_{3-\delta}$ and $BaZr_{0.95}Yb_{0.05}O_{3-\delta}$. Among these discoveries, the highest conductivity, in the order of $10^{-2}S\cdot cm^{-1}$ at 600°C, was achieved by $BaCeO_3$-based materials [8].

2.1.3 Types of conductors

Electrolytes must fulfill several requirements in order to be suitable for use in electrochemical devices. Firstly, electrolytes must be thermodynamically and chemically stable under oxidizing and reducing environments and it is important to present low electronic conductivity. Also, Hittorf

transference number t_i must be equal to unit. Hittorf number gives the fraction of the total charge carried by an ionic species in the electrolyte [9]. This number is described by equation (2.1),

$$t_i = \sigma_i / \sigma_{total} \tag{2.1}$$

One of the main properties that a material must possess, in order to be considered a suitable electrolyte, is the ability to provide a pathway for ions to flow while simultaneously blocking electrons. The ability to support current flow by the motion of ions when a potential is applied is called conductivity and it is measured in $ohm^{-1}cm^{-1}$ also known as $S \cdot cm^{-1}$ (S=Siemens). Generally, electrons and ions are generated or used through electrochemical reactions at electrodes, these ions flow through the electrolyte to the oppositely charged electrode in order to maintain charge balance while the electrons are forced to an external circuit.

As seen in **Fig. 1**, solid electrolytes exhibit ionic conductivity in the range of 10^{-5} ... 1 $S \cdot cm^{-1}$ at high temperatures. This range is much better than insulators but considerably worse than metals. However, they present the same order of magnitude as semiconductors and liquid electrolytes. Ion conductivity in solid electrolytes generally occurs due to a hopping process between an occupied and a vacant oxide site. Those vacancies occur by doping the initial oxide with an oxide of lower valent cations than the cations of the first oxide. Electrolytes must exhibit ion conductivity of at least $10^{-3} S \cdot cm^{-1}$ at operating temperatures [1].

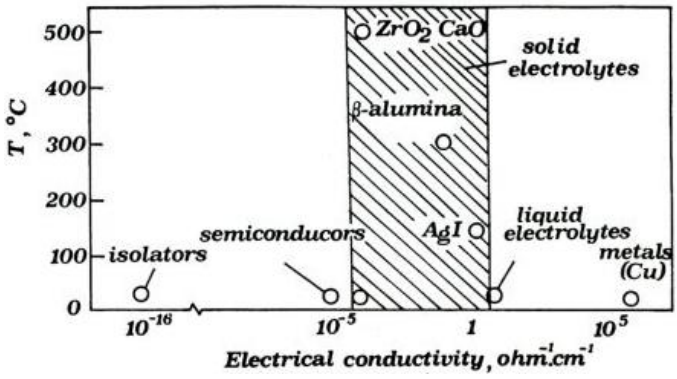

Figure 1: Comparison of the conductivities of: semiconductors, solid electrolytes, liquid electrolytes and metals.

2.1.4 Ionic conductivity

Conductivity in solids is the result of the movement of charged species (ions) when a voltage is applied. An ion needs vacant sites to occupy as it moves and a potential difference to force it to move. Therefore, ionic conductivity is linked with defects. There are many types of defects but two are the most common and most important. The first type is those involving vacant lattice sites (Schottky defects) where ions jump from one vacant site to the next. The second type is those involving species placed between regular sites, in "interstitial" positions (Frenkel defects). In Frenkel defects, ions can jump from one interstitial site to the other or they can push other species into an interstitial position and occupy the regular lattice site [10].

It is observed in **Fig. 1** that solid electrolytes must operate at high temperatures, usually more than 400°C, in order to compete with liquid electrolytes [10]. This means that ionic conductivity (σ) rises as the temperature rises. This can be expressed as an Arrhenius-type form:

$$\sigma = \frac{\sigma_0}{T}\exp\left(\frac{-\Delta E_a}{k \cdot T}\right) \tag{2.2}$$

Where σ_0 is a function of the ionic charge, attempt frequency, jump distance and the concentration of mobile ions, k is Boltzmann's constant, T is the temperature of operation in Kelvin and ΔE_α is the activation energy ranging from 0.7 to 1.4eV [9].

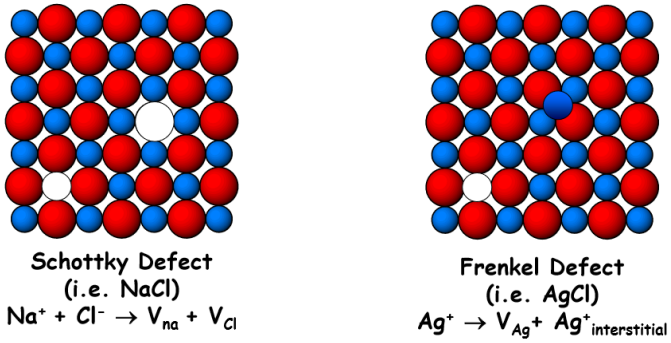

Figure 2: Schematic representation of Schottky and Frenkel defects in NaCl and AgCl [11].

In **Fig.2** is shown Schottky and Frenkel defects in two different solids, NaCl and AgCl respectively. As equations (2.3) and (2.4) suggest, at temperatures above 0, there will

always be an equilibrium of defects. The number of defects at a crystal is calculated by the following equations,

For Schottky defects: $$n_s = N \cdot \exp\left(\frac{-\Delta H_s}{2 \cdot k \cdot T}\right) \quad (2.3)$$

For Frenkel defects: $$n_s = (N \cdot N_i)^{1/2} \cdot \exp\left(\frac{-\Delta H_F}{2 \cdot k \cdot T}\right) \quad (2.4)$$

Where n_s, N and N_i are the number of defects, the number of lattice sites and the number of interstitial sites, respectively, and ΔH_s, ΔH_F are the enthalpy of formation of one Schottky or Frenkel defect, respectively [9].

2.1.4.1 Oxide ion (O^{2-}) conductivity

Oxygen conductivity in solids depends on the movement of oxide ions through the crystal lattice. Oxygen ions are imposed to thermally-activated jumps from normal sites of the crystal lattice to vacancies with a fixed direction depending on the applied electric field. Consequently, ion conductivity depends strongly on temperature. The ceramic electrolytes exhibit zero ion conductivity at room temperature, but at higher temperatures their conductivity can be compared to that of liquid electrolytes, reaching values up to $1 S \cdot cm^{-1}$.

In structures similar to yttria-stabilized zirconia (YSZ), guest cations (Y^{3+}) replace the host's ions (Zr^{4+}) and generate oxide-ion vacancies in order to retain electrical neutrality. The oxygen ion vacancies when ZrO_2 is doped with Y_2O_3 are created according to the reaction,

$$Y_2O_3 \xrightarrow{ZrO_2} 2Y_{Zr}^{'} + V_O^{"} + 3O_O^x \quad (2.5)$$

where $Y_{Zr}^{'}$ is yttrium ion in normal cation site, $V_O^{"}$ is the oxygen vacancy created by the doping process and O_O^x is the oxygen ion normal lattice site.

2.1.4.2 Proton (H^+) conductivity

Protons are always covalently bonded to a negatively charged ion, such as oxygen ions in oxides, or they are shared from two atoms, in bonds like O–H···O. Hydrogen ions or protons can't be found free in solids under equilibrium conditions, because they interact with the

negatively charged oxygen ions. In high-temperature proton conductors (HTPCs), there can be realized a transport mechanism known as proton-hopping mechanism or Grotthuss mechanism. This mechanism is a result of a thermally-activated jumping process. However, this process requires the breaking of the O-H bonds. The proton conduction mechanism takes place in two steps, first, the proton rotates around the oxygen ion and second the proton hops to a neighboring oxygen ion. The second step is the rate-determining step of the process. According to the Grotthuss-type mechanism, the activation energy of the second step is about 0.5eV that is less compared to that of the first step which is below 0.1eV [8]. Most solid proton-conducting materials produce new structure element when they interact with water vapor, according to the reaction,

$$H_2O + V_O^{"} + O_O^x = 2OH_O^{'} \tag{2.6}$$

where $OH_O^{'}$ is the proton defect responsible for the proton conductivity. For example, in the well-known proton-conductor Y-doped $BaZrO_3$ the oxygen vacancies are formed according to the reaction (2.7),

$$Y_2O_3 \xrightarrow{BaZrO_3} 2Y_{Zr}^{'} + V_O^{"} + 3O_O^x \tag{2.7}$$

2.1.5 Classification of solid electrolytes

Good ionic conductivity in solids is not a usual phenomenon. Over the years, researchers have discovered many solid electrolytes that show high ionic conductivity being insulators for electrons. These solid electrolytes are also known as superionic conductors because, in terms of ionic conductivity, they can be compared with the well-established liquid electrolytes. There are several ways to classify solid electrolytes, for example here they are characterized based on the transported ion. Ionic species such as O^{2-}, Ag^+, Na^+, Li^+, H^+ are reported to move fast in crystalline ion conductors [7].

- **Oxygen ion (O^{2-}) conductors**

The ionic conductivity in those solid solutions occurs via oxide ionic vacancies ($V_O^{"}$) generated by doping the host crystal with a lower valent oxide such as CaO, Y_2O_3, MgO, Sc_2O_3.

Thus a cubic fluoride-type solid structure is made that is structurally stable, as shown in **Fig. 3**. For instance, they can be formulated, as $Zr_{1-x}Ca_xO_{2-x}$ and $Zr_{1-x}Y_xO_{2-x/2}$, containing x and x/2 mole of oxide-ion vacancies per formula unit, respectively. High temperature is required to accomplish high ionic conductivity in solid oxides. The conductivity is also related to the concentration of the aliovalent guest cations at the first stage of doping. However, there is a maximum value for aliovalent concentration, after this, further doping has the opposite result. This maximum differs for every aliovalent guest and it is about 5-10% for CaO and 6-10% for Y_2O_3. This type of oxide ion conductors has a fluorite structure.

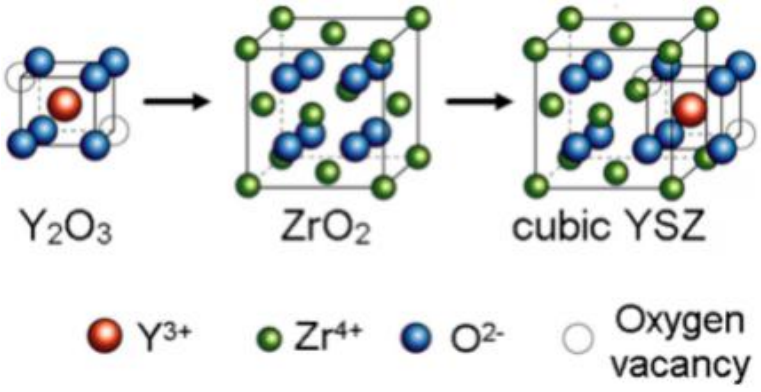

Figure 3: Cubic form of zirconia doped with 12% or more Yttria [12].

These materials have been used in electrochemical gas sensors, oxygen separators, oxygen pumps, steam and/or carbon dioxide electrolyzers and various types of fuel cells [13]. It is interesting that for a certain temperature the maximum ionic conductivity can be found at the right amount of Y_2O_3. For example, in the well-known YSZ electrolyte, the Y_2O_3 concentration that provides the best possible ionic conductivity doesn't depend on the temperature. However, high ionic conductivity can be found at elevated temperatures. In **Fig. 4**, the conductivity of a YSZ electrolyte at different temperatures and with different Y_2O_3 concentrations is depicted.

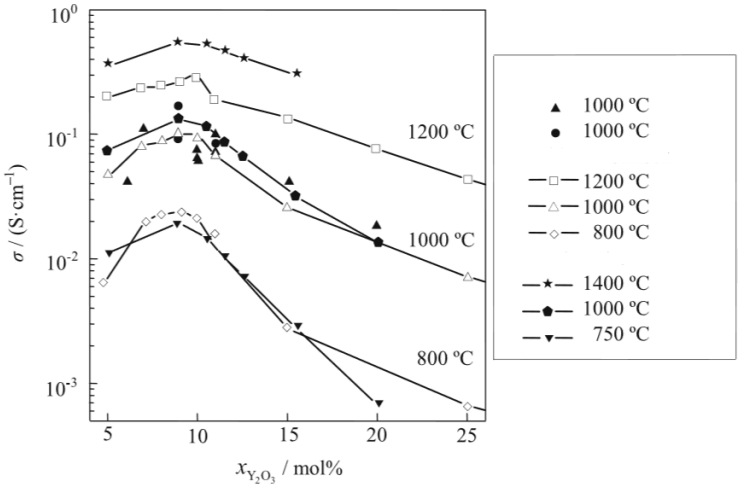

Figure 4: Conductivity of yttria-stabilized zirconia plotted against the content of Y_2O_3 for different temperatures [14].

Even if YSZ is the best-known electrolyte, there are many reports of other materials used as a dopant for ZrO_2. Generally, ZrO_2 needs to be stabilized with the aid of a dopant. Those dopants are divided into two categories, alkaline earth oxide and rare earth oxides. There are reports of alkaline earth oxide like CaO and MgO and rare earth oxide-stabilized zirconia like Sc and Ce [14].

Expect the YSZ oxygen-ion conducting electrolytes, cerium based and lanthanum gallate-based solid electrolytes have also been extensively investigated for operation at lower temperatures. Cerium-based electrolytes, compared to the zirconia-based electrolytes, exhibits a considerably higher ionic conductivity at lower temperatures. An example of such a cerium-based oxide-ion conducting electrolytes is the solid $Ce_{1-x}M_xO_2$ (where M is samarium (Sm) or gadolinium (Gd)). Similar to zirconia, ceria has a fluorite structure and ceria is doped with trivalent cations such as Sm^{3+} and Gd^{3+} for the formation of oxygen vacancies. Considering that these electrolytes show higher ionic conductivity than zirconia-based electrolytes at lower temperatures they are suitable for lower operating temperatures. Moreover, $Ce_{1-x}Gd_xO_2$ presents excellent chemical stability in contact with cathode materials. However, a major drawback of ceria-based electrolytes is that when operating in reducing environments, cerium ion changes its valence state from Ce^{4+} to Ce^{3+} as a result, electronic conductivity appears through the electrolyte. Due to the presence of electronic conductivity in the electrolyte, the system's efficiency deteriorates [15].

On the other hand, perovskite oxides are purely oxide-ion conductors and are employed as electrolytes for application in intermediate temperatures (600-800°C). Among the materials of the perovskite family, lanthanum gallate ($LaGaO_3$)-based materials were the only ones that proved suitable for application as electrolytes. Ishihara and his group in Japan [16-18] were the firsts who developed the optimized materials of general stoichiometry $La_{1-x}Sr_xGa_{1-y}Mg_yO_{3-\delta}$ (LSGM). LSGM exhibits even higher conductivity at intermediate temperatures than the materials belonging to the fluorite structure and is also a promising electrolyte for application in devices operating at lower temperatures than the pre-existing YSZ-based devices.

Another family of oxide-ion conductors is the BIMEVOX family. The materials of this family are conductors based on Bi_2O_3 oxide. Bi_2O_3-based conductors doped with a transition metal (such as Cu or Mg) and vanadium (V) exhibit ionic conductivity of the order of $0.1 S \cdot cm^{-1}$ at 600°C [15]. The ionic conductivities of some of the most promising oxide-ion conductors belonging to the abovementioned families are presented in **Fig. 5**.

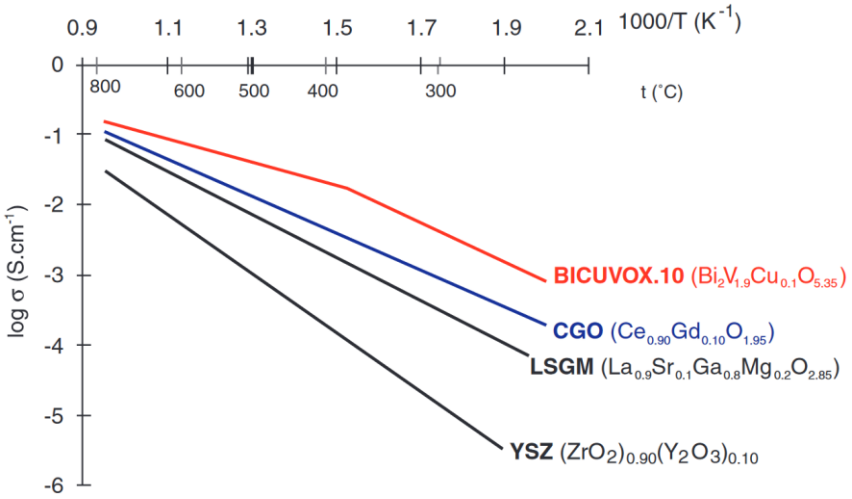

Figure 5: The ionic conductivity of some of the most promising oxide-ion conductors as a function of the inverse temperature [15].

- **Ag^+ Conductors**

Ag^+ conductors were the first solid electrolytes that showed high ionic conductivity even at room temperatures. The most popular Ag^+ conductor is the α-AgI discovered in 1914 by C.Tubandt and E.Lorentz. Most Ag^+ conductors display high ionic conductivity at high

temperatures. However, phases like $RbAgI_5$ with a similar structure to α-AgI exhibit considerably high Ag^+ conduction at low temperatures [7].

- **Na^+ Conductors**

Materials in the family of β-aluminas show exceptionally high conductivity of Na^+ and the ability to exchange Na^+ by a wide variety of other monovalent cations. Sodium β-alumina and sodium β"-alumina are the last members of a family of sodium aluminates whose composition ranges from approximately Na_2O-$11Al_2O_3$ to Na_2O-$5Al_2O_3$. An important advantage of beta aluminas is that they can exchange Na cations for a wide variety of divalent and trivalent cations [19].

- **Li^+ Conductors**

High-density, rechargeable Li-ion batteries that are mainly used in transportable electronics and electric vehicles were the driving force for more funding and research in Li^+ conductors. A commonly used ceramic electrolyte for lithium-ion batteries is lithium metal oxides that allow lithium-ion transport through the solid more readily due to the intrinsic lithium. Those electrolytes can exhibit good ionic conductivity at room temperature [7].

- **H^+ Conductors or proton conductors**

Electrochemical devices such as fuel cells and sensors were the driving force for the development and optimization of solid proton conductors. According to the temperature range of operation, they are divided into two groups. Electrolytes for low and moderate working temperatures are solid-state, acids and the family of β-aluminas. In high temperatures, oxides belonging to the perovskite family are typically used [7]. High-temperature proton conductors or HTPCs are the most promising electrolytes for devices that operate at elevated temperatures and aggressive environments, such as solid oxide fuel cells and electrolysis cells or electrochemical gas sensors. As expected, there are several properties that an electrolyte should satisfy to be considered suitable for application. Electrolytes must exhibit acceptable proton conductivity and low electronic or oxygen-ion conductivity, excellent chemical and thermodynamic stability at reducing, oxidizing or corrosive environments and good mechanical and ceramic properties [8].

Most oxide compounds that exhibit proton conductivity, usually, also exhibit electronic or oxygen-ion conductivity. For example, two well-known proton-conducting electrolytes, $BaZrO_3$ and $BaCeO_3$, depending on the environment of operation, may exhibit electronic (p- or n-type), oxygen-ion or proton conductivity. Also, $SrZrO_3$ and $CaZrO_3$ present similar behavior. High electronic conductivity affects the electrical potential difference between the two sides of the electrolytes and, as a result, reduces the response of the sensor. Considering that the proton-conducting electrolytes for electrochemical sensors operate at high temperatures and for a long period of time, they must exhibit significant stability in reducing, oxidizing and corrosive atmospheres.

Oxygen ion conductors and proton conductors are the most promising electrolytes for many electrochemical devices in the nearest future. Among the oxygen ion conductors, yttria-stabilized zirconia (YSZ) is the most popular.

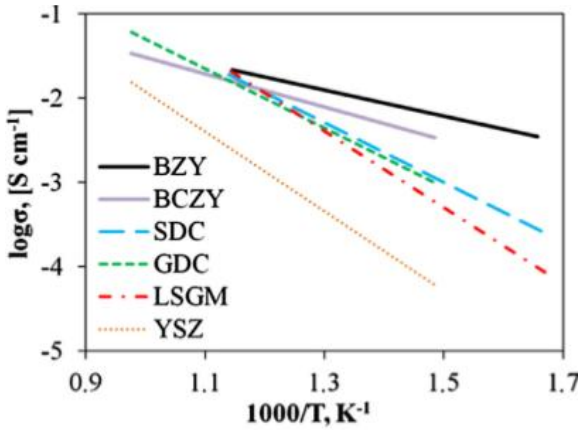

Figure 6: Ionic conductivities of different electrolytes plotted against temperature, $BaZr_{0.8}Y_{0.2}O_{3-\delta}$ (BZY), $BaCe_{0.7}Zr_{0.1}Y_{0.2}O_{3-\delta}$ (BCZY), $Ce_{0.8}Sm_{0.2}O_{2-\delta}$ (SDC), $Ce_{0.8}Gd_{0.2}O_{2-\delta}$ (GDC), $La_{0.8}Sr_{0.2}Ga_{0.8}Mg_{0.2}O_{3-\delta}$ (LSGM) and 8 mol% Y_2O_3-doped ZrO_2 [20].

As far as the proton conductors, two popular electrolytes are the ceramic materials based on $BaZr_{0.8}Y_{0.2}O_{3-\delta}$ (BZY) and $BaCe_{0.7}Zr_{0.1}Y_{0.2}O_{3-\delta}$ (BCZY). **Fig. 6** shows the conductivities of some oxygen-ion conductors and some proton conductors plotted against temperature [20].

2.2 Fundamentals of electrochemistry

2.2.1 Electromotive force

The movement of electrons in a wire or the movement of ions through an electrolyte to an electrode requires a work cost. This is similar to the pumping of water from one point to

another. In order to pump water, work cost is required. This analogy can be further expanded. Water flow requires a pressure difference. Water flow starts from a high-pressure point to a low-pressure point. The needed work for the movement through a pipe is related to water volume and the pressure difference. As in the flow of water, an electrical charge needs a potential difference to move from one point to the other. Electrons move from high voltage to lower voltage. The necessary work for the movement of electrons through a closed circuit is related to the potential difference and the charge being moved. Potential difference is the voltage between two points. Maximum potential difference is referred to as *Electromotive Force* (*EMF*) or E_{cell}. During the operation of the galvanic cell potential difference between the two electrodes is less than the expected maximum potential difference of the cell. This deviation from potential's difference maximum value is due to the movement of electrical charges through the cell. Consequently, potential difference decreases as the electric current increases resulting in its maximum value when no current flows through the system(open-circuit conditions). Cell's *EMF* is equal to the cathode's potential minus anode's potential [21].

$$E_{cell}^{0} = E_{cathode}^{0} - E_{anode}^{0} \tag{2.8}$$

2.2.2 Nernst's equation

Gibb's energy, ΔG^0, of a reaction is equal to the maximum useful work of this reaction. In a voltaic cell, this work is the electric work produced.

$$\Delta G^{0} = -n \cdot F \cdot E_{cell}^{0} \tag{2.9}$$

where n is the number of transferred electrons and F=96.485Cb·mol^{-1} is the Faraday's constant. It is also known that ΔG is related to ΔG^0 under standard conditions following the equation,

$$\Delta G = \Delta G^{0} + R \cdot T \cdot \ln \frac{[\mathrm{Re}\, d]}{[Ox]} \tag{2.10}$$

From the two equations above Nernst's equation is obtained which gives the *EMF* of the cell,

$$E_{cell} = E_{cell}^{0} + \frac{R \cdot T}{n \cdot F} \ln \frac{[\mathrm{Re}\, d]}{[Ox]} \tag{2.11}$$

where E_{cell}^{0} is *EMF* under standard conditions, R=8.314J/kmol is the ideal gas constant, T is the absolute temperature and [Red], [Ox] are the concentrations of the reductant and the oxidant consumed or generated by the redox reaction, respectively [22], [21].

2.2.3 Faraday's law

Faraday's law correlates the total charge, Q [C], passed through a cell to the amount of product, N [mol].

$$Q = n \cdot F \cdot N \tag{2.12}$$

In electrochemistry, Faraday's law can be used in different ways considering what is known. If the electricity that passes through the cell is known, the amount of substance produced in one of the electrodes can be calculated (electrogravimetry) or it is possible to calculate the total electricity that is needed for the complete electrolysis (coulometry). It can also be used for finding the number of electrons implicated in an electrolytic process [22], [21].

2.2.4 Kinetics

Overpotential

An overpotential $\eta = U - E_{cell}^{0}$ is the difference between the applied voltage and the *EMF* of the system.

Butler-Volmer equation and Tafel plot

The Butler–Volmer equation or current-overpotential equation calculates the current that results from an overpotential when mass-transfer limitations are eliminated.

$$i = i_0 \cdot \left(\exp\left(\frac{\alpha_a \cdot \eta \cdot F}{R \cdot T} z \right) - \exp\left(-\frac{\alpha_c \cdot \eta \cdot F}{R \cdot T} z \right) \right) \tag{2.13}$$

Where i is the total current density, i_0 the exchange current density and α_a, α_c are the anodic and cathodic charge transfer coefficients, respectively, and z is the number of electrons

involved in the reaction. Constants α_a, α_c are not two independent coefficients, generally $\alpha_\alpha+\alpha_c=1$, and relate how the applied potential favors cathodic reactions over anodic reactions or the other way around [22].

From the Butler-Volmer equation it is observed that the overall current density can be presented as the difference of two terms, namely the anodic current i_a and the cathodic current i_c.

$$i_a = i_0 \cdot \left(\exp\left(\frac{\alpha_a \cdot \eta \cdot F}{R \cdot T} z \right) \right) \tag{2.14}$$

$$i_c = i_0 \cdot \left(\exp\left(-\frac{\alpha_c \cdot \eta \cdot F}{R \cdot T} z \right) \right) \tag{2.15}$$

There are two cases of the Butler-Volmer equation. The first case is called the overpotential region and can be further divided into two subcases, the positive overpotential and the negative overpotential region. At this region, the equation (2.14) presents a Tafel behavior where one of the two terms of the equation becomes negligible. The sign of the overpotential shows the favorable direction of the reaction. When η>>0 the anodic term dominates the Butler-Volmer equation and the cathodic term becomes negligible. On the other hand, when η<<0 the cathodic reaction dominates over the anodic. This behavior can be seen in **Fig. 7**. When the voltage (η) increases, so do and the anodic current (red line). However, the cathodic current (blue line) tends to zero. The opposite behavior is observed when η<<0.

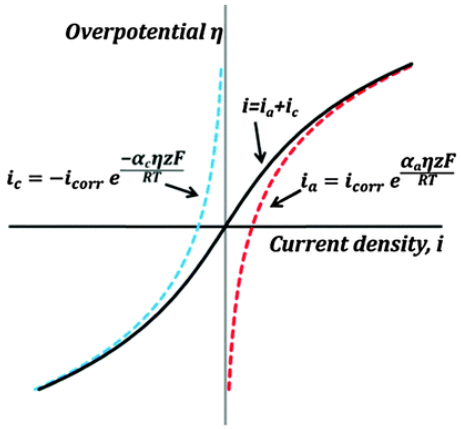

Figure 7: Typical i vs. n dependency based on the Butler-Volmer equation [23].

It is observed in **Fig. 7** that for high overpotentials (over 50mV) the current increases exponentially. So the equations (2.14) and (2.15) can be expressed with the aid of logarithms as,

$$\ln(i) = \ln(i_0) + \frac{\alpha_a \cdot F \cdot \eta \cdot z}{R \cdot T} \qquad \text{for } \eta>0 \qquad (2.16)$$

$$\ln(i) = \ln(i_0) + \frac{\alpha_c \cdot F \cdot \eta \cdot z}{R \cdot T} \qquad \text{for } \eta<0 \qquad (2.17)$$

These equations are known as anodic and cathodic Tafel equations, respectively. Tafel's equation is usually presented as,

$$\eta = \frac{R \cdot T}{\alpha \cdot F} \ln(i_0) + \frac{R \cdot T}{\alpha \cdot F} \ln(i) \qquad (2.18)$$

In equation (2.18), the y-axis corresponds to no overpotential condition so it can be used to measure graphically the exchange current i_o. Equation (2.18) can be written in a simplified form as,

$$\eta = a + b \ln(i) \qquad (2.19)$$

Where in equation (2.19), a and b are constants and can be easily identified by equation (2.18). Equations (2.16) and (2.17) show a linear behavior for *high overpotential*. This region of the Butler-Volmer equation is known as the Tafel region and the log(i)-η plots are known as Tafel plots, **(Fig. 8)**. It can be seen in **Fig. 8** that Tafel plots are composed of two branches, one is the anodic branch for positive overpotential and the other is the cathodic branch for negative overpotential. The oxidation and reduction slopes of the linear region on the Tafel plot are equal to,

$$\text{Reduction slope} = -\frac{\alpha_c \cdot \eta \cdot F}{2.3 \cdot R \cdot T} \qquad (2.20)$$

$$\text{Oxidation slope} = \frac{\alpha_a \cdot \eta \cdot F}{2.3 \cdot R \cdot T} \qquad (2.21)$$

Where 2.3 results due to the conversion from natural to decimal logarithms. Tafel's plots are useful because from the reduction and oxidation slope one can calculate the anodic and cathodic charge transfer coefficients and the exchange current density [22]. For example, for a reduction/oxidation slope equal to 9 and at 25°C, the charge transfer coefficient is calculated by equation (2.20)/(2.21), respectively, and it is equal to about α=0.5. Also, the exchange current density is graphically measured from the intercept with the y-axis and it is equal to $\log|i_o|=-7$ or $i_o=10^{-7}$A.

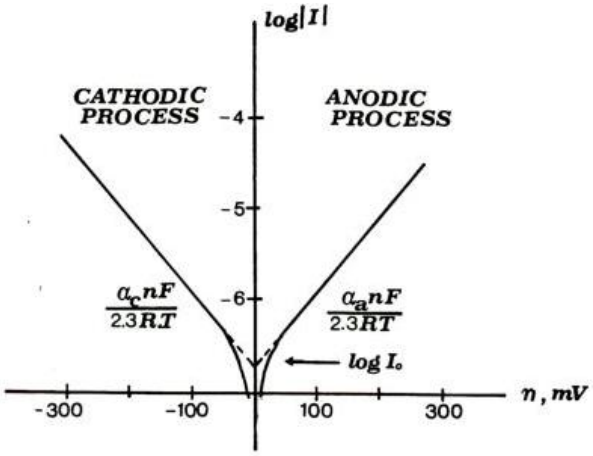

Figure 8: Tafel plots for anodic and cathodic branches [22].

The second case of the Butler-Volmer equation is the *low overpotential region*. This region is called the ohmic region because. for small values of η, the current density varies linearly resulting in a similar to Ohm's law correlation between i and η. For low overpotential, the Butler-Volmer equation changes to,

$$i = \frac{i_0 \cdot (\alpha_a + \alpha_c) \cdot F \cdot \eta}{R \cdot T} \tag{2.22}$$

2.3 Diffusion of gas in porous media

One of the main advantages of electrochemical sensing technologies is the linear output. There are types of sensors designed such that the gas flow is limited by diffusion barriers and the current generated by the sensor is controlled by the quantity of gas that reacts at the electrodes. This way, the gas concentration is linearly proportional to the generated

current. Laws of diffusion describe the net flux of molecules from higher concentration to points of lower concentration or the movement of substance due to a concentration gradient. There are three types of diffusion, molecular, Knudsen and mixed diffusion. The dominant mechanism depends on the characteristics of the measured gas and the microstructure of the solid porous media. To identify which mechanism dominate each time, it is necessary to calculate the Knudsen number (Kn). Molecular diffusion dominates at Kn<<0.1, Knudsen diffusion at Kn>>10 and between 0.1 and 10, all mechanisms contribute to gas diffusion. Knudsen number is the ratio of gas mean free path to the pore diameter as shown in the equation (2.23),

$$K_n = \frac{\lambda}{d_P} \tag{2.23}$$

Concluding, in Knudsen diffusion the mean free path of gas molecules is at least one order larger than the porous diameter, so the collisions between gas molecules and porous wall are dominant, as shown in **Fig. 9**.

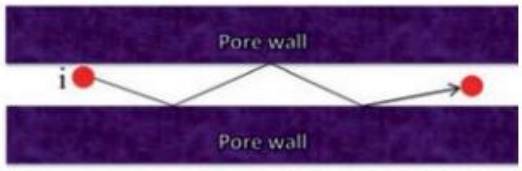

Figure 9: Pure Knudsen diffusion [24].

In molecular diffusion, porous diameter is much larger than the mean free path of gas molecules, resulting in negligible Knudsen diffusion, as shown in **Fig. 10**. For both mechanisms to participate in gas diffusion, λ and dp must have the same order of magnitude.

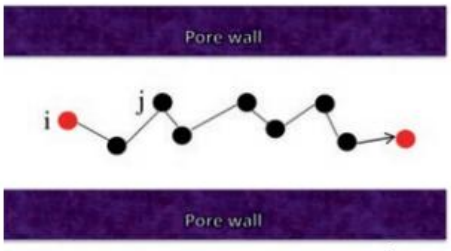

Figure 10: Pure molecular diffusion [24].

Fick's first law is the most important mathematical model for diffusion. Fick in 1855 described in a simple mathematical model how the diffusion flux relates to the gradient of concentration. He explained that diffusion flux starts from high to low concentration regions.

$$J = -D\frac{dC}{dx} \tag{2.24}$$

Where D is the diffusivity and x is the position. The main difference in the calculations of the three mechanisms is the term D of Fick's law. For porous solids, the porosity factor εand the tortuosity factor τ have to be considered in both mechanisms. The diffusivity is modified as,

$$D^{eff} = \frac{\varepsilon}{\tau} D \tag{2.25}$$

where D is different for every type of diffusion and it is calculated as follows [24].

2.3.1 Molecular diffusion

For molecular diffusion, Fick's law is $J = -D_{AB}^{gs}\frac{dC}{dx}$, where D_{AB}^{gs} is the binary diffusion coefficient for mixtures of gases and is calculated from Chapman-Enskog theory,

$$D_{AB}^{gs} = 0.001834 \cdot \left(\frac{\sqrt{T^3 \cdot \frac{Mr_A + Mr_B}{2 \cdot Mr_A \cdot Mr_b}}}{p \cdot \sigma_{AB}^2 \cdot \Omega_D} \right) \tag{2.26}$$

Where T is the absolute temperature, Mr is the molecular weight, p is the pressure,σ is the average collision factor for gases A and B and Ω is collision integral.

2.3.2 Knudsen diffusion

Knudsen diffusion is a selective transport mechanism that becomes important when the mean free path of the particles is greater or even comparable to the porous diameter. The diffusion coefficient for Knudsen's diffusion is estimated from:

$$D_k = \frac{d_p}{3}\sqrt{\frac{8 \cdot R \cdot T}{\pi \cdot Mr}} \tag{2.27}$$

Where dp is the porous diameter, R is the ideal gas constant and T is the absolute temperature. Generally, Knudsen diffusion is important at low pressure and/or small pores [24].

During the operation of most electrochemical devices, the diffusion of the gas fuel or the analyzed gas in the porous electrodes needs to take place for the heterogeneous reaction to occur. In solid electrodes, conditions of pressure and pore diameter are such that both mechanisms participate (0.1<Kn<10) [24]. Both D_{AB}^{gs} and D_k apply and the diffusion coefficient in this case obey the following equation,

$$\frac{1}{D^*} = \frac{1}{D_{AB}^{gs}} + \frac{1}{D_k} \tag{2.28}$$

2.4 Electrochemical devices

2.4.1 Electrochemical cells

The electrochemical cell is the heart of every electrochemical device. An electrochemical cell is composed of two half cells, one contains the oxidation half-reaction and the other contains the reduction half-reaction. The basic configuration involves the electrolyte, two electrodes and the necessary sealants, electronics and fuel distribution mechanisms. However, a third electrode known as the reference electrode is commonly used. A commonly used experimental setup is presented in **Fig. 11**.

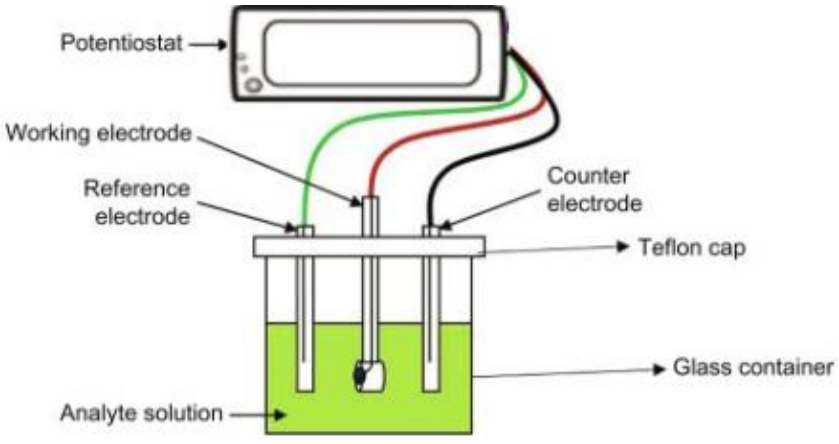

Figure 11: Experimental setup of electrochemical cells [25].

The first electrode is the anode (also referred to as sensing or working electrode). Usually, oxidation takes place at the anode, generating ions and electrons. The reduction reaction occurs at the cathode using both the ions and the electrons from the anode to complete the circuit. To reach the cathode (also referred to as the counter electrode) and complete the reaction, the as-generated ions move through the ion conductive electrolyte and the electrons through the external electrical circuit. The desirable properties of electrodes are good electronic conductivity, good electrocatalytically activity and chemically and thermodynamically stability in the operating environment.

Electrolyte separates anode and cathode. Its role is to provide a pathway for ions to flow from anode to cathode while blocking electrons. Electrolytes are either solid (gels, dry polymer, ceramics) or liquids (alkali, molten carbonate, phosphoric acid). It is also important for electrolytes to be chemically stable at oxidizing and reducing environments and stable at operating temperatures. It is important to note that material selection for every device takes into consideration the operating requirements, conditions and optimization. Resulting in a wide variety of materials for electrodes and electrolytes.

The principle of operation of the electrochemical cell is simple and similar for every electrochemical device. Oxidation takes place at the anode generating electrons and ions. Electrons flow through an external circuit and meet with ions at the cathode side where the reduction reaction occurs. Usually, the reduction reaction is the rate-limiting step of the process. The movement of electrons provides the desirable electrical voltage (electric energy) [26].

Oxidation: $\text{Reductant} \rightarrow \text{Ox.product} + e^-$

Reduction: $\text{Oxidant} + e^- \rightarrow \text{Red.product}$

Overall Reaction: $\text{Reductant} + \text{Oxidant} \rightarrow \text{Ox.product} + \text{Red.product}$

2.4.2 Fuel cells

In 1838, C.F. Schönbein talked about the principles of a fuel cell. Later Sir W.R. Grove, based on his work, demonstrated the first fuel cell. This fuel cell had as electrodes iron sheets and a solution of sulphate and dilute acid as the electrolyte. Fuel cells are devices that convert the fuel's chemical energy to electrical energy through redox reactions. A fuel cell in its simplest

form consists of an electrolyte placed between two porous electrodes, the working (or anode) and the counter (or cathode) electrode and an external circuit for electrons to flow. Hydrogen-rich gases or even pure hydrogen are fed to the anode and an oxidant gas, usually, air or pure oxygen is fed to cathode. A simple and well-known fuel cell is the proton exchange membrane fuel cell (PEMFC) **Fig. 12**. In this type of fuel cell, gaseous fuel containing, e.g. H_2, is fed continuously to the anode compartment and an oxidant e.g. oxygen or air is fed continuously to the cathode compartment. The electrons move through the external circuit providing electrical energy and meet with the protons and oxygen at the cathode where the reduction of oxygen takes place. Theoretically, a fuel cell can provide energy forever as long as there is fuel.

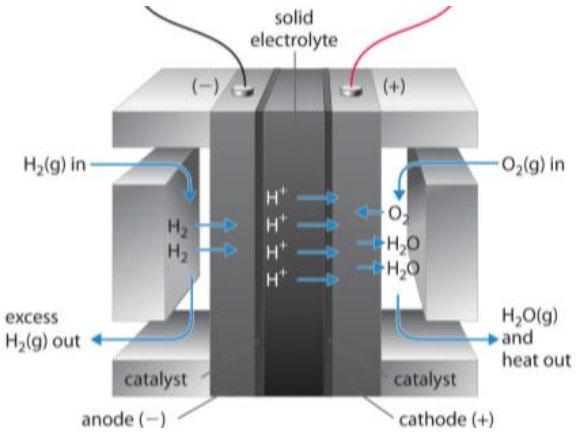

Figure 12: Proton exchange membrane fuel cell [26].

Fuel cells present plenty of advantages over other energy generating devices leading to plenty of research over the years. Fuel cells are used in a wide range of applications including portable, transportation, stationary and emergency backup power applications. Furthermore, fuel cells present many important advantages over the already well-established combustion technologies. First of all, in terms of efficiency, fuel cells operate with overall efficiencies up to 60%, in contrast to combustion engines that achieve efficiencies varying from 30% to 40%. Also, there are types of fuel cells that have low to zero emissions. When pure hydrogen is used as fuel, it emits only water and heat, so there are no greenhouse gases in its emissions.

There are many types of fuel cells categorized based on the electrolyte, the fuel, the working temperatures and the applications. Basic information about the main available technologies are listed in **Table. 1**.

Table 1: Types of fuel cells [27].

	TEMPERATURE °C	Electrolyte	Ions in electrolyte	Applications	Released power
AFC (alkaline)	<100	KOH	OH^-	vehicles, portable, energy storage, space	5-150kW
PEMFC (polymer electrolyte membrane)	20-80	Proton exchange membrane	H^+		5-250kW
DMFC (direct methanol)	60-120	Nafion membrane	H^+		<5kW
PAFC (phosphoric acid)	160-220	immobilized liquid phosphoric acid	H^+	stationary power systems	50kW-11MW
MCFC (molten carbonate)	600-800	immobilized liquid molten carbonate	CO_3^{2-}	stationary systems and transportation (train, boats,…)	100kW-2MW
SOFC (solid oxide)	800-1000	YSZ	O^{2-}		100-250kW

Besides the fact that they show significant advantages, fuel cells aren't yet commercially used as most technologies are still under development and burdened by many problems. Those problems make them less competitive against technologies that are already in use. The rate-determining step of fuel cell's efficiency is the reduction that takes place at the cathode. Therefore, catalysts are employed in order to accelerate both oxidation and reduction reactions. The most effective catalysts for fuel cells are platinum and other noble metals of the same family, such as Ru, Ir, or Pd. The necessary noble metal load for fast reaction increases the cost of the fuel cell [27]. Furthermore, hydrogen, which is the main fuel for most fuel cell technologies, is expensive as there isn't still a network for its distribution and an easy and efficient method for mass production. Also, it needs great pressure to confine the desirable quantity of hydrogen in fuel containers making its distribution even more expensive. Lastly, hydrogen is an invisible, odorless, flammable and potentially explosive gas making it, alongside the great pressures, a dangerous fuel [28].

2.4.3 Batteries

Batteries are devices able to store electric energy in the form of chemical species. When there is a need for this stored energy, chemical reaction takes place inside the battery generating electrical energy. The first step for solid-state ionics was the discovery of solid electrolytes Ag_2S and PbF_2 by Michael Faraday around 1834. Solid-state batteries were developed in the 1950s for the first time using Ag^+ conductors. These batteries had a very high internal resistance and limited current

densities. As most of those batteries were based on Ag^+ conducting electrolytes it was necessary to use silver as the anode. Resulting in low cell voltage and low energy densities. However, the batteries did exhibit a long shelf life and good mechanical stability [29].

A battery consists of two electrodes, anode and cathode, separated by the electrolyte. When connected to the external circuit redox reactions take place inside the cell, generating electrons and ions. Ions move through the electrolyte and electrons through the external circuit providing electric energy. The electron flow stops when one of the two reactions stop. Batteries are usually classified, based on their reactions, in primary and secondary batteries. In primary batteries, the reactions are irreversible, while the opposite applies to secondary batteries. Reversible reactions indicate that the battery can be recharged, after the use, back to its pre-discharged condition [30].

The lithium-ion batteries are well-known and promising rechargeable batteries, employed in many portable devices and electric vehicles. A typical lithium-ion battery uses lithium metal oxide (e.g. $LiCoO_2$) and graphite electrodes and polymer gel as the electrolyte. Reactions during charge and discharge inside a typical lithium-ion rechargeable battery are,

Cathode: $$LiCoO_2 \rightarrow Li_{1-x}CoO_2 + xLi^+ + xe^- \quad (2.29)$$

Anode: $$xLi^+ + xe^- + xC_6 \rightarrow xLiC_6 \quad (2.30)$$

Overall reaction: $$LiCoO_2 + xC_6 \rightarrow Li_{1-x}CoO_2 + xLiC_6 \quad (2.31)$$

where x=0.5 and it represents the transferred moles during the reaction. When an external source is connected, electrons and ions are detached, according to the reaction (2.29), from the metal oxide and move through the electrolyte and the external circuit, respectively, to the anode. Reaction (2.30) takes place at the anode. However, when the source disconnects, both ions and electrons stay trapped in an unstable condition. When a load is connected, the charged species and the reactions follow the opposite direction. The charge and discharge of a typical lithium-ion battery are presented in **Fig. 13**.

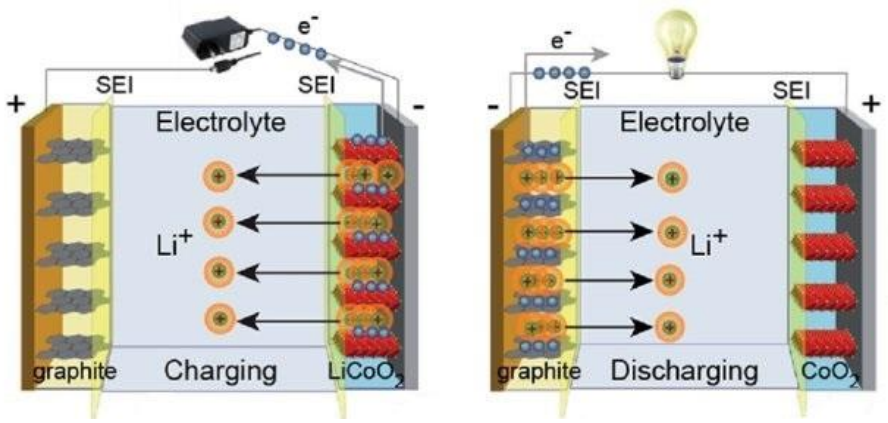

Figure 13: Charge and discharge of a typical Li-ion battery using $LiCoO_2$ and graphite electrodes [31].

In **Fig. 13,** the positive electrode (or cathode) is lithium metal oxide $LiCoO_2$ and the negative electrode (or anode) is grapheme. In contrast to more conventional batteries with liquid or polymer electrolytes, solid-state batteries employ solid electrolytes and solid electrodes. Solid-state batteries offer many advantages over conventional batteries making them a potential alternative in near future. Among these advantages, they exhibit higher stability and energy density with a low risk of flammability or other failure conditions. Concluding, solid-state batteries exhibit higher performance and safety at a lower cost compared to batteries based on liquid or polymer electrolytes [32].

2.4.4 Capacitors-Supercapacitors

In their simplest form, capacitors consist of the dielectric placed between two parallel plates. The dielectric needs to present zero electronic conductivity (e.g. air) and it is utilized as an insulator between the electrodes. In their neutral phase, both plates have an equal amount of electrons and are neutral. When voltage is applied, electrons are forced to move from one plate to the other. Due to the charge difference between the two plates, an electric field is created. Electrons can't move through the dielectric so when the voltage source disconnects, the electrons remain at the plates and the capacitor remains charged. Thus, capacitors are devices able to store electrical energy in the form of an electric field established by the opposite charge of the two plates. The amount of stored energy known as capacitance is proportional to the surface area of the plates and inversely proportional to the dielectric thickness between these two conductive plates [33]. Capacitance is measured according to equation (2.32),

$$C = \varepsilon_o \cdot \varepsilon_r \cdot \frac{A}{D} \tag{2.32}$$

Where ε_o and ε_r are dielectric constants about the free space and insulating material between the electrodes, A is the electrodes surface area and D is the distance between the electrodes. Also, the stored energy E in a capacitor is calculated from equation (2.33),

$$E = \frac{1}{2} \cdot C \cdot V^2 \tag{2.33}$$

Where V is the applied voltage required to charge the capacitor. Usually, capacitors are represented as a circuit with a resistance R. A conventional charged capacitor is presented in **Fig. 14.**

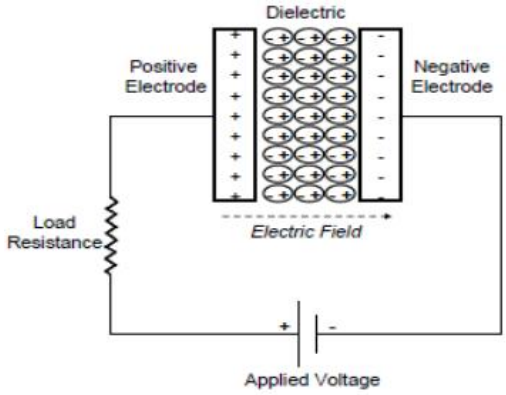

Figure 14: Scheme of a charged conventional capacitor [34].

Considering that no electrochemical reaction takes place during the discharge/charge, capacitors provide high power densities. However, their energy density is considerably lower than that of other energy storage devices such as batteries and supercapacitors. Larger capacitance or more energy density can be accomplished by increasing the electrode's surface area or using a thinner dielectric. Supercapacitors or ultra-capacitors or electric double-layer capacitors are high-capacity electrochemical devices able to compete with most pre-existing energy storage devices. Typically, supercapacitors consist of two porous electrodes that provide high surface area, an electrolyte and a very thin separator. Depending on the requirements and the application, used electrolytes are either solid-state or organic aqueous-type. In supercapacitors there is no dielectric. Between the two plate there is an electrolyte that contains a mixture of positive and negative charge carriers. When a voltage

source connects, an opposite polarity charge layer is formed on both sides creating an electric double-layer as shown in **Fig. 15**, thus the name double layer capacitor [35].

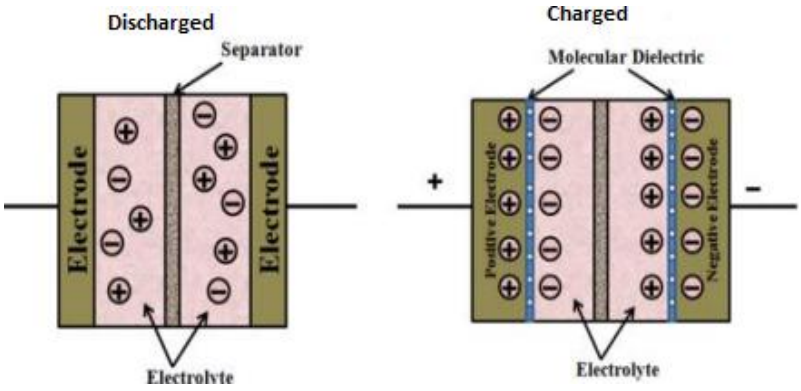

Figure 15: Schematic representation of the basic double layer principle in a charged capacitor [35].

Commercially used supercapacitors typically use liquid organic electrolytes. Liquid electrolytes are already well-established and it is well-known that they provide high ionic conductivity and fast discharge/charge kinetics. However, liquid electrolyte based-supercapacitors are vulnerable devices with a high risk of electrolyte leakage or evaporation, unable to operate in harsh environments. So rigid packaging is required to protect and retain the liquid electrolyte. Many of the problems associated with liquid electrolytes are solved by replacing them with solid-state electrolytes. Solid electrolytes are more stable even in harsh environments, providing design freedom. Concluding, efforts to increase the performance and the energy density of solid-state supercapacitors involve the development of progressively higher ion-conducting and electrochemically reactive materials for both electrodes and electrolytes [36].

Energy production from renewable energy sources such as wind or sun is becoming more and more important. The main problem with such energy sources is their irregular nature. Because of this problem, there is a need for energy storage devices that are safe, cost-effective, environmentally friendly and able to store energy when in excess and provide it when there is a need. Concluding, the optimization of electrochemical energy storage devices such as fuel cells, batteries and supercapacitors, plays an important role in the future of environmentally friendly energy production.

Chapter III

Experimental techniques for materials and sensors characterization

Abstract

In the present chapter, a general background of the experimental techniques for the characterization of the materials and the devices is provided. Techniques for the electrochemical analysis of the materials are reviewed. The three-electrode configuration is presented as it is the basic configuration for most of the electrochemical experiments and then common techniques such as CV, LSV, EIS, chronoamperometry and RDE are discussed. Physicochemical techniques for the analysis of the chemical and physical composition of the material's surface are also discussed. The most common techniques are reviewed, such as TEM, SEM, XPS and RS.

3.1 Electrochemical techniques

An electrochemical analysis is an efficient way to understand the electron and ion transfer reactions underpinning electrochemical devices. More and more researchers are interested in further understanding electrochemistry to optimize and advance their research [37].

3.1.1 Conventional three-electrode cell

Most electrochemical characterization techniques are accomplished through voltammetry experiments. These experiments study current as a response to an applied potential. In these methods, with the help of a potentiostat connected to the electrodes, an electric potential is applied to the working electrode in order to drive the transfer of electrons from and to the electrolyte. A second electrode is needed to maintain a stable reference potential to monitor the sensing electrode's potential and to complete the redox reactions. However, a three-electrode setup is employed as it is difficult to maintain a stable potential when current passes through the second electrode. Consequently, the most common experimental configuration is the three-electrode cell. This setup consists of three electrodes, the anode or working/sensing electrode, the reference and the cathode or counter electrode. All three electrodes are immersed in the liquid electrolyte. A scheme of a two-electrode and a three-electrode experimental setup is presented in **Fig. 16**.

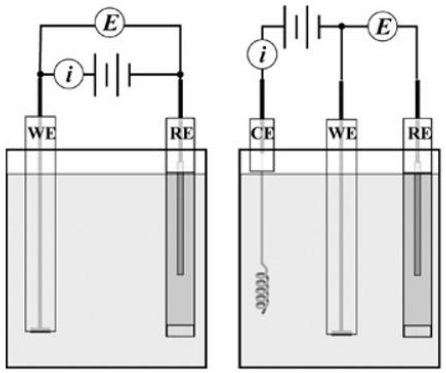

Figure 16: Two and three-electrode setups, WE is the working electrode, CE is the counter electrode and RE is the reference electrode [22].

In this method, the potential difference is measured between the sensing and the reference electrode and the current passes between the sensing and the counter electrode. In order to provide a stable reference potential, there must be no or low current through the reference electrode. This is accomplished with a high input resistance to the potentiostat. Ohmic resistance has a negligible impact on this potential because the reference electrode is placed as close as possible to the sensing electrode, thus reducing the solution resistance. Note that the reference tip should not block the mass transfer of the electrolyte [22].

3.1.2 Cyclic voltammetry (CV)

Cyclic voltammetry is a simple method used in many electrochemical studies. This method is being applied to obtain analytical (concentration of the mixture), kinetic (rate of the reactions), thermodynamic (equilibrium constants and potentials) and mechanistic information about electrochemical processes affected by redox reactions. When performing cyclic voltammetry, the working/sensing electrode is scanned from an initial potential E_1 to a potential E_2 at a fixed rate. The scan rate depends on the conditions and the reactions of interest, and it usually varies between 1 and 100mV·s^{-1}. During cyclic voltammetry, the potential scan starts from E_1 until the set potential E_2 is reached, and then it changes in the other direction back to E_1. The voltage changes are measured between the sensing-reference electrodes and the current response between sensing-counter electrodes. The applied voltage results in the measurement of a current response (A) at the working electrode. Plotting the applied voltage at the x-axis and the measured current at the y-axis results in a plot known as a cyclic voltammogram, **Fig. 17(left)**. The two set points are selected in such a way to contain the redox reactions of interest [38].

For example, when a solution of ferrocenium $[Fe(C_5H_5)_2]^+$, abbreviated as Fc^+, is swept from zero to negative potentials, it is reduced to Fc locally according to the reaction (3.1),

$$Fc^+ + e^- \rightarrow Fc \tag{3.1}$$

Due to this reaction, a current response and a decrease of Fc^+ close to the electrode are observed. The potential is scanned gradually from E_1 to E_2 (A to D). The concentration of Fc^+ decreases close to the electrode as it is reduced to Fc. However, there is a point where the volume of Fc continues to grow to the point that it slows down the mass transport of Fc^+ to the electrode's surface. At this point, the peak cathodic current ($i_{p,c}$) is observed, and it is also observed that the current decreases as the potential increases. When the set potential E_2 (at point D) is reached, the scan direction is reversed and the Fc reduced at the electrode's surface is oxidized back to Fc^+ according to the reaction (3.2),

$$Fc \rightarrow Fc^+ + e^- \tag{3.2}$$

this way a similar peak is observed. The cyclic voltammogram is presented in **Fig. 17(left)**. In **Fig. 17(right)**, the potential steps during the process are presented.

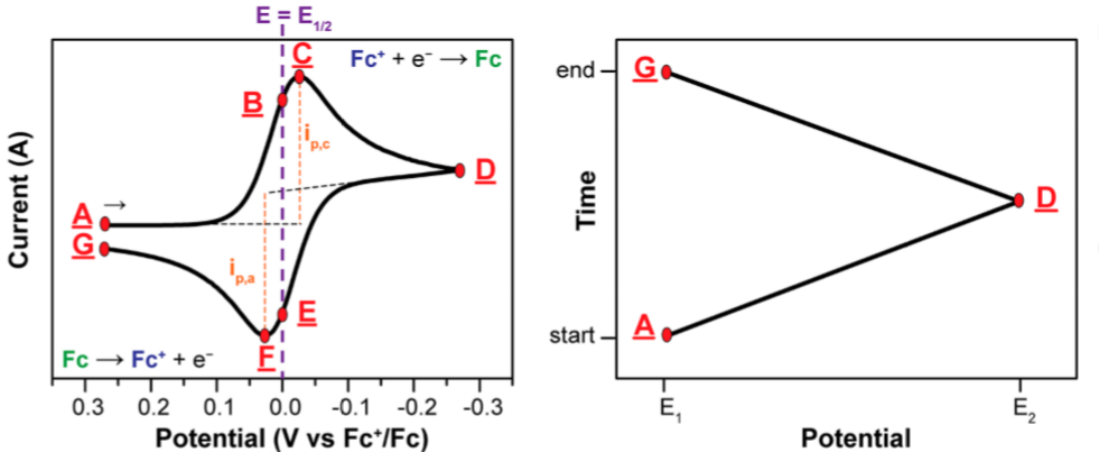

Figure 17: (left) Cyclic voltammogram of the reversible reaction from Fc^+ to Fc, at a scan rate of 100mV·s^{-1} and (right) Applied potential steps as a function of time for a cyclic voltammetry experiment [38].

The important parameters from a cyclic voltammogram are the two potential peaks E_{pa} and E_{pc} and the two current peaks $i_{p,a}$ and $i_{p,c}$, where a stands for anode and c for cathode. It is important to note that, for a reversible reaction, the position of the peak current isn't affected by the potential scan rate. Consequently, it is possible to calculate the value of the current peak through equation (3.3),

$$i_p = 2.69 \cdot 10^5 \cdot n^{3/2} \cdot A \cdot D_o^{1/2} \cdot v^{1/2} \cdot C_o \qquad (3.3)$$

where i_p is the peak current, n is the number of electrons transferred due to the redox reaction, A is the area of the electrode's surface, D_o is the diffusion coefficient, v is the scan rate and C_o is the concentrations of the reactant in the bulk solution. From these values, important information about the electrochemical processes is obtained [39].

3.1.3 Linear sweep voltammetry (LSV)

A similar method to cyclic voltammetry is linear sweep voltammetry. In LSV the scan begins from low values of voltage where there is no current response. As the voltage increases, a current response is observed and eventually reaches a peak before dropping, just like in cyclic voltammetry. In LSV current response is also plotted against applied voltage. When

the peak is observed, the concentration flux of the reactant around the electrode is not fast enough compared to the reaction rate, so the current starts to drop. This analysis ends when the set value E_2 is reached. The characteristics of the linear sweep voltammogram depend on the reaction rate, the reactivity of the components and the scan rate. CV and LSV can be used to identify unknown species and measure the concentration of a solution [38].

3.1.4 Chronoamperometry

A simple but one of the most employed voltammetric methods is chronoamperometry. In its simplest form, a chronoamperometry analysis includes applying a voltage step to the working electrode and measuring the current response. This simplicity is what makes chronoamperometry ideal for basic electrochemical measurements. For example, consider a basic electrochemical cell that is composed of two electrodes, working and reference, and an electrolyte solution. The electrolyte solution contains only the oxidized form of the analyte, O, at a concentration of C_O. During chronoamperometry measurements, at time t_0, a high voltage (E_a) is applied between the two electrodes such that almost all the O around the electrode is instantly reduced to R. Due to the high voltage all the O that reaches, through diffusion, the electrode is instantly reduced, resulting in a great depletion of the O content close to the electrode. The transferred charge (Q) during the reaction is calculated from Faraday's law,

$$Q = n \cdot F \cdot N \cdot A \tag{3.4}$$

By differentiating the equation (3.4) and with the aid of Fick's first diffusion law, equation (2.24), the equation for the faradic current is obtained. Equation (3.5) is also known as the Cottrell equation. Cottrell equation is important because it describes the current response, of a reversible redox reaction, at any time after the potential step.

$$i_f(t) = \frac{n \cdot F \cdot A \cdot C_O \sqrt{D_O}}{\sqrt{\pi \cdot t}} \tag{3.5}$$

where n is the number of the electrons participating in the reaction, F is the Faraday's constant, C_O is the concentration of the reactant, A is the area of the electrode and t is the time after the potential step. The plot of the current response against time can be seen in **Fig. 18(right)**. At t_0=0, when the potential step is applied, the current response from

equation (3.5) is technically infinite, but in real systems, the faradaic current also depends on the electron transfer and the current supply from the electronic equipment. As observed in **Fig. 18(right)**, the current instantly drops and gradually tends to zero [40]. **Fig. 18(left)** shows the potential-time plot.

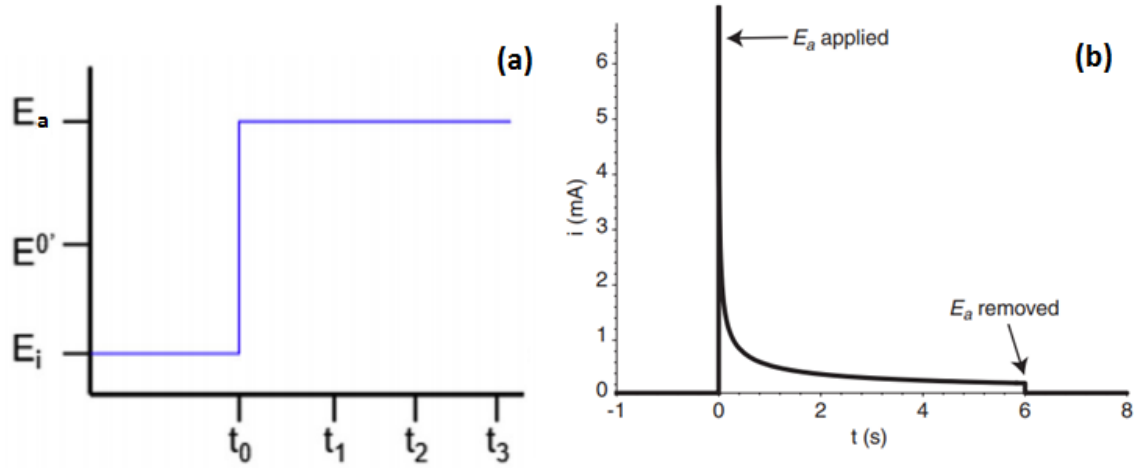

Figure 18: (a) Potential step from E_i to E_a at time t_0 and (b) ideal chronoamperometric current response to step E_a [40].

3.1.5 Electrochemical impedance spectroscopy (EIS)

Electrical resistance is the tendency of a circuit to resist the movement of electrons. It's measured by Ohm's law R=E/I. However, Ohm's law only applies to the ideal resistor. This is because the perfect resistor has many simplifying properties. First, it follows Ohm's law at every value of current and voltage. Second, its resistance doesn't depend on the frequency, and last, AC voltage and current through a resistor are in phase. However, those simplifying properties can't be applied to every system, so impedance is used for more complex systems. Impedance, similarly to resistance, is the tendency of a system to resist the flow of electrons but it requires no simplifying properties. When an AC potential is applied to an electrochemical device, an electrochemical impedance is measured. It is called impedance spectroscopy as it is carried out at a wide range of frequencies. From the relation between impedance and frequency, information about the electrochemical processes is obtained.

The main concept of EIS is that it's possible to imitate every electrochemical process by an equivalent electric circuit. Different chemical or physical characteristics of the cell are represented as an electric circuit that consists of a resistor, a capacitor or a pinion. For

example, the equivalent electric circuit for a simple electron transfer is shown in **Fig. 19**. The electrolyte, between the two electrodes, exhibits an ionic conductivity with a resistance equal to R_Ω, so R_Ω corresponds to the electrolyte's ohmic solution resistance. During the operation of the cell, redox species react at the surface of the electrode. Through these reactions, the faradaic current (i_f) is observed. Faradaic current describes the rate of electron and mass transfer. The electron transfer is described through the charge transfer resistance (or R_{ct}), and the mass transfer is described by the Warburg resistance (or Z_w). Note that the faradaic resistance is equal to the sum of R_{ct} and Z_w. Last, C_d describes the double layer capacitance, and it depends on the electrolyte and the electrode's surface.

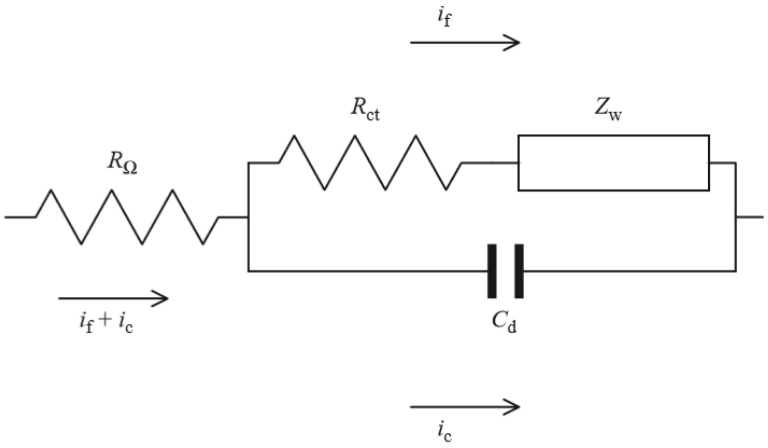

Figure 19: Equivalent electric circuit for a simple electron transfer [41].

To perform EIS at a cell, a small AC is applied, resulting in a measurement of impedance response. EIS is a popular analytic technique as it offers much in-situ information about the kinetics of processes, capacitance, surface areas and resistance. Also the small imposed AC results in a pseudo-linear behavior. At first electrochemical impedance spectroscopy or AC impedance was applied for the calculation of double layer capacitance. Now EIS has many more applications. From processes at the surface of the electrodes and electrolyte, such as reduction and oxidation reactions, adsorption, electrosorption and kinetics of heterogeneous/homogenous reactions, to geometric effects, such as type of mass transfer and the determination of solution resistance and applications in electrochemical devices (batteries, fuel cells) for electrocatalytic reactions and corrosion studies. Information from EIS is presented in complex plots such as Nyquist or Bode plots. Nyquist plots are more

popular in electrochemical studies as they are easily related to electrical models and offers an accurate prediction of cell's elements [42], [43]. The impedance can be described as a complex number,

$$Z_{cell} = Z_{\mathrm{Re}} + i \cdot Z_{\mathrm{Im}} \tag{3.6}$$

In equation (3.6), Z_{Re} and Z_{Im} are functions of R_{Ω}, R_{ct}, ω and C_d. If the real part is plotted on the x-axis and the imaginary part on the y-axis, the resulting plot is known as a Nyquist plot, **Fig. 20**. Note that in the Nyquist plot, the y-axis is reversed, and each point describes the impedance for a certain frequency. The frequency starts from zero at the right side of the diagram and increases when moving towards the left side. A typical Nyquist plot with all the important information is presented in **Fig. 20.**

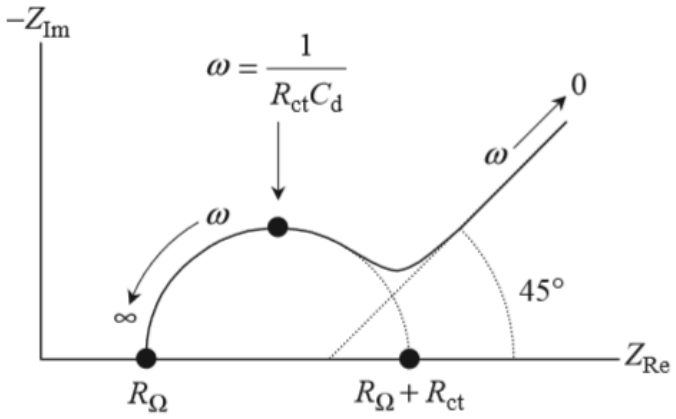

Figure 20: Key information of a Nyquist diagram [41].

From the characteristics of the plotted circle in the Nyquist plot, information about the solution resistance, charge transfer resistance and double layer capacitance are obtained. For example, at the region of high frequencies (left), the intercept on the real axis indicates the value of the solution resistance (R_{Ω}), and the intercept at the region of low frequencies (right) indicates the value of the sum of solution resistance and charge transfer resistance (R_{Ω}+R_{ct}). The frequency at the top of the circle provides information for the double layer capacitance (C_d) [41].

3.1.6 Rotating disk electrode (RDE)

The current response measured during a voltammetry experiment is disturbed due to the bulk movement of the solution. In order to provide accurate measurements, researchers need to take into consideration any disturbance due to the convection. Thus, it is important to control convection. Generally, there are two approaches to address this problem, either the experiment is conducted in a non-stirred solution with zero impact from convection, or the experiment is conducted in a solution stirred in a well-defined and controlled manner. In long-duration experiments, either due to distinctive vibrations or thermal differences, there is always convection. Consequently, on longer timescales, well-defined forced convection is a better approach. Rotating disk electrode (RDE) is the most popular and used hydrodynamic method. In this method, a disk electrode is embedded in an insulator and rotates at a fixed rate, dragging the liquid electrolyte around it [44]. In **Fig. 21a** is presented a typical RDE set up, with the working electrode embedded in an insulator and connected with a rotating mechanism. **Fig. 21b** shows the velocity profile and the mass transfer around the RDE.

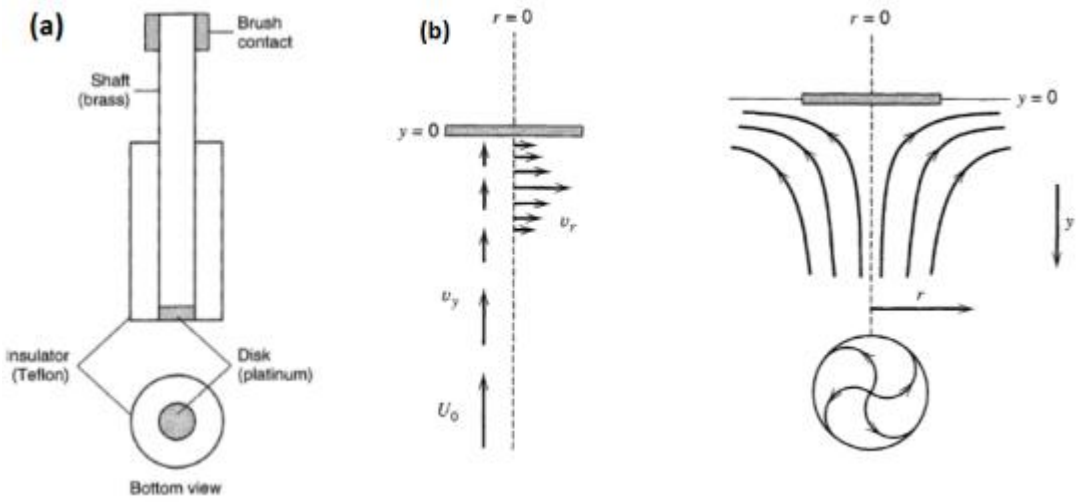

Figure 21: (a) Rotating disk electrode configuration and (b) representation of fluid velocity near the RDE and mass transfer streamlines around the RDE [44].

The steady-state laminar flow conditions are exploited to provide information about the reaction kinetics at the electrode's surface. The rotating disk electrode drags material from the solution towards its surface. When steady-state conditions are established, the solution close to the electrode is considered stationary, because it rotates with the same

angular velocity as the electrode. While the solution away from the electrode is well-stirred. The movement of material from the bulk solution to the electrode surface is described by convection and diffusion concepts. First, the reactant enters the stationary area due to the convection. Then, when the material is inside the stagnant area, the movement is dominated by diffusion as the convection has a negligible impact. In order, the molecule, to reach the electrode's surface it needs to diffuse through a very thin layer, known as the diffusion layer. The thickness of this layer is calculated as follows,

$$\delta_d = 1.61 \cdot D_F^{1/3} \cdot \nu^{1/6} \cdot \omega^{-1/2} \tag{3.7}$$

where D_F is the diffusion coefficient, v is the viscosity of the liquid electrolyte and ω is the angular velocity of the disk electrode. Diffusion layer thickness is inversely proportional to the angular velocity, thus when the angular velocity increases the thickness decreases. However, in experiments, the angular velocity should remain relatively low to maintain a laminar flow for the solution and the RDE theory continues to apply. Generally, its values range from 100 to 1000rpm.

A Levich study is a linear sweep voltammetry technique where an initial low potential is applied to the working electrode without triggering electrochemical reactions and it gradually increases. When the applied potential is high enough and steady-state conditions have been established, the concentration of the reactant at the electrode's surface is decreasing. When there is no reactant close to the electrode's surface, the rate of the reaction depends on the diffusion rate of the reactant through the diffusion layer. Under these conditions, the current response is limited by the diffusion rate of the species and is calculated by Levich's equation,

$$i_L = 0.62 \cdot n \cdot F \cdot D^{2/3} \cdot A \cdot \nu^{-1/6} \cdot \omega^{1/2} \cdot C \tag{3.8}$$

where i_L is the limiting current, n is the number of electrons transferred, F is the Faraday constant and C is the concentration of the reactant. In a Levich study, different voltammograms are acquired over different angular velocities. Current responses measured during the experiments are plotted against the square root of angular velocity. As observed

in equation (3.5), limiting current is proportional to the square root of angular velocity, so perfect squares of angular velocity are usually imposed on the electrode [22].

3.2 Physicochemical techniques

Electrochemical techniques help researchers to understand various processes that take place during operation. To further optimize efficiency and overcome problems, researchers need to understand the physical and chemical composition of the material's surface. The surface is where the interaction with the outer environment takes place. Physicochemical techniques are non-destructive methods able to provide the abovementioned information [37].

3.2.1 Scanning electron microscopy (SEM)

Scanning electron microscopy is a common and simple technique employed for identifying the microstructure's morphology and chemical composition. The images of the surface, from scanning electron microscopy, are produced by hitting the sample with a focused beam of electrons. The generated signals from these interactions give data about the surface structure and composition. The basic composition and principle of operation is simple and is presented in **Fig. 22**. At first, the electrons are generated by the electron source. Then, they are accelerated by the positively charged anode, and with the help of electromagnetic lenses (condenser and objective lenses), are focused on the sample.

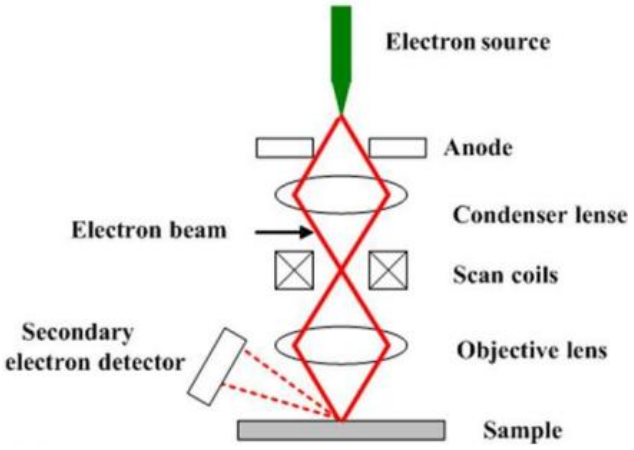

Figure 22: Schematic diagram and basic components of SEM [45].

There is a need, for the entire system, to be under vacuum. It needs to be protected from contamination, vibrations, noises and other atoms. External disturbances affect the electron beam and as a result, the image quality deteriorates. After the impact, many electrons, photons and irradiations are generated. For SEM images, only backscattered and secondary electrons are used. The detection of backscattered is accomplished with solid-state detectors located above the sample. On the other hand, the detection of secondary electrons is mainly accomplished with the Everhart-Thornley detector. Some SEMs achieve resolution close to 1nm [46].

3.2.2 Transmission electron spectroscopy (TEM)

A similar method to SEM is the transmission electron microscopy, abbreviated as (TEM). The transmission electron microscope configuration is similar to that of the scanning electron microscope. It consists of three main parts. The electron gun and the image-producing and recording systems. The electron gun produces the electron beam, and with the aid of the condenser lenses, the electron beam is focused on the sample. The image-producing systems refocus the electrons that pass through the specimen to produce a high-quality image. The image-recording systems transform the image in order to be perceptible from humans. During the operation of the TEM, a high-energy (some keV or even 1MeV) electron beam is transmitted through the sample. The targeted sample is usually a thin layer, even less than 100 nm. As the beam penetrates the sample, a 2D image is formed depending on the interactions between electrons and the sample's material. Usually, the material employed for the image-recording is a fluorescent screen.

Even though SEM and TEM are similar methods, there are some major differences. The image produced in TEM is based on the electrons that pass through the specimen while in SEM the image is produced from scattered electrons. TEM provides information about the internal components, while SEM is used only for surface analysis. Furthermore, images in SEM are three-dimensional in contrast to the two-dimensional images generated from TEM. Last, the images from TEM, usually, have higher resolution compared to SEM's images [40].

3.2.3 X-ray photoelectron spectroscopy (XPS)

X-ray photoelectron spectroscopy is a method used to determine the chemistry of the sample's surface. XPS provides information about chemical surface of the sample. It is an analytical technique mainly based on the photoelectric effect. The photoelectric effect is the emission of electrons when electromagnetic radiation, such as light, interacts with a material. This phenomenon was described in detail by Albert Einstein in 1905. XPS belongs to the family of photoemission spectroscopies in which electrons are generated by irradiating a material with the help of X-rays. Sample properties are obtained from the measurement of the number and the kinetic energy of the generated electrons, with the help of a detector, **Fig. 23.**

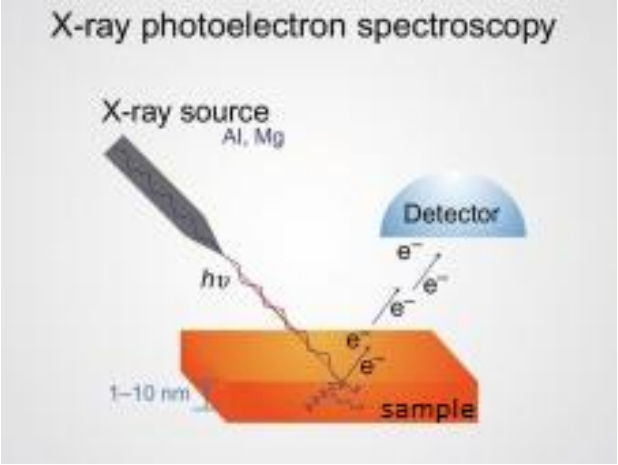

Figure 23: X-ray photoelectron spectroscopy [47].

Material properties are calculated from the measurement of the kinetic energy and the number of the generated electrons. XPS also needs high vacuum conditions. The popularity of XPS stems from its ability to identify all elements except H_2(hydrogen) and He(hellion) in the outer surface of the solid sample and the ability to reveal the chemical environment where the element exists [47].

3.2.4 Raman spectroscopy (RS)

Raman spectroscopy is a scattering technique that provides information about the chemical structure of a sample. It is based on the interaction of photons from a high-intensity light source with the surface of the analyzed material. When the light beam is focused on the

surface, most of the reflected light is at the same wavelength as before, but a small percentage is reflected at different wavelengths. This shift in photon's energy is related to the chemical composition of the surface, thus it provides useful information about it [48].

Chapter IV

Electrochemical gas sensors

Abstract

In chapter IV, an analytical description of the configuration, materials, components and the principle of operation of gas sensors is conducted. The importance of the abovementioned characteristics is described. Also, the different types of gas sensors are reported. The principle of operation and the configuration of potentiometric, amperometric, combined (amperometric-potentiometric), resistor-type and impedancemetric gas sensors is discussed.

4.1 Introduction

Apart from energy storage and production, electrochemical devices have a lot more to offer. Electrochemical sensing technologies are utilized to analyze the composition of various environments in real-time without the need for samples. Electrochemical sensors provide information about the concentration of a wide range of gases through oxidizing and reductive reactions. Electrochemical sensing technologies dominate over other technologies as they provide information in real-time with considerably good selectivity, accuracy, simple design and low cost. Ideally, the response from the electrochemical sensor is directly related to the quantity of a specific chemical species [49].

4.2 History

Coal miners during the 19th century used the first gas detection methods for harmful gases. They moved a torch across the mine, and if there were combustible gases such as methane, the torch would ignite. Another method involved canaries. Workers would bring birds into the tunnel with them and as long as the bird was alive and vivid they knew the atmosphere was safe, otherwise, the mine had to be evacuated. Such methods couldn't provide any information about the type of gas or its concentration and had many flaws resulting in many accidents.

After many years and a lot of research, electrochemical sensors have dominated over other sensing technologies. First electrochemical sensors were mainly used for the detection of oxygen and date back to 1950. Later, in 1980, the first effective electrochemical sensors for a wide range of toxic gases were ready for commercial use. Now, they are employed nearly everywhere from factories and vehicles for better combustion efficiency and monitoring of exhaust gases to medical applications for monitoring biological processes and control of metabolism. Depending on the electrolyte and electrodes, electrochemical sensors can operate in many environments and withstand temperatures from −30 up to 1600°C [50].

4.3 Composition and principle of operation

An electrochemical gas sensor generally consists of the working or sensing electrode, the counter electrode and an electrolyte separating them, all of which are contained within a housing with a gas-permeable membrane. When needed, there is a third electrode, known as the reference electrode. This configuration is presented in **Fig. 24.**

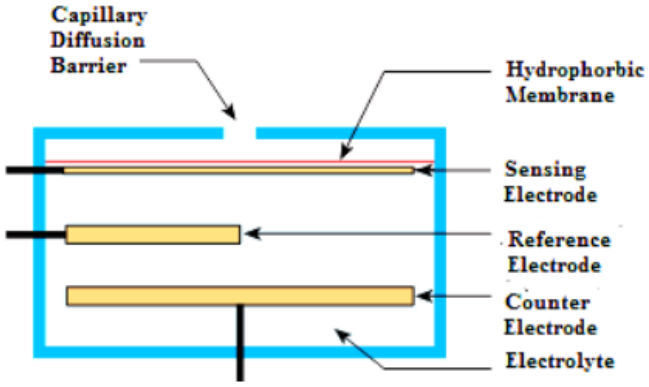

Figure 24: Basic structure of an electrochemical sensor [51].

The housing membrane allows gas, but not liquid or dust molecules, to pass into the sensor. When the gas of interest reaches the sensing electrode, either a reduction or oxidation reaction occurs depending on the reactant. These reactions are catalyzed by the coating material that is specifically chosen for the targeted gas. An oxidation reaction generates electrons that move from the working to the counter electrode, while a reduction reaction causes electrons to move the other way round, from counter to sensing electrode. With an external circuit connected across the electrodes, an electrical current proportional to the gas concentration flows between the working and counter electrodes, thus electrochemical gas sensors are often referred to as amperometric/potentiometric gas sensors or micro fuel cells. From this current, information about the gas concentration is obtained. Some sensors use external electrical energy to force certain reaction at the working electrode. These sensors require a stable and constant potential at the sensing electrode. Due to the electrochemical reaction, the potential at the sensing electrode is disturbed, resulting in a deterioration of the sensor's performance. To eliminate this problem, a reference electrode is placed within the electrolyte, as close as possible to the sensing electrode in order to maintain the value of the applied potential [50].

4.4 Importance of major components individually

- **Gas permeable membrane or hydrophobic membrane**

Its role is to protect the working electrode and in some cases to control the amount of gas that passes into the sensor. These barriers are either low porosity or high porosity Teflon membranes and the sensors are called membrane clad sensors. There are also sensors with a capillary that controls the amount of gas that reaches the electrode's surface, referred to as capillary type sensors. The pore size and the capillary have to be carefully selected in order to allow the proper amount of gas molecules. Sometimes a filter is installed to block unwanted gases. Activated charcoal is the most effective filter as it efficiently filters out many species, except hydrogen and carbon monoxide. By properly selecting the filter, the sensor's efficiency and selectivity are increased.

- **Electrolyte**

The role of the electrolyte is to provide a pathway for the generated ions to move across the electrodes efficiently. Depending on the application, the electrolyte is specifically synthesized to exhibit conductivity for a unique ion. Common electrolytes are oxide-ion and proton-conductors. Also, electrolytes need to present zero electronic conductivity and to be compatible with the materials used in the sensor. Electrolytes must be dense and have excellent tightness to properly separate the gases at each side. Last, they must exhibit excellent thermodynamic and chemical stability for a long period of time.

- **Electrodes**

The reactions take place at the surface of the electrodes. In order to accelerate the reaction and improve the selectivity, the selection of the electrode's material is important. Typically, the electrodes are coated with a noble metal, such as platinum, that is used as a catalyst for the redox reactions. Also, electrodes have porous surface to provide more surface for the interaction of the catalyst with the gas. The selection of the materials takes into consideration the design of the sensor, the targeted gas and the desired life span [50].

4.5 Types of electrochemical sensors

Based on their principle of operation and the employed electrolyte, electrochemical sensors are classified as potentiometric, amperometric, resistor-type and impedance-based sensors [52].

4.5.1 Equilibrium potentiometric gas sensors

During the operation of a potentiometric sensor, an equilibrium potential is established at the interface between the electrolyte and the sensing electrode. This potential depends on the concentration of the gas of interest. Also, with the help of a reference electrode, a standard and known potential is established. The sensing electrode's potential is measured by this standard potential. Electrodes are coated with a catalyst, usually a noble metal like platinum, to increase reaction speed and thus to improve the sensor's performance [20]. Typically, potentiometric sensors are made of two electrodes, the sensing or working and the reference electrode, on each side of the electrolyte. However, Type-III potentiometric sensors use an auxiliary phase as a sensing electrode [52].

The principle of operation of potentiometric sensors is based on open-circuit voltage (OCV) measurements where no electrical current flows through the sensor. The sensor operates as a concentration cell with different chemical potentials of ionic species on each side. The open-circuit voltage can be calculated by equation (4.1),

$$E = -\int_{\mu_2}^{\mu_1} \frac{t}{n \cdot F} d\mu_i \tag{4.1}$$

where μ_i is the chemical potential, t_i is the ionic transport number, F is Faraday's constant and n is the number of electrons. Chemical potential can be calculated by equation (4.2),

$$\mu_i = \mu_i^o + R \cdot T \cdot \ln\left(p_i\right) \tag{4.2}$$

By combining equation (4.1) and (4.2) and integrating, equation (4.3) is obtained,

$$E = -t_i \frac{R \cdot T}{n \cdot F} \ln\left(\frac{p_2}{p_1}\right) \tag{4.3}$$

where R is the ideal gas constant, T is the absolute temperature and p_2, p_1 are the partial pressures of the gases on each side of the sensor. If operating conditions, characteristics of reference atmosphere and experimental OCV are known the composition of the targeted atmosphere can be analyzed. Most equilibrium potentiometric sensors follow this principle [50]. For example, for an oxygen sensor with an oxygen ion conductor, equation (4.3) is,

$$E = -t_o \frac{R \cdot T}{4 \cdot F} \ln\left(\frac{p^{sensing}O_2}{p^{reference}O_2}\right) \tag{4.4}$$

where t_o is equal to unity, as already discussed in chapter II, for solid oxide electrolytes with no electronic conductivity, n is equal to 4 and p_{O2} is the partial pressure. A well-known potentiometric oxygen sensor with a solid oxide electrolyte (YSZ) is the lambda sensor usually employed for the detection of oxygen in exhaust gases **Fig. 25** [53].

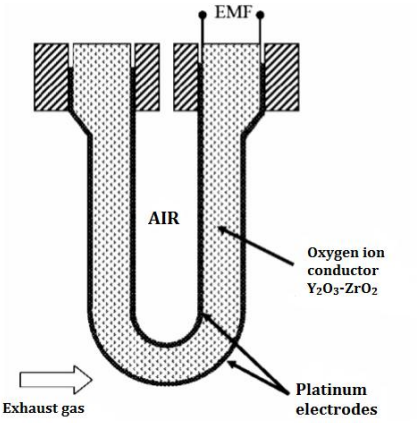

Figure 25: A typical potentiometric sensor for the detection of oxygen in exhaust gases [54].

Based on the mobile ions within the electrolyte and the working principle, potentiometric gas sensors are categorized in Type-I, Type-II and Type-III [52].

- When the transferred ions inside the electrolyte are related to the reactant gas, the sensor is classified as Type-I. A popular Type-I potentiometric sensor is the lambda sensor that is utilized for the analysis of oxygen in the exhaust gases of vehicles. Lambda sensors are composed of Yttria-stabilized Zirconia (YSZ) solid electrolyte (conductor of oxygen anions) between two Pt coated electrodes and air as the reference gas. **Fig. 26a** presents the principle of operation of a typical Type-I potentiometric sensor. This sensor can be described as an electrochemical cell with different partial pressures on each side of the solid oxide electrolyte. The partial pressure at the reference side is kept constant. During the sensor's operation, oxygen gas reduces on one side and oxidizes at the other side [52].

Reduction: $$O_2 + 4e^- \rightarrow 2O^{2-} \quad (4.5)$$

Oxidation: $$2O^{2-} \rightarrow O_2 + 4e^- \quad (4.6)$$

The partial pressure on each side indicates which reaction will take place on that side. The measured *EMF* of the potentiometric sensor determines the partial pressure at the sensing side.

- The principle of operation and configuration of Type-II potentiometric sensors is similar to Type-I. However, in this type, the gas doesn't equilibrate with mobile ions in the electrolyte but it equilibrates with, non-related to it, immobile ions in the electrolyte. CO_2 sensors, for example, function as Type-II sensors where the concentration of CO_2 is determined by equilibrating with K^+ ions in the K_2CO_3 electrolyte. **Fig. 26b** shows the principle of operation

of a carbon dioxide sensor. Here, the carbon dioxide concentration is determined with the help of a K^+ ion conductor [52]. The overall reaction that take place here is,

Overall reaction: $$2K^+ + CO_2 + \frac{1}{2}O_2 + 2e^- \rightarrow K_2CO_3 \quad (4.7)$$

The equation (4.8) for this sensor is modified to,

$$E = \frac{R \cdot T}{n \cdot F} \ln\left(\frac{\left(P_{CO_2}^{sensing} \cdot (P_{O_2}^{sensing})^{1/2} \right)}{\left(P_{CO_2}^{reference} \cdot (P_{O_2}^{reference})^{1/2} \right)} \right) \quad (4.8)$$

Equation (4.8) is simplified to equation (4.9) because the partial pressure of oxygen is kept equal to both sides.

$$E = \frac{R \cdot T}{n \cdot F} \ln\left(\frac{\left(P_{CO_2}^{sensing} \right)}{\left(P_{CO_2}^{reference} \right)} \right) \quad (4.9)$$

Concluding, if the partial pressure of CO_2 at the reference side is known the partial pressure at the sensing side can be determined.

- Lastly, Type-III sensors function differently. In this Type, an auxiliary phase is attached to the electrolyte and functions as the sensing electrode. This auxiliary phase contains the same ionic species as the gas of interest. Thus, the auxiliary phase provides an equilibrium reaction between the gas of interest and the mobile ions in the electrolyte, resulting in a measured *EMF* related to the concentration of the target gas. **Fig. 26c** presents a type-III potentiometric CO_2 sensor with Au electrodes separated by NASICON (Na^+ conductor) electrolyte and Na_2CO_2 auxiliary phase. Type-III sensors are considered more effective for SO_x and NO_x emissions [52, 55].

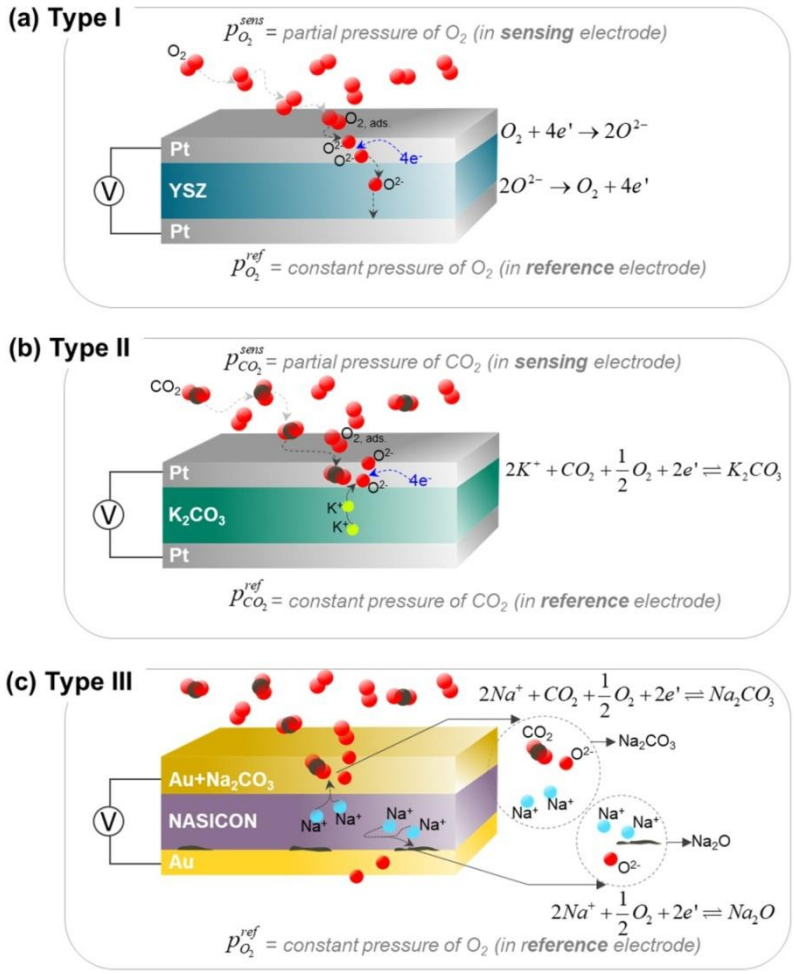

Figure 26: (a) Type-I potentiometric oxygen (O_2) sensor, (b) Type-II carbon dioxide (CO_2) potentiometric sensor, (c) Type-III carbon dioxide (CO_2) potentiometric sensor [56].

Besides the fact that potentiometric sensors are effective tools for gas detection, there are several weak points that limit their usage. Firstly, potentiometric sensors require the supply of a reference gas to operate properly. In industrial conditions, the stable and continuous supply of a reference gas might be problematic. Also, due to the logarithmic dependence of the sensor's *EMF*, most potentiometric sensors provide low sensitivity in atmospheres with high concentrations [57].

4.5.2 Non-equilibrium potentiometric gas sensors

Mixed sensors' design and principle of operation is similar to that of potentiometric gas sensors. In an equilibrium potentiometric sensor, oxidation and reduction reactions occur between the electrodes and the gas until a steady potential is established. However, in non-equilibrium sensors, the targeted gas participates in more than one reactions. As a result, no

equilibrium is established in the interface between the electrode and the electrolyte, and a mixed potential is observed. This behavior is known as non-Nernstian. As in equilibrium sensors, this mixed potential provides information about the gas of interest. These sensors are employed for the detection of H_2, CO, hydrocarbons or NO_x in non-equilibrium gas mixtures [50, 55].

4.5.3 Amperometric gas sensors

Potentiometric gas sensors' operation is based on open-circuit conditions where no external voltage is applied. However, for the operation of amperometric sensors, an external voltage is required. This applied voltage drives certain reactions at the electrodes. Amperometric sensors are designed such that the gas supply at the sensing electrode is limited by diffusion, resulting in a linear output proportional to the targeted gas's concentration. Amperometric sensors have an inner cavity and inside this cavity is the sensing electrode. In order for the gas to reach the anode, it must diffuse through the diffusion or capillary barrier [52]. **Fig. 27** shows a typical amperometric sensor.

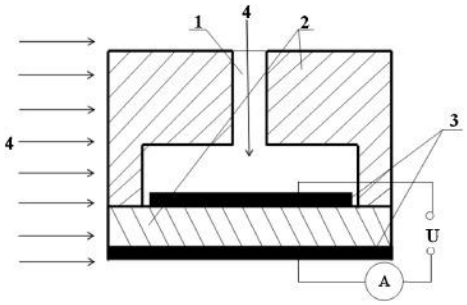

Figure 27: Principle of operation of an amperometric sensor: (1) the diffusion barrier, (2) the solid electrolyte, (3) sensing and counter electrode, (4) surrounding gas [58].

When the sensor is placed in the tested atmosphere, the empty cavity fills with the gas. Then, an external voltage is applied to the working electrode and the oxidation of the targeted gas at the anode's surface begins. This way, a balance is established between the amount of gas pumped out from the cavity and the ambient gas that diffuses through the diffusion barrier. According to Faraday's law, the electrical current generated relates to gas diffusion as follows,

$$J(gas) = \frac{I}{n \cdot F} \tag{4.10}$$

where I is the observed current, F is Faraday's constant and n is the number of electrons involved in the reaction. As the applied voltage increases, so does the reaction rate until a certain value, where the concentration of the targeted gas inside the sensor is negligible. At this point, the applied voltage is so high that when the molecules reach the electrode's surface, they immediately react, so diffusion through the capillary barrier is the rate-limiting step. The reactant's concentration inside the sensor is negligible because the reaction rate is higher than the diffusion rate. Under this condition, a further increase in the applied voltage doesn't affect the current response. This condition is referred to as limiting current [58]. Limiting current is measured from equation (4.11),

$$I_{\lim} = -\frac{n \cdot F \cdot D_{(gas)} \cdot A \cdot P}{R \cdot T \cdot L} p_{(gas)} \tag{4.11}$$

where I_{lim} is the limiting current. D_{gas} is the diffusion coefficient, A is the area of the diffusion barrier and L the length of the diffusion barrier. P, R, T are the absolute pressure, ideal gas constant and absolute operating temperature, respectively and p_{gas} is the partial pressure of the targeted gas. Note that the diffusion coefficient depends on operating conditions according to the equation (4.12),

$$D = D_0 \left(\frac{T}{T_0} \right)^m \frac{P_0}{P} \tag{4.12}$$

where D_0, T_0, P_0 are the diffusion coefficient, temperature and pressure at standard conditions (25°C and 1 atm) while P and T are the pressure and temperature at operating conditions and m is a coefficient that ranges from 1.5 to 1.9 [58].

The linear relationship between the gas's concentration and the current response makes amperometric sensors a more suitable tool for detecting high gas concentration in contrast to potentiometric sensors. With many different employed materials and geometries, amperometric sensors are capable of identifying many different gases, such as O_2, H_2, CO, NO_x, SO_x, H_2S [52]. Amperometric sensors also present several weaknesses during their operation. In amperometric sensors, the limiting current depends on the diffusion barrier. Particles from the analyzed atmosphere can block the diffusion barrier and change its characteristics, resulting in wrong limiting current measurements. Furthermore, if

additional gas reaches the electrode's surface from cracks in the sealant or the electrolyte, there will be an increase in the limiting current [57].

4.5.4 Combined gas sensors (Amperometric-Potentiometric)

Combined sensors consist of two electrochemical cells. The first one, the amperometric cell, works as an electrochemical pump, transferring ions in or out of the sensor's chamber, while the second one, the potentiometric cell, measures the *EMF*. The joints between the potentiometric/amperometric cells or the cells and the capillary barrier are sealed with high-temperature glass sealant. The principle of operation of these devices is more complex than a single potentiometric or amperometric cell. During their operation, one cell operates as an amperometric sensor, pumping gas in or out of the sensor's chamber and measuring the limiting current. While, the second cell operates as a potentiometric cell, measuring the *EMF* and giving information about the analyzed gas concentration or the proper operation of the amperometric cell.

One of the problems of potentiometric oxygen sensors is the stable and continuous supply of reference gas. The first combined oxygen sensor was designed by Haaland to eliminate the need for a reference atmosphere [59]. In this sensor, the amperometric cell operates as an oxygen pump. Depending on the applied voltage, the oxygen is electrochemically pumped in or out of the chamber. At first, the voltage is applied such that the oxygen inside the chamber is electrochemically pumped out. When there is no oxygen, the pumping is reversed in order to create inside the sensor the same oxygen's partial pressure as outside. Under these conditions, the observed *EMF* tends to zero. The measurements of the oxygen's partial pressure in the analyzed gas is accomplished with the aid of the ideal gas law and Faraday's law [50].

Another use of the double cell configuration is to control the output of the amperometric sensor and the overall performance of the system. In the combined oxygen sensor in **Fig. 28**, the amperometric cell serves for electrochemically pumping oxygen out of the sensor's chamber while the potentiometric cell measures the concentration of the oxygen inside the chamber and controls the operation of the system according to the calibration curves.

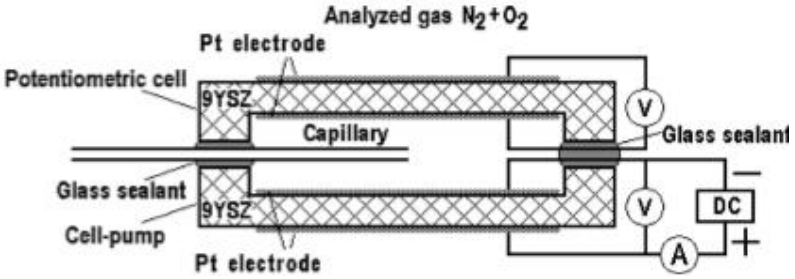

Figure 28: Scheme of operation of a combined oxygen sensor [57].

During the operation, an external potential is applied at the electrochemical pump, driving the oxygen reduction reaction inside the sensor's chamber, generating oxygen ions. These ions move through the electrolyte (YSZ) to the anode, to be oxidized back to oxygen.

Cathode reaction: $$O_2 + 4e^- \rightarrow 2O^{2-} \tag{4.13}$$

Anode reaction: $$2O^{2-} \rightarrow O_2 + 4e^- \tag{4.14}$$

So, the cell pumps oxygen to the outer gas. The measured current is known as limiting current and it is related to the geometry parameters of the capillary and the oxygen concentration in the chamber, as shown in equation (4.15).

$$I_{\lim} = \frac{4 \cdot F \cdot D_{O_2} \cdot P \cdot A}{R \cdot T \cdot L} p_{O_2} \tag{4.15}$$

where 4 is the number of transferred electrons ($O_2 + 4e^- \rightarrow 2O^{2-}$) and p_{O2} is the partial pressure of the oxygen. In the sensor's chamber, the gas mixture contains traces of oxygen. The second cell, the potentiometric cell, measures oxygen concentration inside the chamber using the gas outside of the sensor as a reference atmosphere. The potentiometric cell's *EMF* is calculated by equation (4.16).

$$E = \frac{R \cdot T}{4 \cdot F} \ln\left(\frac{p_{O_2}^{out}}{p_{O_2}^{in}} \right) \tag{4.16}$$

The sensor's ability to measure, simultaneously, the limiting current and the cell's *EMF* increases its reliability and efficiency [50], [57]. From the measurements of the *EMF* and the limiting current, the proper operation of the sensor is verified. For example, when the limiting current is observed, the *EMF* should be equal to the set value, otherwise the sensor

is malfunctioning. Higher *EMF* than the set value indicates that the diameter of the capillary barrier has decreased, while lower indicates the existence of additional leakage [57].

4.5.5 Resistive gas sensors

Resistor-type gas sensors based on metal oxide electrolyte such as SnO_2, TiO_2, In_2O_3, WO_3, NiO are another common type of sensor. These sensors measure changes in electrical resistance of the semiconducting oxide caused by the interactions between the sensing electrode and the gas which generally involve electrons generation and transfer. Due to these surface interactions, an important change in electrical resistance is observed, related to the concentration of chemical species in the gas. Based on these surface phenomena, resistor sensors can be divided into two major types, one that shows changes in the surface conductance and changes in the bulk conductance [56]. As far as for the latter, the main bulk deflects are the oxygen vacancies, so changes in the bulk conductance are due to oxygen's partial pressure at operating temperatures up to 600-1000°C that the oxygen vacancies can quickly diffuse from the interior of the grains to the surface. The main application of this type is to detect oxygen at high temperatures. On the other hand, the second principal type is based only on changes in surface conductivity at lower temperatures <600°C. These sensors are used to detect other reactive gases such as CO, NO_x, SO_x or HCs [52].

However, resistor-type gas sensors show disadvantages that limit the field of applications, such as poor reproducibility and long-time instability. In addition, these sensors aren't linear devices so most of the time more than one sensor or operation mode of the same sensor is required to determine the gas concentration [52].

4.5.6 Impedancemetric gas sensors

Lastly, the impedancemetric gas sensors employ a different approach for detecting the gas of interest. The design of impedance-based sensors is similar to that of mixed-potential sensors. For their operation, a sinusoidal voltage is applied to the sensors and the current response is measured. Knowing the applied voltage and the current response, the impedance is calculated. As already discussed in electrochemical methods, impedance spectroscopy is used to analyze every component individually due to their frequency-based

behavior. Impedance-based techniques are applied to both semiconductor-based sensors and solid oxide-based sensors. There are reports of YSZ-based impedancemetric sensors for detecting steam (H_2O), NO_x and CO [52].

Chapter V

Electrochemical gas sensors based on solid oxide electrolytes

Abstract

In this chapter, the description of different electrochemical sensors based on solid electrolytes for the detection of common gases is presented. The materials, design and principle of operation of the sensors employed for the detection of combustible gases, such as carbon oxides, hydrocarbons and hydrogen are thoroughly discussed. Sensors for the detection of nitrogen oxides and ammonia are also presented. Oxygen and humidity sensors are also described. Different sensors are reported, operating in a wide range of temperature from 300°C to 1000°C, based on different materials for electrolytes and electrodes.

5.1 Introduction

Electrochemical sensors based on solid oxide electrolytes are progressively employed in more and more applications, such as environmental control (combustion, air, industrial wastes monitoring, etc.), chemical processing, laboratory analysis, etc. These sensors, among other gas sensing technologies, seems the most promising technology, offering simple design and operation, high sensitivity, real-time response and scope for miniaturization even in really

harsh environments. Moreover, the output of these sensors is an electrical signal that provides information directly about the measured chemical quantities. These advantages make these sensors an attractive and promising technology to address emission-related problems. Despite the targeted gas or the design, most of the electrochemical sensors have the same principles of operation. These sensors are classified based on their operation into two categories. First, the active sensors, where the sensing signal is the voltage between the two electrodes and no external applied voltage is needed. In this category belong the equilibrium potentiometric (EPSs) and mixed potential sensors (MPSs). Second, the passive sensors where an externally applied voltage is required and the output current is the sensing signal. Here belong the amperometric sensors. In this chapter, the description is limited to solid oxide-based sensors. Among the solid oxides that present ionic conductivity, the oxygen-ion conductors and proton-conductors are emphasized.

Solid-state gas sensors are the most common type for gas detection at high temperatures and harsh environments. Generally, oxygen sensors are the primary tool to optimize combustion processes, however, nitrogen oxides (NO_x), sulfide oxides (SO_x), carbon oxides (CO_x), hydrogen sulfides (H_2S) and hydrocarbons (HCs) sensors are also important for emission control and the combustion monitoring.

5.2 Combustible gas sensors

5.2.1 Electrochemical sensors for the detection of CO_x (CO, CO_2) and C_nH_{2n+2} hydrocarbons

Nowadays, concerns about flammable and toxic gases are increasing. Toxic gases appear in both industrial and domestic environments, causing several life-threatening issues to humans and being harmful to the environment. Solid-state oxygen sensors is a well-known technology for the regulation of internal combustion engines emissions. However, the control of more stringent pollutant emissions requires the development of electrochemical sensors capable of detecting carbon monoxide (CO) and unburned hydrocarbons (HCs). Future emission control strategies and on-board diagnostic (OBD) systems, need sensors to detect such gases in low concentrations, usually a few ppm, at temperatures between 800-1000°C. During internal combustion, CO is generated when carbon in the fuel isn't fully

burned. Its control is important because it is harmful to the environment and humans, and also its concentration provides information about combustion's efficiency. Unburned hydrocarbons appear in rich combustion conditions. For direct OBD strategies, solid-state electrochemical sensors capable of operating at high temperatures and detecting those combustible gases are employed downstream of a three-way catalytic converter (TWC). These sensors are reported to be more effective than dual oxygen sensors [52].

5.2.1.1 Mixed combustible sensors

Usually, solid-state electrochemical gas sensors employed for detecting hydrocarbons and CO, operate under the potentiometric regime. The sensor's signal in these sensors is the electromotive force between the two electrodes. The most popular solid electrolyte is the YSZ, and Pt is the most widely used noble metal for the electrodes. Many reports suggest $Ce_{0.8}Ga_{0.2}O_{1.9}$ (CGO) or β-aluminas as electrolytes. The main requirement that solid electrolytes should fulfill to be suitable for a mixed potential sensor is the reaction kinetics at the three-phase boundary and not the conductivity. These sensors are suitable for a temperature range between 500-600°C as they operate in non-equilibrium conditions. At higher temperatures, the system will approach equilibrium resulting in a decrease in the response signal.

Researches on mixed potential sensors for combustible gases mainly focus on finding new material for the electrodes. WO_3, Nb_2O_5 and Nb_2O_5-Ta_2O_5 are some of the most popular materials for electrodes for CO and HCs electrochemical sensors at operating temperature in the range of 500-700°C. Furthermore, doped-oxides and perovskites have also been investigated as materials for sensing electrodes. Mixed potential sensors suffer from poor selectivity because of their detection mechanism. Also, mixed potential sensors exhibit high cross-sensitivity as both HCs and CO react with oxygen [52].

5.2.1.2 Resistor-type combustible sensors

The most widely used electrochemical sensors for the detection of CO and hydrocarbons at the temperature range of 300-500°C are the resistor-type sensors. These sensors detect the gas of interest through the desorption and the adsorption of the gas species on the metal oxide. During the operation of resistor-type sensors at high temperatures, the targeted

gases react with the lattice oxygen to form oxygen vacancies in the metal oxide. Because of this, it is really difficult for the sensor to exhibit good reproducibility, recoverability and stability in such environments. Considering that, only a few metal oxides can effectively detect reducing gases in high-temperature environments, above 500°C.

Three different mechanisms take place depending on the operating temperature and the carrier mobility of oxides, as shown in **Fig. 29**. First, at low temperatures, direct chemisorption of the reducing gas on the surface of the metal oxide, resulting in the transfer of electrons into the metal oxide. At intermediate temperatures, reactions at the surface lead to oxygen defects at the surface. At temperatures close to 1000°C, the reactions with lattice oxygen change the equilibrium of crystal defects. This mechanism requires high temperatures to gain high defect mobility. Due to the reaction between the gas and the surface or the bulk of the metal oxide, the sensor's response changes. The advantage of these types of sensors is the considerably improved reproducibility compared to mixed potential sensors. One of the materials that exhibited promising results as far as the detection of HCs and CO at high temperatures is Ga_2O_3. Generally, Ga_2O_3 is a common material for resistor-type oxygen sensors that operate at temperatures above 900°C based on the bulk-volume-defect equilibrium (third mechanism).

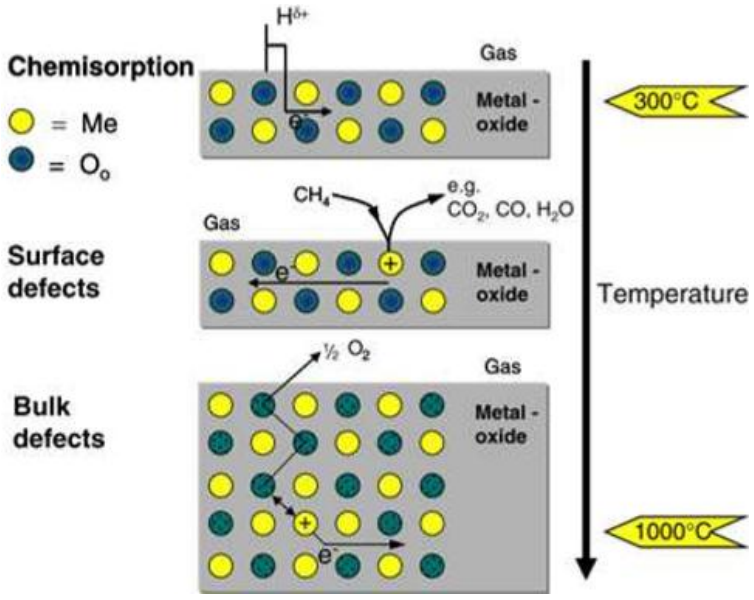

Figure 29: Interaction between the gas phase and the metal oxide for different temperatures [52].

At the operating temperature of resistor-type combustible sensors, the dominant mechanism is the second one (surface defects). However, investigations on the ability of SnO_2 doped Ga_2O_3 and pure Ga_2O_3 to detect CO and HCs at an operating temperature between 600-1000°C showed promising results. The sensors based on those materials exhibited sensitive, stable and recoverable responses for both targeted gases. Similar behavior is observed from TiO_2 with additions of CuO and La_2O_3. Yet, mainly because of the sensing mechanisms, resistor-type sensors suffer from high cross-sensitivity [52].

5.2.1.3 Amperometric combustible sensors

The most common and well-established sensor for the control of exhaust emissions is the lambda sensor. This sensor is based on yttria-stabilized zirconia and operates under the potentiometric regime. It's the most reliable technology among sensing technologies, as it is employed in gasoline-based vehicles for about 40 years now. Considering that, YSZ has been proven to be a suitable material for sensing devices. Among the advantages of YSZ is its great mechanical and chemical stability over a long period of time and its excellent oxygen anion conductivity. Consequently, there is a potential for different YSZ-based sensors for the detection of different gases at high temperatures. Apart from YSZ-based electrochemical potentiometric sensors, amperometric sensors have also been proposed. Amperometric sensors present several advantages, including the operation without the need for a reference gas and the establishment of an equilibrium potential.

Even if amperometric sensors have many advantages over potentiometric sensors, there aren't many reports about the design of amperometric sensors for the detection of combustible gases in harsh environments. Additionally, the detection of combustible gases in mixtures of combustible gas+N_2 is interesting from a practical point of view, because most thermal catalytic analyzers can't effectively detect combustible gases in oxygen-free atmospheres. Recently, an amperometric sensor for the detection of H_2, CO and CH_4 in nitrogen atmospheres was fabricated by E.Gorbova et al. for intermediate temperatures (450°C). The abovementioned sensor consists of two cells based on 9YSZ solid electrolyte ($0.91Zr+0.09Y_2O_3$). The cells are sealed with glass sealant such that an inner chamber is formed between them. This chamber connects through a metal capillary with the

environment. At the opposite sides of one of the cells are deposited Pt electrodes with wire current leads. The sensor's configuration is presented in **Fig. 30**.

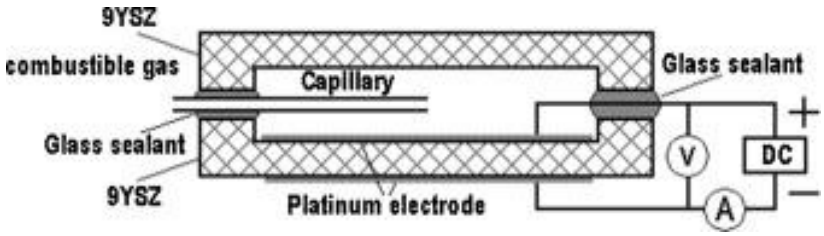

Figure 30: Schematic representation of the amperometric sensor [60].

The principle of operation of amperometric sensors has already been discussed. A positive potential is applied to the electrode inside the sensor forcing certain reactions. Due to the applied voltage, steam and carbon dioxide react at the outer electrode according to the reactions,

$$H_2O + 2e^- \rightarrow H_2 + O^{2-} \quad (5.1)$$

$$CO_2 + 2e^- \rightarrow CO + O^{2-} \quad (5.2)$$

Decomposition of steam is possible because there is some residual humidity (10 ppm) in nitrogen and so at the analyzed gas, while carbon dioxides in mixtures of CH_4 and $CO+N_2$ appear due to the oxidation of CO and CH_4 due to the oxygen in nitrogen. Generated oxygen anions from reactions (5.1) and (5.2) move through YSZ to the inner electrode and react with the H_2, CO and CH_4 at the chamber according to the reactions,

$$H_2 + O^{2-} \rightarrow H_2O + 2e^- \quad (5.3)$$

$$CO + O^{2-} \rightarrow CO_2 + 2e^- \quad (5.4)$$

$$CH_4 + 4O^{2-} \rightarrow CO_2 + 2H_2O + 8e^- \quad (5.5)$$

As the applied voltage increases, the rate of oxygen pumping also increases. Due to the reactions, the concentration of the combustible component inside the chamber decreases and a concentration gradient at the opposite spaces of the capillary is created. The diffusion flux of the combustible gas, through the capillary, reaches its maximum value when its concentration inside the chamber is zero. Under these conditions, the current response is

stable and it isn't affected by the voltage. These conditions corresponds to the limiting current which is calculated for every gas from equation (5.6).

$$I_{k,\lim} = z_k \cdot D_k \cdot X_k \frac{P \cdot F \cdot S}{L \cdot R \cdot T} \tag{5.6}$$

where k represents the gas of interest (k=H_2, CO or CH_4) and X_k is the concentration of the targeted gas. If equation (5.6) is expressed for the diffusion coefficient, the following equation is obtained,

$$D_k = \frac{I_{k,\lim}}{X_k} \frac{L \cdot T \cdot R}{z_k \cdot P \cdot S \cdot F} \tag{5.7}$$

As far as the experimental part, the tests were carried out in different gas mixtures of combustible gas+nitrogen at an operating temperature of 450°C. In **Fig. 31** the relation between the applied voltage and the current response of the sensor is shown. In the three figures, the plateau region is observed when the limiting current is observed. From these curves, information about the tested system is obtained. More specifically, for different gases and different concentrations, the slope at the start varies. At first, the slope provides information about the characteristics of the total internal resistance. While the latter part provides information about the polarization resistance of the electrodes and the Ohmic resistance of the electrolyte.

Fig. 31a shows the ampere vs. volt curves for the mixture of N_2+H_2 for different hydrogen concentrations, starting from 0.5 to 2, 4 and 6 vol.% H_2. All curves reach the plateau region between 0.2 and 0.25 V. From these curves, the sensor's total resistance can be calculated. For example, from **Fig. 31a** for the mixture of N_2+6%H_2 at 450°C the total sensor's resistance is about 4 kΩ. From the total resistance, about 12.5% is the electrolyte's resistance (about 0.5 kΩ) and the rest is the electrode's polarization resistance. **Fig. 31b** depicts the curves for the N_2+CH_4 mixture for different CH_4 concentrations. Similar behavior to the H_2+N_2 mixture is observed with the curves reaching the plateau region between 0.2 and 0.25V and at slightly higher current values. The total sensor's resistance, for the N_2+6%CH_4 mixture, here is about 5 kΩ, close to the value obtained for the N_2+H_2 mixture.

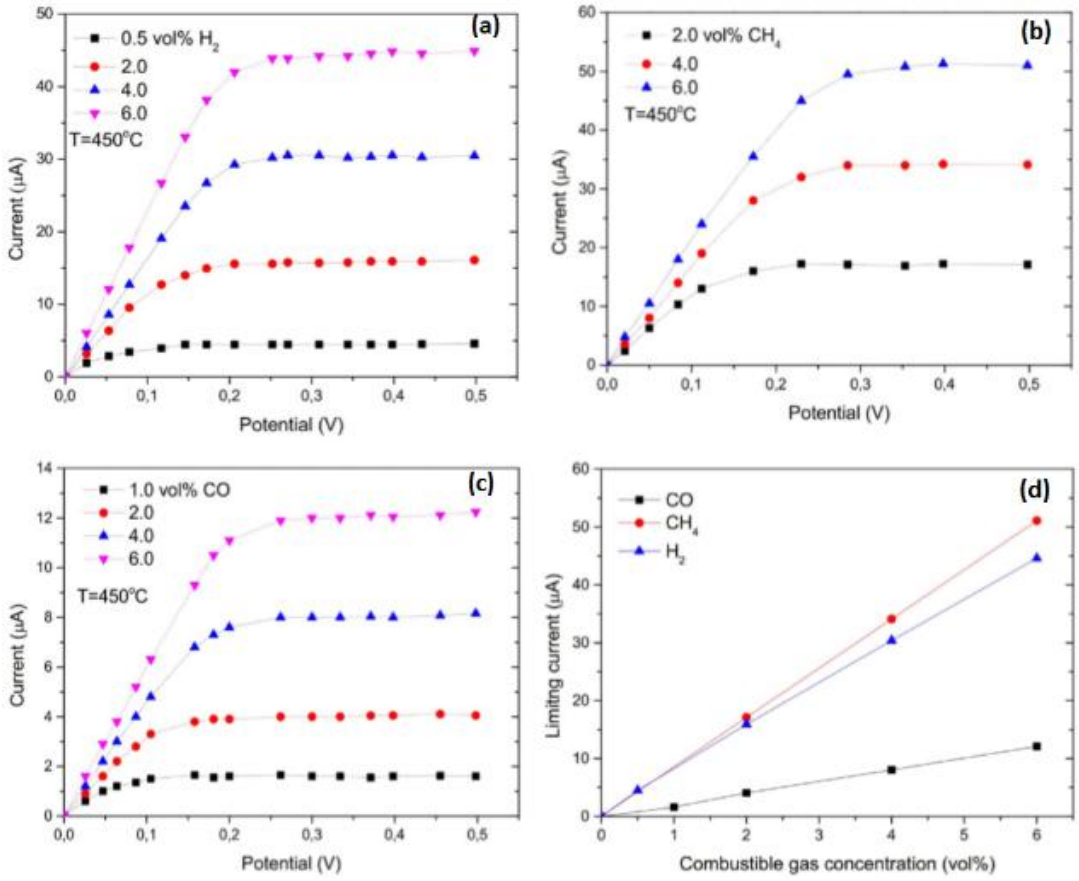

Figure 31: (a) Ampere-volts characteristic curves of the tested sensor at 450°C, (a) for the mixture N_2+H_2 for different H_2 concentrations (0.5, 2, 4, 6 vol.% H_2), (b) for the mixture N_2+CH_4 for different CH_4 concentrations (2, 4, 6 vol.% CH_4) and (c) for the mixture N_2+CO for different CO concentrations (1, 2, 4, 6 vol.% CO). (d) the relation between the limiting current and different concentrations of the three tested combustible gases (H_2, CH_4 and CO) [60].

In **Fig. 31c**, the ampere vs volt curve of the N_2+CO mixture for different CO concentrations is presented. It is observed that the current response is considerably lower than that of the two previous components. As the author suggests, the main reason is the considerably lower diffusion rate of CO in N_2 compared to that of CH_4 and H_2. Furthermore, due to the higher electrode's polarization resistance for the reaction (5.4), the sensor's total resistance is much higher compared to the previously tested gases. For the mixture of N_2+6%CO, the sensor's resistance is about 16 kΩ. In all the tested combustible gas components, the limiting current is linearly proportional to the concentration, so the condition is satisfied. This linear behavior can be seen in **Fig. 31d** [60].

Last, from equation (5.7) and from **Fig. 31d**, the diffusion coefficient for the tested gases is calculated. In equation (5.7) L, S are characteristics of the system, z_k is the number

of electrons of the reaction and F is Faraday's constant. T, P and X_k are parameters given to the system and the $I_{k,lim}$ is obtained from the experiment, so D_k can be measured. The calculated diffusion coefficient for H_2, CH_4 and CO is equal to 3.601, 0.952, 1.053cm^2/s, respectively. The diffusion coefficient values from this experiment are in good agreement with the data from the literature.

5.2.2 Hydrogen (H_2) sensors

Over the years, apart from solid electrolytes that exhibit oxygen-ion conductivity, there have been developed other types of electrolytes that exhibit proton conductivity. These materials have attracted the attention of electrochemical devices researchers as they can operate under a wide range of temperatures, from medium to high, and can be implemented in many electrochemical devices, such as electrolysis cells, fuel cells and sensors. In many industrial fields such as metallurgy, nuclear or thermal power plants and the petrochemical industry, the processes that take place require high temperatures. By measuring the concentration and analyze the emissions, it is possible to reduce the released hazardous gases and also to optimize the combustion. These measurements require sensors capable of withstanding the operating conditions and effectively operating under them. A well-known electrolyte for these sensors is the well-established yttria-stabilized zirconia. YSZ is a stable and effective electrolyte with good ion conductivity at elevated temperatures. Considering that, there are many investigations for sensors based on oxygen-conducting electrolytes for the detection of hydrogen using a mixed potential method. However, such sensors aren't yet suitable for measuring hydrogen. Consequently, for the development of electrochemical hydrogen sensors, researchers report the use of solid oxide proton conductors. There have been reported many proton-conducting solid electrolytes, but materials belonging to the perovskites family are considered the most promising and effective so far. Well-known hydrogen conductors that exhibit both stability and acceptable conduction are electrolytes based on barium cerate ($BaCeO_3$) and strontium cerate ($SrCeO_3$).

5.2.2.1 Amperometric H_2 sensors

Amperometric sensors seem to provide more advantages over potentiometric ones as they can operate without a reference atmosphere. The establishment of a reference

atmosphere, for the proper operation of a hydrogen potentiometric sensor, can be really problematic due to the environment of operation of these sensors. The working temperature is usually above 600°C. Some major advantages of amperometric sensors include the linear dependence of limiting current to the gas concentration and the absence of a reference gas. This way, amperometric sensors are more precise at medium and high concentrations and are considered more reliable. Consequently, amperometric sensors have attracted more attention for the detection of hydrogen.

The most fully investigated materials, as far as their proton-conducting properties, are the oxides based on $BaCeO_3$ and $BaZrO_3$. In addition to those materials, other protonic conductors such as $LaNbO_4$, $Ba_2In_2O_5$ and $LaYO_3$ are used in solid oxide electrochemical hydrogen sensors even if they exhibit lower proton conductivity. Among them, $LaYO_3$ was the first oxide material that Iwahara and Takahashi observed proton-conducting properties. Kalyakin et al. synthesized a Sr-doped $LaYO_3$ proton conductor for its application in hydrogen amperometric sensors. This sensor is composed of two different cells, the first one is based on a solid proton-conducting electrolyte, $La_{0.9}Sr_{0.1}YO_{3-\delta}$, while the other one is based on an oxygen ion-conducting electrolyte, YSZ. Both electrolytes have Pt electrodes on the opposite sides. The two cells form a chamber between them that connects with the ambient gas through a ceramic capillary barrier. **Figs. 32** depicts the scheme of operation principle and the experimental cell of the hydrogen amperometric sensor, respectively.

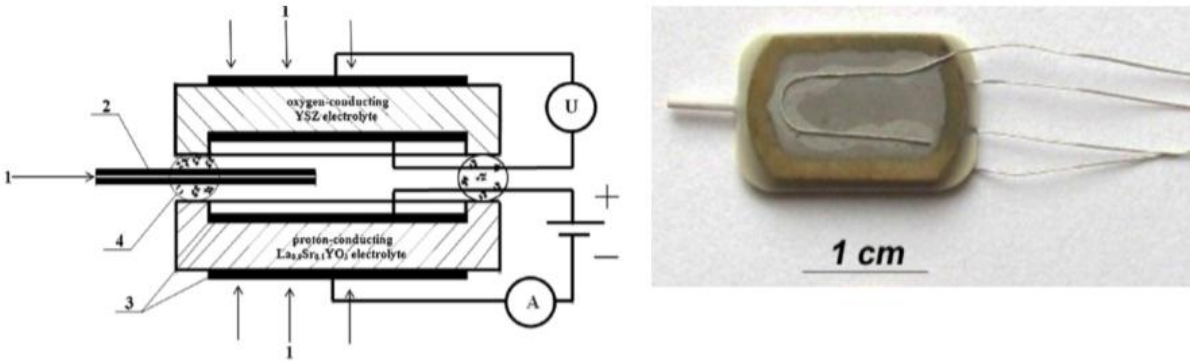

Figure 32: Schematic representation of the hydrogen amperometric sensor (left): (1) the ambient gas, (2) the ceramic capillary, (3) the Pt electrodes and (4) the glass sealants. (right) the experimental cell [61].

For the testing part, the as-fabricated sensor is placed inside an oven and is fed with a fixed mixture of N_2+H_2, to imitate the operating conditions. When the sensor is placed in the N_2+H_2

mixture and the analyzed gas fills the sensor, a DC voltage is applied to the electrodes of the protonic conductor. Consequently, hydrogen molecules are electrochemically pumped-out of the sensor through the $La_{0.9}Sr_{0.1}YO_{3-\delta}$ electrolyte. The hydrogen that is pumped out from the sensor is compensated with hydrogen permeating through the ceramic capillary. However, as the applied voltage increases, the pumping out of the sensor dominates over the diffusion through the capillary, resulting in a decrease in hydrogen's concentration. When the concentration of hydrogen inside the sensor is negligible, a further increase in the voltage doesn't affect the current response. This condition corresponds to the limiting current. From equation (5.8), the limiting current of the sensor for hydrogen is calculated,

$$I_{\lim} = \frac{2 \cdot F \cdot D_{(H_2)} \cdot S \cdot P}{R \cdot T \cdot L} p_{H_2} \tag{5.8}$$

So the purpose of the first cell is to calculate the current response to the applied voltage. The second cell operates as an oxygen gauge. Due to the decomposition of humidity inside the chamber, oxygen is produced in the sensor, according to the reaction (5.9).

$$H_2O \xrightarrow{K} H_2 + \frac{1}{2}O_2 \tag{5.9}$$

The cell with the YSZ electrolyte continuously monitors the content of oxygen inside the sensor, as the hydrogen pumping continues. Oxygen partial pressure is calculated from equation (5.10).

$$p_{O_2} = \left(\frac{K \cdot p_{H_2O}}{p_{H_2}} \right)^2 \tag{5.10}$$

In equation (5.10), K is the equilibrium constant of the reaction, p_{H2O} and p_{H2} are the water and hydrogen partial pressures. Note that due to the electrochemical pumping of the hydrogen, hydrogen's partial pressure inside the sensor decreases during the operation. This change is monitored with the aid of the Nernst equation (5.11) based on the open-circuit voltage of the second electrochemical cell.

$$\Delta V_{OC} = \frac{R \cdot T}{4 \cdot F} \ln \left(\frac{p'_{O_2}}{p''_{O_2}} \right) \tag{5.11}$$

The *I-V* characteristics curves of the tested sensor for different H_2 concentrations in mixtures of N_2+H_2 at different operating temperatures are shown in **Fig. 33a,b**. The current-voltage curves are distinguished in three regions for every H_2 concentrations. At the first region, the current is proportional to the applied voltage until a certain point where the limiting current is observed and a plateau is formed. At this point the current is constant and it isn't affected by the voltage. The current starts to increase again at really high values of the applied voltage. It is important to note that the limiting current value greatly increases as the H_2 content in the mixture increases. Also, in **Fig. 33c**, the linear relation between the limiting current and the H_2 concentration is depicted. This is an important condition for amperometric sensors to be considered suitable for the detection of the targeted gas [61].

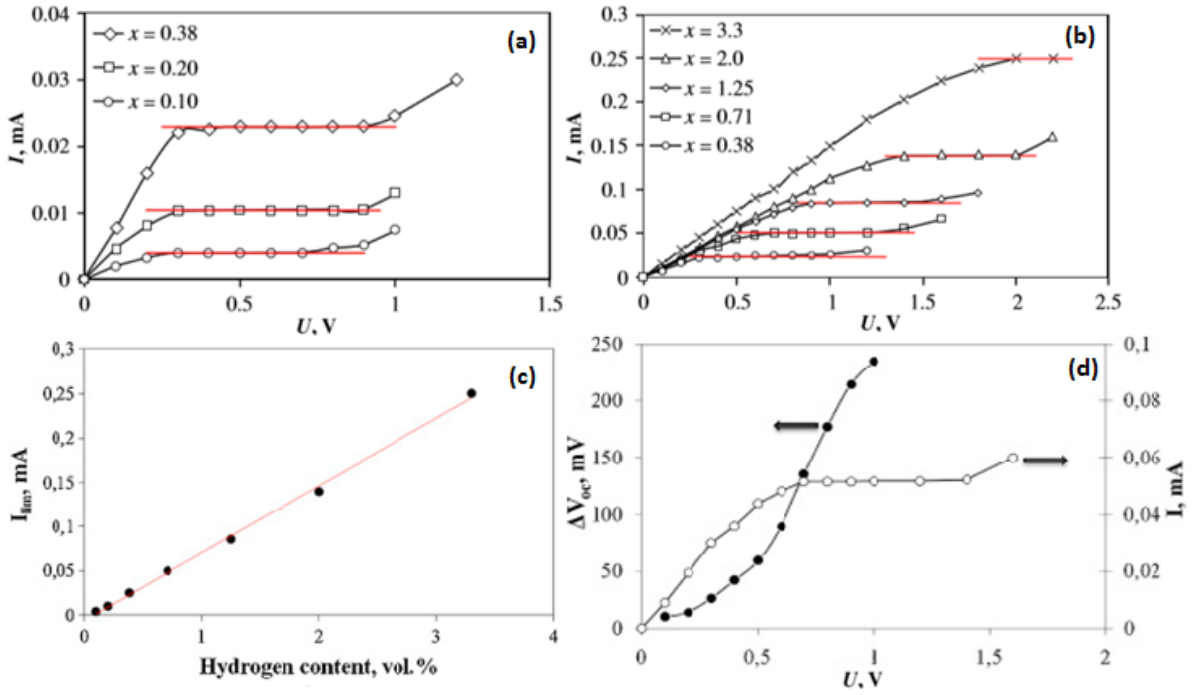

Figure 33: (a, b) Dependence of current on the applied voltage for x vol.% H_2 in N_2+H_2 mixture at 550°C, (c) Dependence of limiting current to hydrogen content and (d) I and ΔV_{oc} plotted against U for the 0.7 vol.% H_2+N_2 mixture at 550°C [61].

Fig. 33d shows the dependence of the limiting current and open circuit electric potential (ΔV_{oc}) on the applied voltage. This diagram is obtained at 550°C for 0.7 vol.% hydrogen in the mixture of H_2+N_2. As it is observed, the limiting current increases with the applied voltage until a certain point, where a plateau is observed. For this concentration, the plateau is observed at 0.7 applied voltage. This current is referred to as limiting current and

it remains constant until voltage's value reaches about 1.5 V. This rise is due to either the partial decomposition of the used materials or the presence of electronic conductivity in the solid electrolyte. At the same time, the ΔV_{oc} value measured with the aid of the YSZ-based cell increases smoothly with the increase of the applied voltage. However, when the concentration of hydrogen inside the sensor tends to zero, there is a sharp increase at the ΔV_{oc} value. As the author suggests, as far as the conditions in **Fig. 33d,** at the limiting current region, the hydrogen's concentration is less than 8 parts per million (ppm).

Hydrogen amperometric sensors were also fabricated based on $La_{0.95}Sr_{0.05}YO_3$, $CaZr_{0.90}Sc_{0.1}O_3$ and $CaTi_{0.95}Sc_{0.05}O_3$ proton-conducting solid electrolytes. These electrolytes were synthesized and tested by Kalyakin et al. for application in amperometric hydrogen sensors. Three hydrogen amperometric sensors were fabricated based on the abovementioned electrolytes and they were tested in a H_2+N_2+H_2O gas atmosphere in an operating temperature of 800°C. Each of the abovementioned electrolytes was employed in one of the fabricated cells.

The configuration of the three cells is similar. Two parts of the solid electrolyte were sealed together with the aid of a glass sealant such that an empty chamber is formed between the two plates. Two Pt electrodes were placed at the opposite sides of one of the plates. The sensor's configuration is presented in **Fig. 34**. In these sensors, the leakage between the sealed parts and through the porous solid electrolyte has the role of the diffusion barrier. For the experimental study of the three sensors, they were placed into a furnace in order to reach the needed temperature, around 800°C. Then the N_2+H_2+H_2O gas mixture was fed to the sensor.

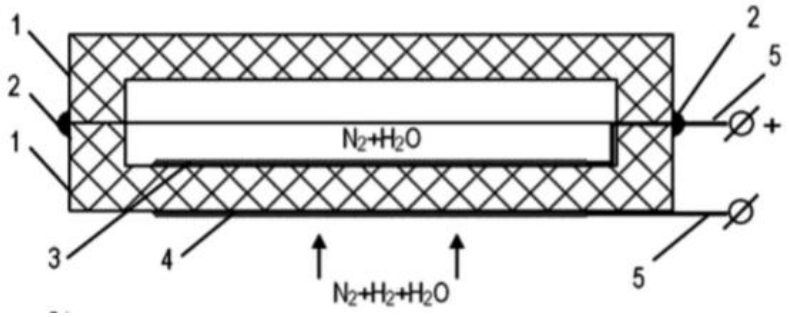

Figure 34: Schematic representation of the amperometric sensor, (1) proton-conducting electrolyte, (2) glass sealant, (3-4) Pt electrodes, (5) platinum lead [62].

When the chamber inside the sensor is filled with N_2+H_2+H_2O, at the beginning of the experiment, a DC voltage is applied to the electrodes to electrochemically pump-out the hydrogen from the chamber. As already discussed, hydrogen's concentration inside the chamber decreases and eventually reaches zero. It is known that at this stage the limiting current is observed.

On the basis of the electrochemical study, the voltage-current curves of the electrochemical cell were obtained. The ohmic resistance of the solid electrolyte and the electrode polarization resistance affect the slope of the *I-V* curve. While the limiting current value depends on the characteristics of the diffusion barrier and the composition of the fed gas.

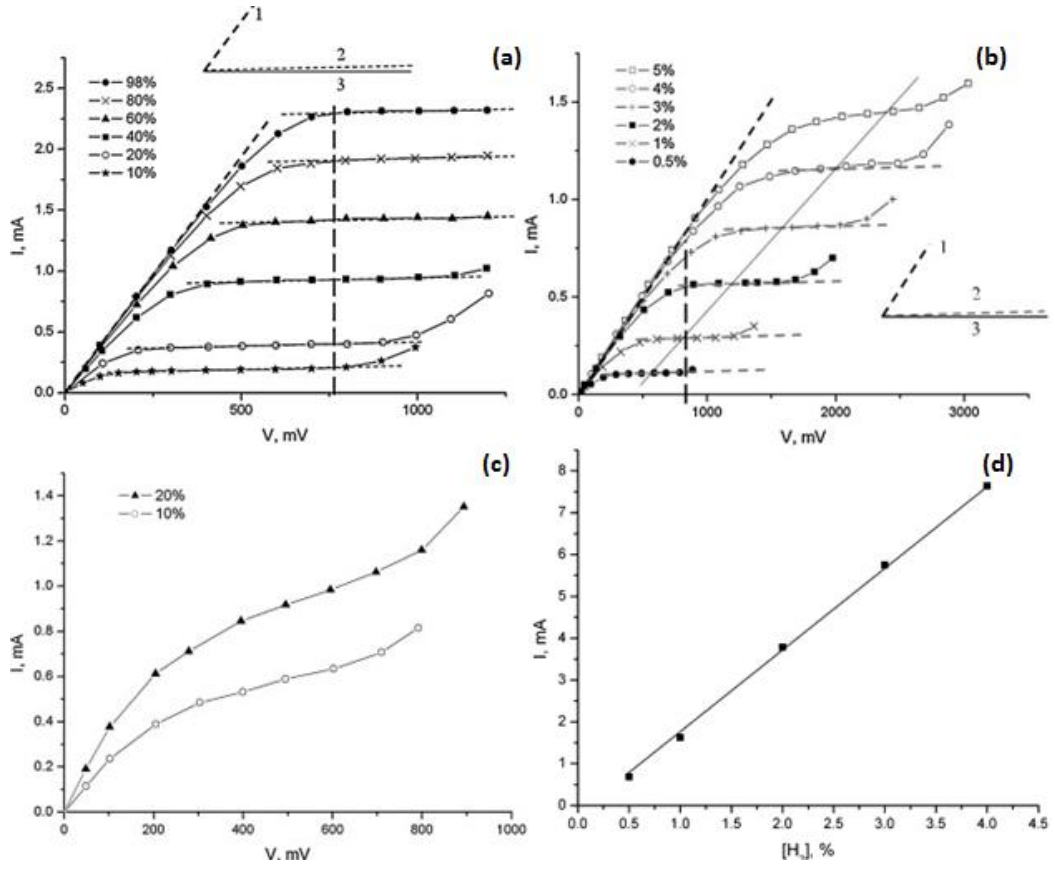

Figure 35: Voltage current curves for (a) $La_{0.95}Sr_{0.05}YO_3$ electrolyte-based cell, (b) $CaZr_{0.90}Sc_{0.1}O_3$ electrolyte-based cell, (c) $CaTi_{0.95}Sc_{0.05}O_3$ electrolyte-based cell, for different H_2 concentrations in mixtures of N_2+2%H_2O+H_2 at operating temperature of 800°C and (d) dependence of limiting current on hydrogen content for cell-1 [62].

The *I-V* curves of the cell 1,2,3 based on $La_{0.95}Sr_{0.05}YO_3$, $CaZr_{0.90}Sc_{0.1}O_3$ and $CaTi_{0.95}Sc_{0.05}O_3$, respectively, is presented in **Fig. 35a,b,c**. In the first sensors, based on $La_{0.95}Sr_{0.05}YO_3$ and $CaZr_{0.90}Sc_{0.1}O_3$ the three regions can be distinguished. Cell-1 was tested in high hydrogen

concentration between 10-98% while cell-2 was tested in significantly lower hydrogen concentrations. However, at cell-3 based on $CaTi_{0.95}Sc_{0.05}O_3$ electrolyte, the current-voltage curves never reach a plateau. As the author suggests, this is attributed to the presence of significant electronic conductivity in the solid electrolyte. Consequently, this electrolyte isn't suitable for hydrogen sensors. As far as the relation between the limiting current and H_2 content, it is observed in **Fig. 35d** for cell-1 that it is strictly linear. Therefore, $La_{0.95}Sr_{0.05}YO_3$ electrolyte can be used for the detection of high hydrogen concentration in mixtures with N_2 at elevated temperatures. From **Fig. 35b** is observed that the dependence of limiting current and H_2 content is also linear. Cell-2 based on $CaZr_{0.90}Sc_{0.1}O_3$, can be implemented for applications in hydrogen sensors for the detection of low H_2 concentration (below 5%) in mixtures of N_2 at elevated temperatures [62].

5.2.2.2 Combined (Amperometric-Potentiometric) H_2 sensors

Apart from devices based on a single cell, more complex devices combining two or more cells have been designed. These devices exhibit increased accuracy and can perform several functions. Usually, one cell is operated under potentiometric regime as a gauge while the other under amperometric regime as an electrochemical pump. Many researchers are showing increasing interest in Zr-substitute $BaCeO_3$-based systems. Materials such as $BaCe_{0.7}Zr_{0.1}Y_{0.2}O_{3-\delta}$ (BZCY) oxide are the main electrolytes for high-temperature gas detection. These materials exhibit great proton conductivity at high temperatures and acceptable stability in the, usually, aggressive environment of operation. $BaCe_{0.7}Zr_{0.1}Y_{0.2}O_{3-\delta}$ (BZCY) was employed in a combined amperometric/potentiometric sensor for detecting hydrogen in mixtures of nitrogen at intermediate temperatures between 450-550°C fabricated by Kalyakin et al. This sensor is made of two $Pt|BaCe_{0.7}Zr_{0.1}Y_{0.2}O_{3-\delta}|Pt$ electrochemical cells with an empty chamber between them. The chamber connects with the environment through a capillary barrier. The joints between the cells and the cell and capillary were sealed with a high-temperature glass sealant. The configuration of the sensor is presented in **Fig. 36**. Cell-1 operates under amperometric regime as an electrochemical pump, while cell-2 operates as a hydrogen potentiometric sensor. Depending on the applied voltage, the sensor operates either in amperometric mode, **Fig. 36b** or potentiometric mode, **Fig. 36a**.

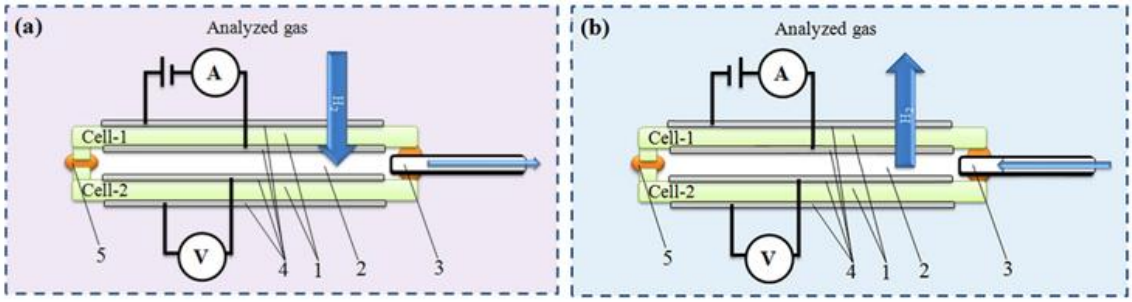

Figure 36: Combined potentiometric (a) amperometric (b) hydrogen sensor, (1) BZCY proton conductor, (2) chamber inside the sensor, (3) capillary barrier, (4) Pt electrodes, (5) glass sealant [63].

During potentiometric mode, a DC voltage is applied to the cell-1 driving hydrogen reaction at the external electrode and generating protons and electrons. Protons move through the proton conductor (BZCY) to the inner electrode and meet with the electrons to form hydrogen molecules again. The electrochemical pumping of hydrogen is described by the following equations,

External electrode: $$H_2 \rightarrow 2H^+ + 2e^- \quad (5.12)$$

Internal electrode: $$2H^+ + 2e^- \rightarrow H_2 \quad (5.13)$$

The two reactions take place at the opposite electrodes of cell-1. Resulting in the pumping of pure hydrogen inside the sensor. Hydrogen gradually replaces nitrogen inside the chamber and a pure hydrogen atmosphere is created. The second electrochemical cell (cell-2) measures the electric potential difference generated between its internal and external electrodes due to the difference in hydrogen concentration. According to Nernst's equation, this potential is described as,

$$E = \frac{R \cdot T}{2 \cdot F} \ln\left(\frac{p'_{H_2}}{p''_{H_2}}\right) \quad (5.14)$$

where p'_{H_2} is the hydrogen partial pressure in the ambient gas and p''_{H_2} is the hydrogen partial pressure inside the sensor. Note that inside the sensor there is a pure hydrogen atmosphere, therefore p''_{H_2} = 1 atm. From the measured *EMF*, hydrogen's concentration in the surrounding gas is calculated. The generated high potential difference at the electrodes enables the tested potentiometric cell to effectively measure low hydrogen concentrations

in N_2+H_2 gas mixtures. Consequently, the potentiometric mode is suitable to detect hydrogen at the operating conditions. **Fig. 37a** presents typical *EMF-V* curves for the cell-2. As the applied voltage at cell-1 increases, the rate of the hydrogen-pumping inside the chamber also increases. As observed, *EMF* grows initially with the applied voltage and then tends to a constant value when ΔU reaches 2-2.5V. The first stage is explained by the partial displacement of nitrogen and steam due to the pumped hydrogen and, as a result, the hydrogen's partial pressure difference growth between the opposite sides. Whereas, at the second stage, there is a pure hydrogen atmosphere inside the sensor, so the pressure difference between the opposite sides has reached its maximum value. The *E-ΔU* curves obtained in this experiment for different hydrogen concentrations are presented in **Fig. 37a**.

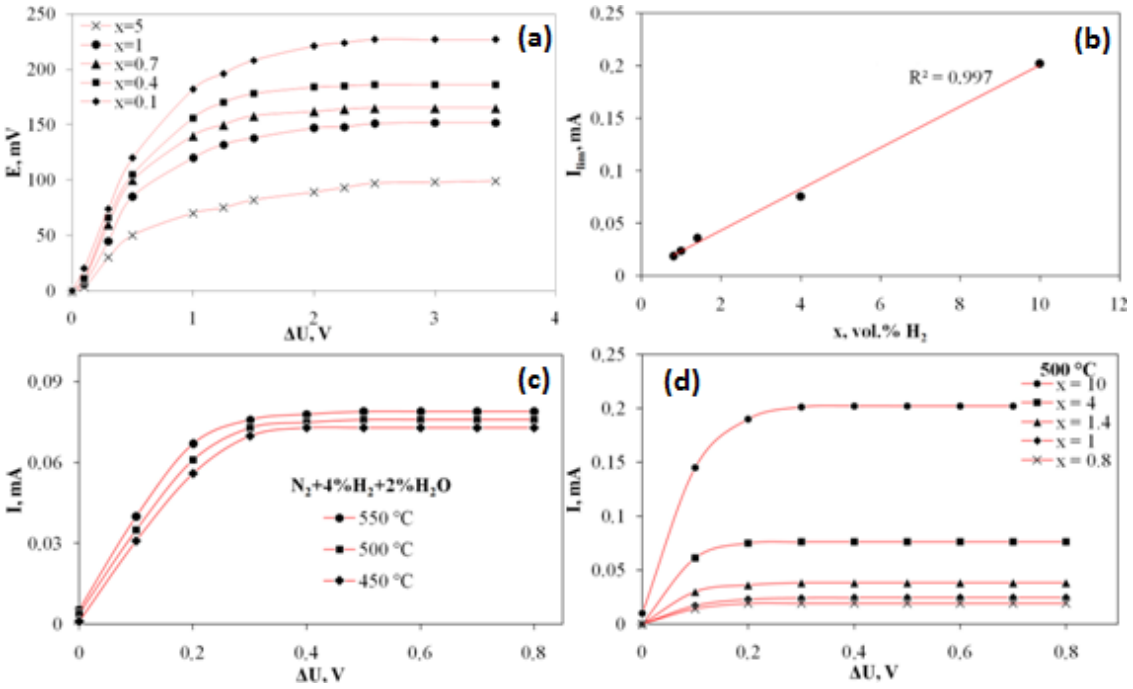

Figure 37: (a) *EMF-V* curves for different hydrogen content in x%H_2+N_2+2%H_2O gas mixtures at 500°C, (b) The limiting current as a function of hydrogen content in N_2+H_2 mixture at 500°C, (c) *I-V* curves for different temperatures of operation and (d) for different H_2 concentrations at 500°C [63].

During the amperometric mode, a DC voltage is applied again between the electrodes of cell-1, **Fig. 37b**. However, this time, the reverse process takes place and hydrogen in the form of protons flow from the chamber to the outside of the sensor. As the hydrogen is pumped out, a concentration gradient is created between the chamber and the environment resulting in a

hydrogen diffusion flux through the capillary. Faraday's law describes the correlation between the diffusion flux and the current response of the sensor.

$$J(H_2) = \frac{I}{2 \cdot F} \tag{5.15}$$

As the applied voltage at cell-1 increases, so does the rate of hydrogen pumped-out of the sensor. At a certain applied voltage, the concentration of hydrogen inside the sensor is close to zero. This condition is known as the limiting current. The limiting current for a hydrogen sensor with a solid protonic conductor is calculated through equation (5.16).

$$I_{\lim} = \frac{2 \cdot F \cdot D_{(H_2)} \cdot S \cdot P}{R \cdot T \cdot L} p_{H_2} \tag{5.16}$$

Fig. 37c displays the *I-V* curves for the mixture of N_2+2%H_2O+4%H_2 for different temperatures. As it is observed, the highest limiting current is observed at the highest temperature of operation. **Fig. 37d** shows the *I-V* curves for different H_2 content at an operating temperature of 500°C. The plateau region is observed between 0.2 and 0.3 applied voltage. The ability of this sensor to operate in either potentiometric or amperometric mode enables the sensor to effectively detect hydrogen in either low or high hydrogen concentrations in mixtures of N_2+H_2O+H_2. The dependence of the limiting current to the hydrogen concentration is presented in **Fig. 37b**. From the analysis, a linear behavior between limiting current and H_2 content is obtained. Concluding, apart from the potentiometric mode, this sensor is suitable for the detection of hydrogen when operating at the amperometric mode [63].

5.2.3 Sulfur dioxide (SO_2) and carbon dioxide (CO_2) sensors

Other gases that need to be monitored for the optimization of energy production processes and due to limitations regarding the greenhouse gases are sulfur dioxide (SO_2) and carbon dioxide (CO_2). CO_2 is one of the main pollutants of every combustion process, while SO_2 is emitted when low-grade sulfur-containing coal is burned. To monitor these gases in real-time, there is a need for a sensor able to operate at high temperatures. Even if electrochemical high-temperature sensors for the detection of such pollutants have been reported, there are still challenges that limit their application in industrial processes. Consequently, usually in industrial fields, the analysis of a

sample at lower temperatures is preferred. Similar to every solid-state electrochemical sensor the main challenge is to find suitable materials for the electrolyte and electrodes that optimize the operation of the sensor.

5.2.3.1 Carbon dioxide (CO_2) sensors

Carbon dioxide sensors operate as Type-II or Type-III potentiometric sensors. Usually, a carbonate electrolyte is employed, where the voltage difference is measured by the difference, at the opposite electrodes, between the carbonate ion concentrations (CO_3^{2-}). According to Nernst's equation cell voltage (E) is,

$$E = \frac{R \cdot T}{n \cdot F} \ln\left(\frac{[CO_3^{2-}]^{sensing}}{[CO_3^{2-}]^{reference}} \right) \tag{5.17}$$

Carbonate ions equilibrate with CO_2 and O_2 according to the following reaction,

$$CO_2 + \frac{1}{2} O_2 + 2e^- \rightarrow CO_3^{2-} \tag{5.18}$$

According to the reaction (5.18), the equation (5.17) is modified to equation (5.19),

$$E = \frac{R \cdot T}{n \cdot F} \ln\left(\frac{((p_{O_2})^{1/2})^{sensing} \cdot (p_{CO_2})^{sensing}}{((p_{O_2})^{1/2})^{reference} \cdot (p_{CO_2})^{reference}} \right) \tag{5.19}$$

For the proper operation of such sensors, it is required to establish a stable reference potential. Usually, as a reference gas, a mixture of CO_2+O_2 is used, with fixed concentrations for both gases. However, as already discussed, reference atmospheres may be problematic in many applications, so reference gases have been replaced from solid-state reference electrodes. Considering that oxygen partial pressure is equal on both sides, equation (5.19) is simplified. Mainly, simple carbonates such as K_2CO_3, carbonated with oxide additions such as Li_2CO_3-MgO and mixed carbonates such as Na_2CO_3-$BaCO_3$ are employed for detecting CO_2. Nevertheless, other systems based on a solid reference are reported. One example is the $LiMn_2O_4$ reference electrode with Li_2CO_3-MgO electrolyte. The equilibrium between lithium ions and CO in Li_2CO_3 makes it an effective material for auxiliary electrodes. Li_2CO_3 has been used with a variety of lithium-ion conductors such as LISICON, Li_3PO_4 and LIPON. The activity in Li_2CO_3 is low and constant, but as long as it is constant, the reference

potential will also be constant. Also, mixed carbonates can be used for auxiliary electrodes, such as the Li_2CO_3-$BaCO_3$, to improve efficiency. The output of different sensors based on the abovementioned electrolytes and sensing electrodes is presented in **Fig. 38a**.

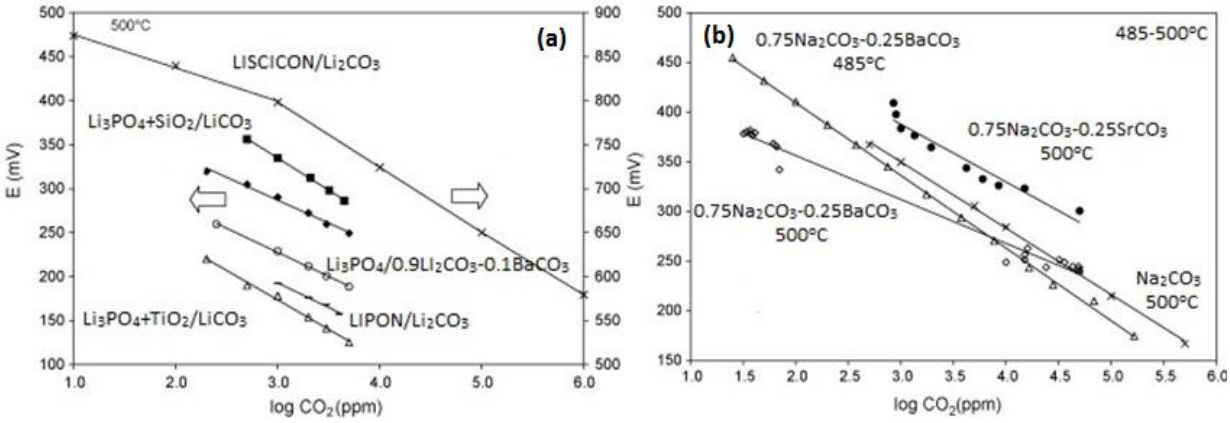

Figure 38: E(mV)-log(CO_2) (ppm) plot of CO_2 sensors based on (a) lithium ion-conducting electrolytes and $LiCO_3$ based auxiliary electrodes and (b) sodium ion-conducting electrolytes and different Na_2CO_3 based auxiliary electrodes [64].

Also, Na-β-alumina, NASCICON and sodium aluminosilicate glass with Na_2CO_3 as an auxiliary electrode have been reported. As with lithium-ion conductors, mixed carbonates have been used with Na_2CO_3 to form a more effective auxiliary electrode. The results from the sensors with Na_2CO_3, Na_2CO_3-$BaCO_3$ and Na_2CO_3-$SrCO_3$ auxiliary electrodes are displayed in **Fig. 38b** [64].

Recently, an amperometric solid-state electrochemical sensor based on a proton-conducting electrolyte was fabricated by Kalyakin et al. for the detection of CO_2 at elevated temperatures and in N_2+2%H_2O+CO_2 gas mixtures. This sensor consists of two $La_{0.9}Sr_{0.1}YO_{3-\delta}$ electrolyte plates sealed together with the aid of high-temperature glass sealant such that a chamber is formed between them. Pt electrodes were deposited at each side of one of the plates. The inner chamber connects with the surrounding environment through a capillary barrier. The sensor's configuration is presented in **Fig. 39**. For the testing part, a N_2+CO_2+2%H_2O gas mixture is fed to the sensor and the sensor is heated to the desired temperature. A DC voltage is applied to the Pt electrodes in order to force the water decomposition reaction at the external electrode. Due to the reaction, H^+ are generated and move through the proton-conducting material to the internal electrode, where CO_2 reduction takes place. The two reactions are as follows,

$$H_2O \rightarrow \frac{1}{2}O_2 + 2H^+ + 2e^- \tag{5.20}$$

$$2H^+ + CO_2 \rightarrow H_2O + CO - 2e^- \tag{5.21}$$

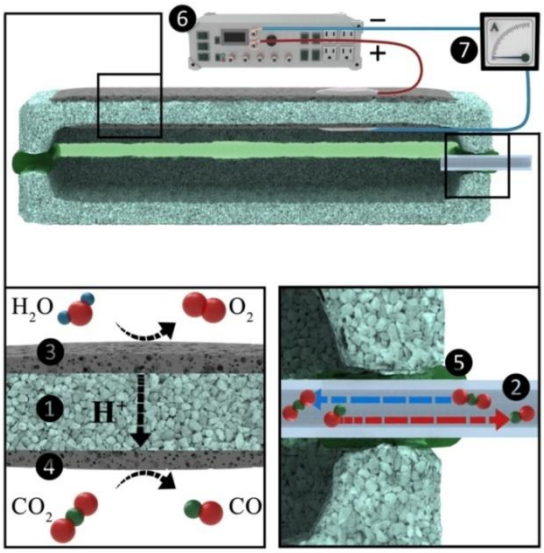

Figure 39: Configuration and operation of the amperometric CO_2 sensor, (1) $La_{0.9}Sr_{0.1}YO_{3-\delta}$ proton-conducting electrolytes, (2) capillary barrier, (3-4) Pt electrodes, (5) glass sealant, (6) DC source and (7) amperometer [65].

As a result, current, in the form of H^+, flow is generated and the concentration of CO_2 inside the chamber decreases. Reaction (5.20) can technically go on forever, as long as there is steam in the atmosphere but reaction (5.21) is limited by the CO_2 concentration in the sensor. As the CO_2 is reduced, more CO_2 flows through the capillary inside the sensor. However, at a certain applied voltage, the reduction rate is much higher than the CO_2 diffusion rate, so the concentration of CO_2 tends to zero. Under this condition, the limiting current is observed. The limiting current is theoretically calculated as follows,

$$I_{\lim} = \frac{n \cdot F \cdot S \cdot P \cdot D_{CO_2} \cdot p_{CO_2}}{R \cdot T \cdot L} \tag{5.22}$$

The diffusion coefficient of CO_2 can be theoretically measured with the aid of equation (5.23). For equation (5.23), it is required to know only the temperature and pressure of operation.

$$D_{CO_2} = D_{0,CO_2} \frac{P_0}{P} \left(\frac{T}{T_0} \right)^n \quad (5.23)$$

As far as the experiment results, the most important diagrams are presented in **Fig. 40**. The *I-V* curves of the sensor are presented in **Fig. 40a,c**. **Fig. 40a** displays *I-V* curves for different CO_2 concentrations from 2.3 to 13.7% at 550°C. As observed, the current increases as the applied voltage increases until a plateau region is formed. That means that after a certain voltage, the current response remains constant. However, by applying a much higher voltage the current starts to rise again. As it is suggested, this is due to the electrolytic decomposition or the presence of electronic conductivity in the electrolyte. In all curves, a plateau region is formed. The plateau is formed between 0.2-0.3V and the current ranges from 1 to 10mA, depending on the CO_2 content in the initial mixture. As expected, as the CO_2 concentration increases the plateau region is formed at higher applied voltages, it narrows and the limiting current value increases.

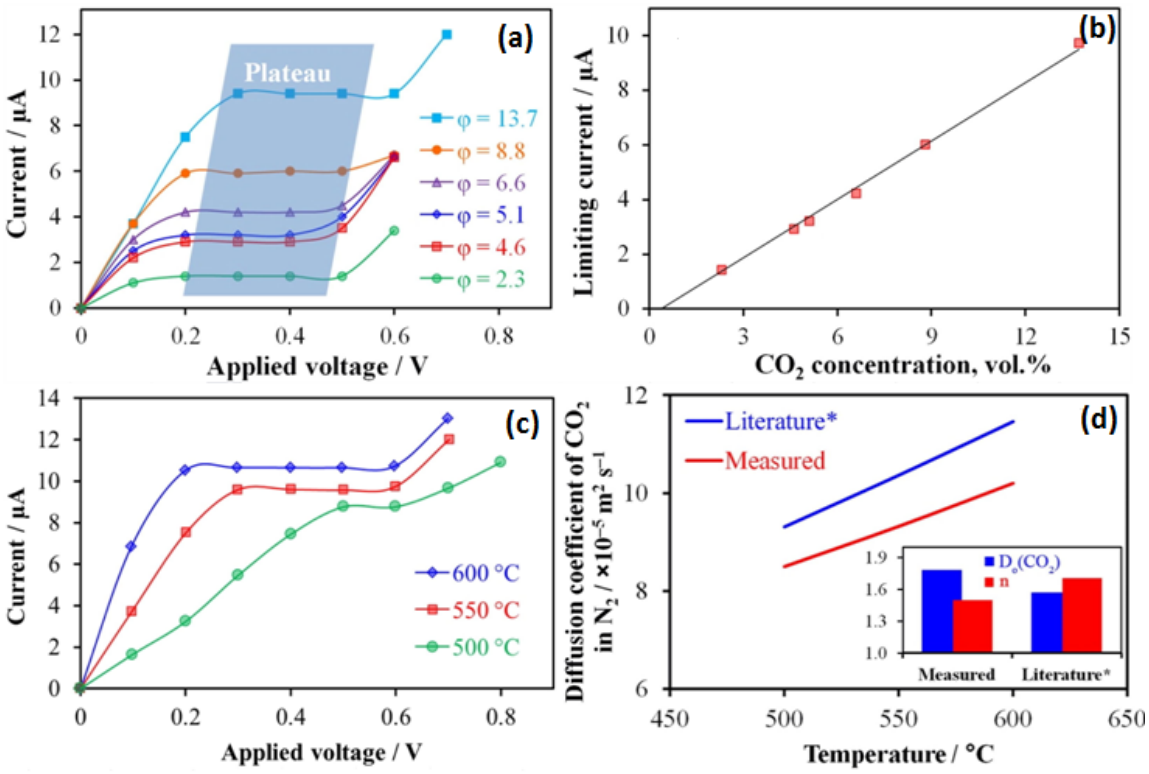

Figure 40: (a) current-voltage curves for N_2+2%H_2O+x%CO_2 (x=2.3 to 13.7) gas mixtures, (b) relation between limiting current and CO_2 concentration, (c) current-voltage curves for N_2+2%H_2O+13.7%CO_2 for 500, 550 and 600°C and (d) experimental D_{CO2} values for different temperatures compared to the values from literature [65].

Also, as presented in **Fig. 40b**, the limiting current dependence on the CO_2 content shows a linear behavior. This dependence can be utilized as a calibration curve that helps to identify the CO_2 concentration in real gas mixtures. **Fig. 40c** depicts the dependence of the *I-V* curve on the temperature of operation. These curves are obtained for the mixture of N_2+2%H_2O+13.7%CO_2 at 500, 550 and 600°C temperature of operation. As the temperature increases, the observed current increases and the plateau region is obtained at lower applied voltages. Also, the width of the plateau is larger at 600°C. Considering that the limiting current region corresponds to stationary conditions, it is highly beneficial to operate at higher temperatures. Last, from this experiment, it is possible to measure the CO_2 diffusion coefficient at any CO_2 concentration and temperature.

The dependence on the temperature of the carbon dioxide's diffusion coefficient in the mixture of N_2+H_2O+13.7% CO_2 is presented in **Fig. 40d**. It is observed that the experimental results are in good agreement with the results obtained from the literature. This suggests that this electrochemical method is suitable and reliable. It is also possible to measure the diffusion coefficient at any given CO_2 concentration. Generally, D_{CO2} slightly increases as the C_{CO2} increases [65].

5.2.3.2 Sulfur dioxide (SO_2) sensors

Sulfur oxide electrochemical sensors, also, operate under the potentiometric regime as Type-II or Type-III potentiometric sensors. Sulfate electrolytes are usually employed for electrochemical SO_2 sensors. The following reaction takes place at the electrolyte,

$$SO_3 + \frac{1}{2}O2 + 2e^- \rightarrow SO_4^{2-} \tag{5.24}$$

In conditions of excess oxygen, the determination of SO_3 partial pressure is achieved through equation (5.26) and the reaction (5.25), between SO_2 and O_2.

$$SO_2 + \frac{1}{2}O_2 \rightarrow SO_3 \tag{5.25}$$

$$p_{SO_3} = \frac{p_{SO_2}}{\left(1+\left(\frac{1}{K\cdot(p_{O_2})^{1/2}}\right)\right)} \tag{5.26}$$

Thus, the cell voltage can be calculated according to Nernst's equation, equation (5.27),

$$E = \frac{R\cdot T}{n\cdot F}\ln\left(\frac{(p_{O_2}^{sens.})^{1/2}\cdot p_{SO_2}^{sens}}{(p_{O_2}^{ref})^{1/2}\cdot p_{SO_2}^{ref}}\right) \tag{5.27}$$

Li_2SO_4-Ag_2SO_4 and Na_2SO_4-$BaSO_4$-Ag_2SO_4 based electrolytes are implemented in electrochemical SO_2 sensors. The addition of Ag_2SO_4 helps for the use of silver metal as the reference electrode. Silver metal, compared to lithium and sodium reference electrodes, is more stable in the operating temperature and better at establishing a reference potential. The potential, due to the Ag_2SO_4, is established through reaction (5.28), or if $AgSO_4$ is used with a silver ion conductor the potential is established according to reaction (5.29). In both cases, Ag_2SO_4 can be used as the reference electrode.

$$2Ag + SO_4^{2-} + 2e^- \rightarrow Ag_2SO_4 \tag{5.28}$$

$$2Ag^+ + SO_3 + \frac{1}{2}O_2 + 2e^- \rightarrow Ag_2SO_4 \tag{5.29}$$

The output of a SO_2 sensor based on Ag-β-alumina electrolyte for different operating temperatures ranging from 475 to 700°C is presented in **Fig. 41a**. Also, NASCICON and Na-β-alumina with Na_2SO_4 and Na_2SO_4-$BaSO_4$ auxiliary electrodes have been used for SO_2 sensors. Usually, to increase the potential reference electrodes, electrolyte chains are used. Dual electrolytes such as NASCICON with Sr-β-alumina electrolyte are used with Na_2SO_4 auxiliary electrode. Outputs of SO_2 sensors based on sodium ion-conducting electrolytes and Na_2SO_4 auxiliary electrodes is presented in **Fig. 41b**.

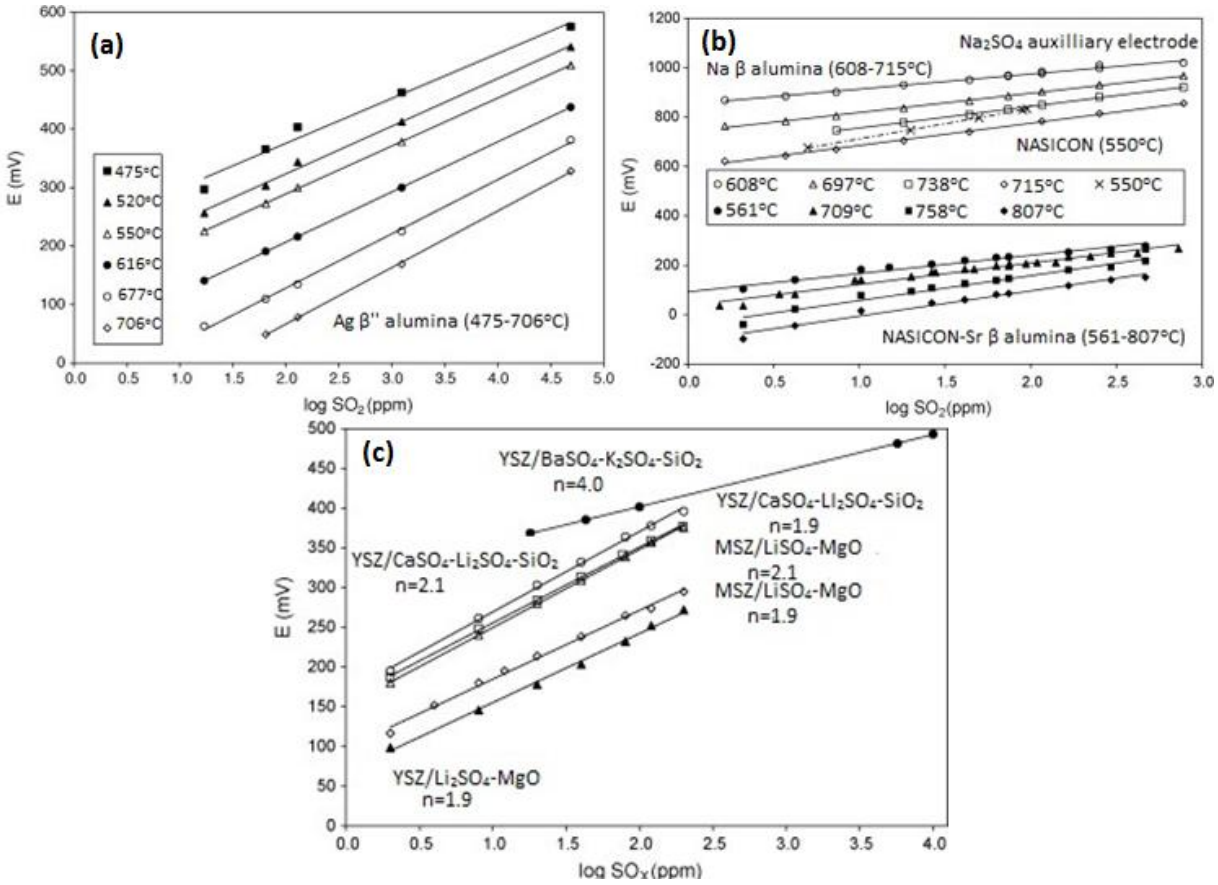

Figure 41: E(mV)-log(SO_2) (ppm) plot for SO_2 sensors based on (a) Ag-β-alumina electrolyte for different temperatures and (b) sodium ion-conducting electrolytes and $NaSO_4$ auxiliary electrode, (c) E(mV)-log(SO_x) (ppm) plot for zirconia-based SO_2 sensors at operating temperature of 650°C [64].

Zirconia based electrolytes have been reported for SO_2 sensors. Stabilized zirconia is preferred due to its high stability in aggressive environments. For SO_2 sensors, usually, a sulfate is employed as an auxiliary electrode. Common sulfates are the $LiSO_4$ and $LiSO_4$-$BaSO_4$ that are combined with magnesium-stabilized zirconia, MSZ, electrolyte or K_2SO_4 with the yttria-stabilized zirconia, YSZ, electrolyte. Also, an oxide is necessary to relate the oxygen anions in zirconia with the cations in sulfate. SiO_2 and MgO are two common oxides that have been reported to improve the sensor's response. The output of zirconia-based SO_2 sensor at 650°C is displayed in **Fig. 41c** [64].

5.2.4 Hydrogen sulfide (H_2S) sensors

The first electrochemical gas sensing technologies were designed in early 1950 for the monitoring of oxygen. Until now, these devices are considered the most suitable for

controlling and detecting hazardous emissions, such as hydrogen sulfide (H_2S). H_2S (hydrogen sulfide) is a colorless gas with a characteristic odor of rotten eggs that is corrosive, poisonous and flammable. H_2S is released through natural sources or industrial activities. As far as the natural sources, it is produced during the decomposition of organic matter. Thus, low concentrations of H_2S can be found in sewer and septic systems. Regarding the human activities, high quantities of H_2S are released through refilling and drilling processes of petroleum and natural gas. Apart from environmental pollution, hydrogen sulfide is also dangerous to humans. Exposure or inhaling of H_2S can cause several damages. Even for a short period of time, H_2S can lead to unconsciousness or damage the eyes, nervous system and respiratory system at low concentration, or it can be fatal at high concentrations. Consequently, it is important to design sensing technologies capable of detecting hydrogen sulfide in real-time. Every sensing technology should fulfill several requirements, including low cost, fast response, miniaturization and the ability to operate at elevated temperatures, to be suitable for commercial use and competitive against the pre-existing technologies.

Today, researches and studies are focused on the development of fast, low-cost, miniaturized and efficient H_2S electrochemical sensors based on various materials such as organic materials, semiconductors or solid electrolytes. Among the abovementioned materials, the latter seems to be the most promising for the development of electrochemical sensing devices to detect low concentrations of H_2S. There are many examples of electrochemical H_2S sensors based on solid electrolytes operating at a wide range of temperatures. An amperometric H_2S sensor based on proton exchange membrane (Nafion) electrolyte and Pt-Rh/C sensing electrode was fabricated by Yang et al. for the detection of low concentration of H_2S (0.1-200 ppm) at room temperature. This sensor showed a linear current response at the concentration range of 0.1 to 200ppm, long term stability and great selectivity. Zhang et al. fabricated a mixed potential electrochemical sensor for operation at low temperatures based on $CoCr_{2-x}Mn_xO_4$ sensing electrode and a sodium-ion conductor (NASCICON) for the detection of sub-ppm concentration levels of H_2S at temperatures around 250°C. Even though these sensors are fulfilling all the above-mentioned requirements the low temperature of operation is a major issue. Considering

that H_2S sensors are employed for the control of H_2S released from industrial processes, usually, these sensors need to operate at much higher temperatures. A material suitable to address this problem is the well-known yttria-stabilized zirconia (YSZ). There are many reports about electrochemical H_2S sensors based on YSZ electrolyte and a great variety of metal oxides as sensing electrodes that show great potential because of the chemical and thermodynamic stability of YSZ at high temperatures and in the presence of oxidizing or reducing gases. A mixed potential electrochemical H_2S sensor based on YSZ electrolyte and WO_3 working electrode was fabricated by Miura et al. This sensor was responding well to 0.25-25 ppm H_2S at temperatures around 400°C. Another similar H_2S sensor was fabricated by Lu et al. based on YSZ electrolytes combined with $NiMn_2O_4$ sensing electrode that exhibited great sensitivity and response to 50 part per billion (ppb) H_2S at the operating temperature of 500 °C. Furthermore, La_2NiO_4 was employed as a sensing electrode in a mixed potential H_2S sensor with a low detection limit of 0.02 ppm H_2S at 500°C. Last, Lu et al. fabricated a mixed potential YSZ-based electrochemical H_2S sensor with a $ZnMoO_4$ sensing electrode for the detection of ppb-level concentrations of H_2S. This sensor exhibited its highest response to 1ppm of H_2S and also showed an acceptable response to 5ppm and 500ppb at 500°C. As it is stated, its lower limit is about 5ppb.

In **Table. 2,** the basic information about the abovementioned solid-state electrochemical H_2S sensors are listed. Even if there already are solid electrolytes-based sensors that exhibit great sensitivity/ selectivity and fast response, there is still potential for optimized sensors by designing more and more efficient materials [66].

Table 2: Solid-state electrochemical H_2S sensors.

Source	Date	Electrolyte	Type	SE	Temperature °C
[67]	2018	Nafion	Amperometric	Pt-Rh/C	20-30
[68]	2014	NASCICON	Mixed	$CoCr_{2-x}Mn_xO_4$	250
[69]	1996	YSZ	Mixed	WO_3	400
[70]	2014	YSZ	Mixed	$NiMn_2O_4$	500
[71]	2018	YSZ	Mixed	La_2NiO_4	500
[66]	2020	YSZ	Mixed	$ZnMoO_4$	500

5.3 Electrochemical sensors for the detection of nitrogen oxides (NO_x) and ammonia (NH_3) gas

5.3.1 Nitrogen oxides sensors

On 1940s, A.J. Haagen-Smit et al., discovered that a certain type of smog is generated by reactions involving nitrogen oxides and reactive hydrocarbons in the atmosphere. Nowadays, this certain type is known as photochemical smog and is generated when the ultraviolent part of the sunlight interacts with the existed nitrogen oxides in the atmosphere. Following this revelation, most of the initial efforts to address this problem were aimed at reducing hydrocarbons emissions, as it was an easier problem at the time to solve. However, during the years, research has also focused on reducing nitrogen oxide emissions. Over the last two decades, the better understanding of nitrogen oxides has led to the development of efficient NO_x control technologies. Furthermore, due to the photochemical smog and acid rain in many urban areas, it is clear that there is a need for a NO_x emission control devices. The seven most common nitrogen oxides are NO, NO_2, NO_3, N_2O, N_2O_3, N_2O_4 and N_2O_5. Among these seven pollutants, the first two, NO and NO_2, are the most important because they are emitted in larger quantities. In combustion exhaust emissions, NO is the main pollutant as it makes 7-80% of the total NO_x content. Apart from environmental issues, NO_x also causes damage to the human respiratory system and nerve. Consequently, it is necessary to develop sensors to detect NO_x emissions in harsh environments and high temperatures. Many devices use NO_x sensors aiming to reduce or eliminate NO_x emissions from combustion processes, resulting in a great need for reliable NO_x sensors able to provide the needed information. NO_x sensors must fulfill some requirements to be considered suitable and used in commercial combustion applications. The most important requirements are the ability to operate at elevated temperatures (600-900°C) for a long period of time and to provide a stable and accurate response in the absence of oxygen or environments with high moisture concentration [72], [52].

5.3.1.1 Amperometric NO_x sensors

Among the NO_x sensors, the most commonly used and successful type is the amperometric sensors. There are many types of amperometric sensors and many configurations that have

shown good results. Most NO_x amperometric sensors consist of two chambers. The first chamber usually operates as an oxygen pump extracting oxygen by exhaust emissions. While in the second chamber, the decomposition of NO to N_2 and O_2 takes place and the total concentration of O_2 is measured. Another NO_x sensor was fabricated by Kalyakin et al. for detecting nitrous oxide (N_2O) and operating as an oxygen amperometric sensor. The sensor's configuration is presented in **Fig. 42**. This sensor consists of two solid electrolyte plates sealed such that an inner cavity is created inside them. Both plates are made of YSZ and there are Pt electrodes on opposite sides of one of the plates.

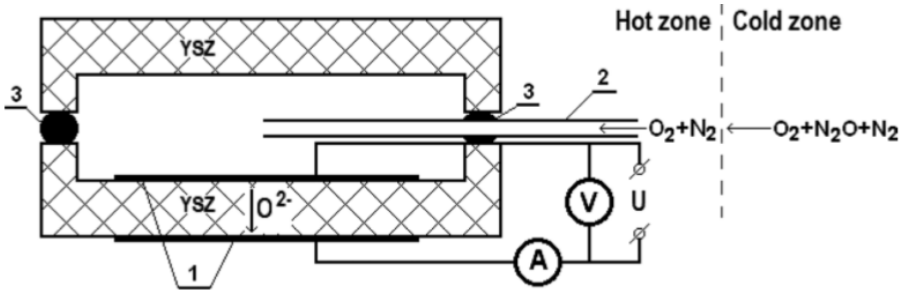

Figure 42: A scheme of an amperometric NO_x sensor. (1) Pt electrodes, (2) capillary, (3) glass sealants [73].

The operation of every amperometric sensor is based on an externally imposed voltage. When the voltage is applied to the sensor's electrodes, oxygen in the form of oxygen ions is electrochemically pumped out of the chamber to the ambient gas resulting in a decrease of the oxygen's concentration inside the chamber. Due to the created concentration gradient, oxygen from the surrounding gas moves into the cavity by diffusing through the capillary barrier. Furthermore, the decomposition of N_2O takes place inside the cavity, forming N_2 and O_2. As the applied voltage increases, more oxygen is pumped out of the chamber until its concentration is close to zero, then the flow through the cavity is at its maximum and the limiting current is observed. By the values of the limiting current and the equation (5.30), the concentration of oxygen is calculated,

$$I_{\lim} = \frac{4 \cdot F \cdot D_{O_2} \cdot P \cdot A}{R \cdot T \cdot L}(1 - X_{O_2}) \qquad (5.30)$$

Knowing the kind of the initial gas mixture, the concentration of oxygen and using the calibration curve in N_2+O_2 mixtures, the concentration of N_2O can be measured by the equation (5.31),

$$X_{O_2}^{*} = \frac{1-0,5\cdot X_{N_2O}}{1+0,5\cdot X_{N_2O}} \tag{5.31}$$

or expressed for the concentration of N_2O as,

$$X_{N_2O} = 2\frac{1-X_{O_2}^{*}}{1+X_{O_2}^{*}} \tag{5.32}$$

This equation slightly differs based on the initial mixture that surrounds the sensor. For example, equation (5.31) for a mixture of N_2O+N_2 is,

$$X_{N_2O} = \frac{2\cdot X_{O_2}^{*}}{1-X_{O_2}^{*}} \tag{5.33}$$

or for a ternary mixture of N_2O+air (N_2+N_2O+O_2) is,

$$X_{N_2O} = \frac{X_{O_2}^{*}-0,209}{0.209-0,5\cdot X_{O_2}^{*}} \tag{5.34}$$

In the operating environments, there are more oxygen-containing gases, such as steam (H_2O) and carbon dioxide (CO_2), that are stable at these temperatures. The value of the applied voltage shouldn't be high enough to trigger the electrochemical decomposition of these gases (lower than 1V at 700°C) [73].

For the experimental part, the sensor was tested in different environments of N_2O+N_2, O_2 or air. The current-voltage curves for all the different mixtures at an operating temperature of 700°C are presented in **Fig. 43**. It is observed in **Fig. 43a,b** that the limiting current for the N_2O+N_2 mixture is reached at 0.2V applied voltage for low concentrations, between 0.67 and 4.7%, and 0.4V for higher concentrations, between 7.4 and 100%. Also, even though the concentration of N_2O increases, the value of the limiting current doesn't exhibit a significant rise.

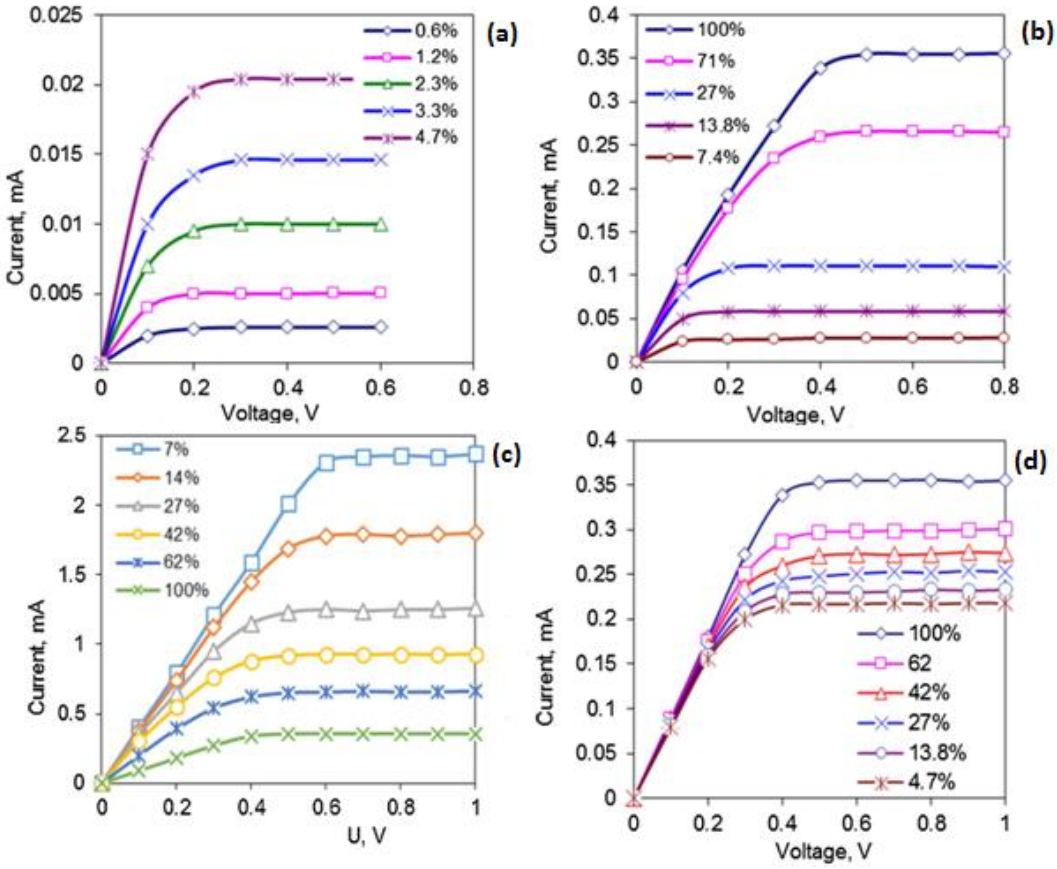

Figure 43: Current-voltage curves at 700°C for different N_2O concentrations in mixtures of, (a, b) N_2O+N_2 , (c) N_2O+O_2, (d) N_2O+air [73].

In **Fig. 43c,** the ampere-volt curves for the mixture x%N_2O+O_2, where x is ranging from 7 to 100%, are presented. Here, the limiting current is observed at 0.6V. Similar to the previously tested mixture, there isn't a significant increase at the limiting current's value as the concentration increases. Note that in the x%N_2O+O_2 mixture, by increasing the initial amount of N_2O, a reduction in the limiting current value is observed. This can be explained by the decrease in oxygen concentration in the initial hot mixture due to the substitution of oxygen by nitrous oxide. Last, the curves for the ternary mixture of N_2O+air are presented in **Fig. 43d**. The concentration of N_2O ranges from 4.7 to 100% and the limiting current is reached at about 0.4V. Concluding, this sensor is capable of detecting N_2O in various mixtures for a wide range of N_2O concentration. However, although these types of NO_x sensors provide a fast and accurate response with minimum degradation over long operation time, their complex design and high cost have limited their application. Therefore, investigations are still required on electrode and electrolyte materials.

5.3.1.2 Mixed NO_x sensors

There are also reports employing potentiometric sensors for the detection of NO_x in high-temperature emissions. Equilibrium potentiometric sensors present several problems during the detection of NO_x emissions in the operating environment. The fundamental problem is that there aren't yet electrode or electrolyte materials that present the desired characteristics at the working conditions. Consequently, non-equilibrium potentiometric or mixed sensors are employed to overcome these problems. These sensors use electrode materials that present different catalytic activities. NO_x sensors require an electrode that exhibits considerable good thermal stability for high-temperature operation. Mixed sensors have been intensively investigated and many metal oxides have been tested.

In earlier years, $ZnFe_2O_4$, $ZnCr_2O_4$, ZnO, $NiCr_2O_4$ and WO_3 were tested for NO_x detection at 600-700°C. Among the tested metal oxides, Ni-family oxides showed the most promising results for operation at temperatures above 800°C. Mixed NO_x sensors based on Ni oxides as electrode material showed great sensitivity in wet or dry environments and the highest sensing temperatures. Furthermore, NiO electrode's characteristics can be further improved by the addition of a noble metal. Noble metals such as Pt, Ir, Pd, Ru and Rh have been tested, among them, Rh provides a significant improvement in electrode characteristics [52].

5.3.1.3 Impedancemetric NO_x sensors

Impedancemetric sensors are the least developed technology for the detection of NO_x. These sensors are detecting even lower concentrations of NO_x in exhaust emissions and in contrast to the abovementioned types, they can measure the total amount of NO_x because the output response for NO and NO_2 is the same in impedancemetric sensors. The complexity of electronics and signal processing equipment limits the application of these sensors. In addition, impedancemetric sensors can't operate properly in the presence of oxygen in the analyzed gas, so there is a need for materials with better selectivity for impedancemetric sensors to be commercially used and competitive for high-temperature gas detection [52].

5.3.2 Ammonia (NH_3) sensors

Most of the ammonia gas in the atmosphere is produced through human activities. Nowadays, 20% of ammonia (NH_3) is produced for application in cleaning products, pharmaceuticals, refrigeration and explosives, while the other 80% for nitrogen-based fertilizers. Those activities are estimated to emit around 2.1 to 8.1Tg of ammonia annually. Today, in the atmosphere, ammonia is at a low ppb-level (1-5ppb). However, ammonia is a toxic and corrosive gas, so even in low concentrations, it causes several life-threatening problems to humans, affecting the skin, eyes and lungs. As the use of ammonia grows and the industry fields employing ammonia expand, so does the need for reliable and effective ammonia sensors. As a rule, in order, for gas sensors, to be suitable for the detection of ammonia over a long period, they must exhibit some major aspects. Among the sensing technologies, electrochemical gas sensors seem to be more suitable for quantifying and detecting NH_3 or other hazardous gases. Electrochemical gas sensors exhibit great sensitivity for individual gas even in ppm or ppb levels in real-time. From the group of perilous gases, more attention has been given to NH_3 gas detection because ammonia is a common manufactured chemical and it is applied in a wide variety of applications around the world.

5.3.2.1 Amperometric NH_3 sensors

Most of the technological processes in metallurgical, chemical and energetic fields need to detect ammonia content in harsh environments and at high temperatures. Consequently, solid-state electrochemical sensors are the most suitable type for operating effectively under these conditions. These sensors normally operate under potentiometric or amperometric regimes. An amperometric ammonia sensor was fabricated by Kalyakin et al. This sensor is based on two electrochemical cells forming an inner chamber and a capillary that connects the surrounding environment with the chamber. Each cell is based on yttria-stabilized zirconia (YSZ) electrolyte and Pt electrodes are deposited at each side of the two cells. The cells are glued together with the aid of a glass sealant. The configuration of this sensor is depicted in **Fig. 44.**

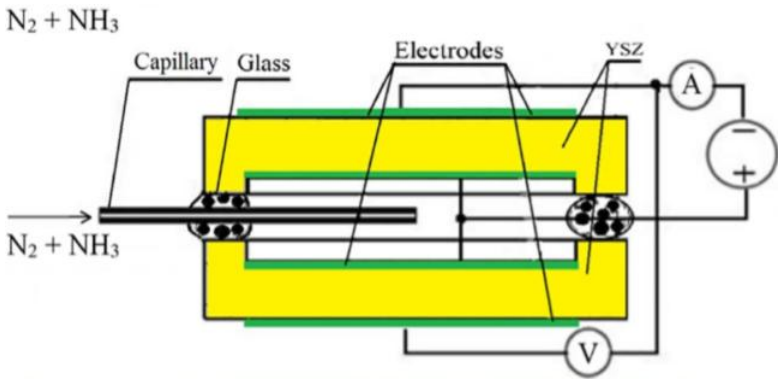

Figure 44: Schematic representation of a NH_3 amperometric sensor [74].

During the experiment, the sensor is placed in the NH_3+N_2 gas mixture. In this experiment, the content of impurities (H_2O steam) in the mixture does not exceed 0.1 vol.%. When the chamber fills with N_2+NH_3 gas mixture, a DC voltage is applied to the electrodes. Due to the applied voltage, the decomposition of H_2O occurs at the outer electrodes according to the reaction,

$$H_2O + 2e^- \rightarrow H_2 + O^{2-} \tag{5.35}$$

Oxygen anions generated by the reaction (5.35) move through the solid electrolyte to the internal electrodes. At the internal electrode, the oxidation of ammonia takes place. The catalytic oxidation of ammonia occurs through three different reactions generating N_2 (molecular nitrogen), NO (nitrogen oxide) and N_2O (nitrous oxide).

$$NH_3 + 1,5O^{2-} \rightarrow 0,5N_2 + 1,5H_2O + 3e^- \tag{5.36}$$

$$NH_3 + 2O^{2-} \rightarrow 0,5N_2O + 1,5H_2O + 4e^- \tag{5.37}$$

$$NH_3 + 2,5O^{2-} \rightarrow 0,5NO + 1,5H_2O + 5e^- \tag{5.38}$$

As the applied voltage further increases, the rate of the reactions also increases. Consequently, the sensor's current response increases and the ammonia concentration in the chamber gradually decreases. As the difference in NH_3 concentration inside and outside of the sensor grows, the ammonia diffusion flux grows as well. When ammonia's concentration in the chamber is zero, the diffusion flux has reached its maximum value. The current observed in this condition is known as limiting current and it indicates that the diffusion is the rate-limiting step of the reactions at the electrodes. Limiting current is calculated through equation

(5.39). According to this equation, the limiting current in a function of the capillary's characteristics, environmental parameters, the electrochemical reactions that take place and the concentration of the targeted gas. From equation (5.39), it is observed that the limiting current is directly proportional to the gas concentration.

$$I_{\lim} = \frac{z \cdot F \cdot D \cdot S \cdot P}{R \cdot T \cdot L} X_{NH_3} \tag{5.39}$$

In amperometric electrochemical sensors, the quantity of interest is the limiting current. In this experiment, the sensor was tested in different ammonia concentrations starting from 0.1 to 5 vol.% at temperatures between 375 and 430°C. For these concentrations, the limiting current is reached for temperatures up to 400°C and it is linearly proportional to the ammonia concentration. So, a calibration curve (limiting current vs NH_3 concentration) is obtained for the determination of ammonia in N_2+NH_3 gas mixtures.

Fig. 45a shows the sensor's current response for a wide range of N_2+NH_3 mixtures plotted against the applied voltage. In these curves, three different regions are distinguished. In the first region, when the DC voltage is applied, the current increases as the voltage increases. In the second region, the concentration of ammonia inside the chamber is zero and the limiting current appears. The limiting current is depicted at the curves as a plateau region. In the third region, the current starts growing again with the applied voltage due to the presence of oxygen inside the chamber. As expected, the limiting current value increases as the content of ammonia in the N_2+NH_3 mixture increases. As already discussed, one of the main advantages of the amperometric sensors is the linear relation between the limiting current and targeted gas concentration. As presented in **Fig. 45b**, this condition is satisfied for the tested sensor, so it is suitable for the detection of ammonia in the temperature range of 375-400°C.

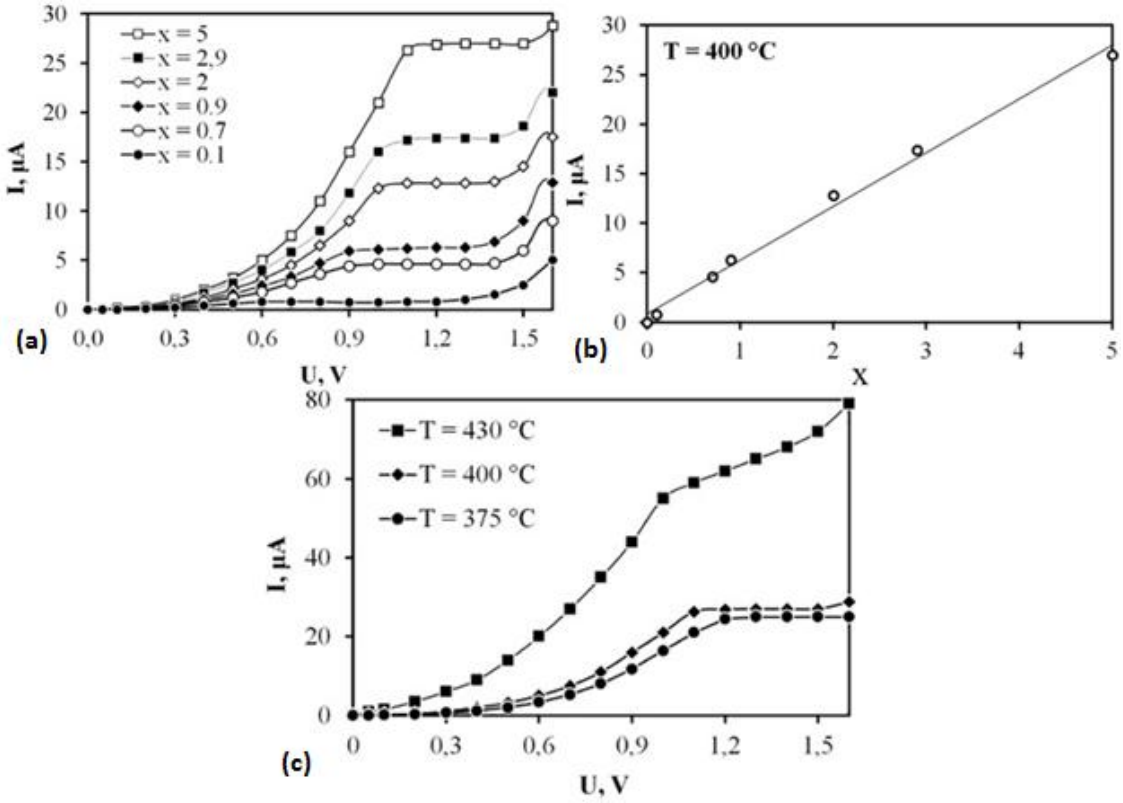

Figure 45: (a) Current response on the applied voltage for different ammonia concentrations at 400°C. x is the NH_3 concentration in vol.%, (b) The relation between the limiting current and different NH_3 concentrations and (c) current-voltage curves for different temperatures for 5 vol.% ammonia [74].

Another important observation from **Fig. 45c** is the effect of temperature on the sensor's operation. From **Fig. 45c** is observed that at low temperatures, between 375-400°C, there is a clear plateau region formed at 1 to 1.2V, while at temperatures up to 430°C, there is no limiting current region. This increase in current is connected with an increase in the cell's internal resistance. At these temperatures, the catalytic decomposition of NH_3 takes place at the chromo-nickel electrode according to the reaction (5.40),

$$NH_3 \rightarrow 0,5N_2 + 1.5H_2 \qquad (5.40)$$

Through reaction (5.40), H_2 is generated at the capillary and then it diffuses inside the sensor. This hydrogen, then, reacts with the oxygen ions that flow through the YSZ electrolyte, according to equation (5.41),

$$H_2 + O^{2-} \rightarrow H_2O + 2e^- \qquad (5.41)$$

The number of electrons required for the oxidation of NH_3, reaction (5.36), are the same as for the oxidation of H_2, reaction (5.41). Concluding, the observed current is higher because hydrogen's diffusion flowrate is higher. From this experiment, it is also possible to identify which reaction, among the reactions (5.36), (5.37), (5.38), dominate inside the sensor and thus which are the main byproducts produced in the chamber. This is accomplished by comparing the measured diffusion coefficients in the gas mixture with the data from the literature. The experimental values were measured with the aid of equation (5.39) expressed for the D,

$$D = \frac{R \cdot T \cdot L \cdot I_{LIM}}{z \cdot F \cdot S \cdot P \cdot X_{NH_3}} \tag{5.42}$$

Using equation (5.42) and changing z for every reaction (5.36-38) without changing the other parameters, the diffusion coefficient can be measured. The results are presented in **Table. 3**. On the other hand, the theoretical diffusion coefficient D_{th} is calculated according to equation (5.43),

$$D_{th} = \frac{0.01858 \cdot T^{1.5}}{P \cdot \sigma^2 \cdot \Omega_{DT}} \sqrt{\frac{1}{M_{N_2}} + \frac{1}{M_{NH_3}}} \tag{5.43}$$

In equation (5.43), Ω_{DT} is the collision integral for diffusion, σ is the characteristic distance for nitrogen/ammonia mixture. P, T is the absolute pressure and temperature, respectively, and M is the molecular mass. In **Table. 3** the results for the experimental and theoretical values for diffusion coefficient are reported.

Table 3: Experimental and theoretical diffusion coefficients for ammonia in nitrogen at different temperatures [74].

T, °C	Equation	Dex·10^4 m^2/s	Dth·10^4 m^2/s	ΔD/Dth %	Byproduct
400	(5.36)	1.11	1.12	0.9	N_2
	(5.37)	0.83		26	N_2O
	(5.38)	0.67		40	NO
375	(5.36)	1.01	1.05	3.8	N_2
	(5.37)	0.76		28	N_2O
	(5.38)	0.60		43	NO

The diffusion coefficient for the reaction (5.36) is the closest to the theoretical one, concluding that the main byproduct from the electrochemical oxidation of ammonia is N_2 and not N_2O or NO [74].

5.4 Electrochemical sensors for the detection of oxygen (O_2) and humidity (H_2O vapor)

5.4.1 Oxygen sensors

Today, there are several concerns about health issues and environmental pollution from gases released by burned hydrocarbons. These concerns have driven legislation and great development and research to reduce worldwide emissions of harmful gases. The most promising technology to address or reduce this issue are the gas sensing devices, resulting in a great turn of interest and research in this field. In particular, the emission control and the optimization of internal combustion engines and boilers used in automobiles and various industries, respectively, have been achieved with the help of solid electrolyte-based oxygen sensors. Based on the number of sensors employed, oxygen sensors are mainly used for the control of the air-fuel ratio in the combustion engine and are an integral part of the on-board diagnostic (OBD) of the exhaust emission control system.

5.4.1.1 Potentiometric Type-I oxygen sensors

Equilibrium potentiometric oxygen sensors are well-known devices usually employed for the control of exhaust emissions. These sensors are one of the most successful applications of solid electrolytes. It is a simple design with a ceramic electrolyte, usually yttria-stabilized zirconia because it is structurally and chemically stable for temperatures up to 1500°C, between two Pt electrodes and air as the reference gas electrode. As already discussed in previous chapters, the operation of these sensors is based on the open-circuit conditions where no current is applied to the sensor. The oxygen concentration in the targeted atmosphere is measured according to Nernst's equation (5.44). By measuring the *EMF* of the cell, generated by the difference between the partial pressure of oxygen at the sensing and the reference side.

$$E = -t_o \frac{R \cdot T}{4 \cdot F} \ln\left(\frac{P_{O_2}^{sensing}}{P_{O_2}^{reference}} \right) \tag{5.44}$$

Where $P_{O_2}^{sensing}$, $P_{O_2}^{reference}$ are the partial pressures at the sensing and reference side, respectively, T is the absolute temperature, R is the ideal gas constant, t_o is equal to one for solid oxide electrolytes and F is Faraday's constant.

Potentiometric sensors need a reference electrode to operate. Conventional YSZ-based oxygen sensors use Pt/air as the reference electrode resulting in some architecture limitations. Considering that they use air as reference gas, these sensors must be in contact with the environment during their operation, so the oxygen concentration can only be measured near the wall of the combustion chamber. Concluding, to achieve miniaturization and simpler configuration of the sensors and more precise measurements of the concentration by placing the sensor in any location inside the chamber, there is a need to change the reference electrode. An alternative that has been proposed is the metal/metal oxide as the reference electrode. There have been investigated many different oxides that can provide stable equilibrium oxygen partial pressure at a fixed temperature, such as Sn/SnO_2, Pd/PdO, Ru/RuO_2, In/In_2O_3 and Ni/NiO. Most of the abovementioned metal/metal oxides operate at temperatures below 500°C. The latter, however, Ni/NiO is the most promising reference alternative for the environment of the combustion chamber [52].

5.4.1.2 Amperometric oxygen sensors

In potentiometric oxygen sensors, as it can be seen in equation (5.44), the output potential depends logarithmically on the oxygen concentration. As a result, when the oxygen concentration is high enough as in the lean combustion gas, potentiometric sensors can't effectively measure oxygen concentration. Consequently, an amperometric sensor is preferable for detecting high concentrations as it gives a linear output that depends on oxygen concentration. The principle of operation of amperometric sensors is discussed in previous chapters. Amperometric sensors' operation is based on limiting current measurements. For a diffusion channel with length L and cross-section A, the limiting current I_{lim} is given by,

$$I_{\lim} = \frac{4 \cdot F \cdot D_{O_2} \cdot P \cdot A}{R \cdot T \cdot L} p_{O_2} \tag{5.45}$$

In equation (5.45), F is Faraday's constant, R is the ideal gas constant, T and P is the absolute temperature and pressure, D_{O2} is oxygen diffusion coefficient and p_{O2} is the partial pressure of oxygen in the sensing electrode.

When the sensor is operating properly, the current response increases linearly with the oxygen concentration, exhibiting great accuracy in measurements and high sensitivity (ppm to ppb). However, the limiting current is related to diffusion barrier characteristics, so there is a need for flawlessly designed diffusion barriers. Also, amperometric sensors show poor long term and thermal stability. For high-temperature amperometric oxygen sensors, yttria-stabilized zirconia (YSZ) is the most effective solid electrolyte. However, Gd and Sm doped CeO_2 has been proposed as a possible alternative. For example, $Ce_{0.8}Sm_{0.2}O_{1.9}$ (CSO) has been reported to present higher ionic conductivity than YSZ at temperatures ranging between 500-700°C. Besides the solid electrolyte, diffusion barriers play an important role in the proper operation of the sensor. Diffusion barriers are expected to perform good thermal stability and electronic conductivity in the working environment. Lanthanum strontium manganate (LSM) is an ionic-electronic conductor for oxygen membranes that shows good diffusion control. High oxygen-ion and electronic conductivity and great electrochemical catalytic activity have also been reported in cobalt-containing perovskites (LCO).

5.4.1.3 Combined oxygen sensors

Apart from purely potentiometric or amperometric cells, there are more sophisticated devices that combine both cells. In these devices, one cell operates under the amperometric regime and works as an oxygen pump, while the other operates under potentiometric regime as an oxygen gauge. The ability of the sensor to measure simultaneously the limiting current in the oxygen pump and the electromotive force (*EMF*) in the potentiometric cell increases the sensor's reliability [52]. A sensor capable of operating simultaneously under both amperometric and potentiometric regimes was fabricated and tested by Kalyakin et al. The sensor consists of two electrochemical cells based on YSZ electrolyte. The exact composition of the solid electrolyte is $0.91ZrO_2+0.09Y_2O_3$. The two cells are fixed together with a heat-resistant glass such that an inner chamber is formed. The Pt porous electrodes are deposited at each side of both plates

and a metal capillary is used to connect the internal chamber with the surrounding environment. The scheme of the described sensor is presented in **Fig. 46**.

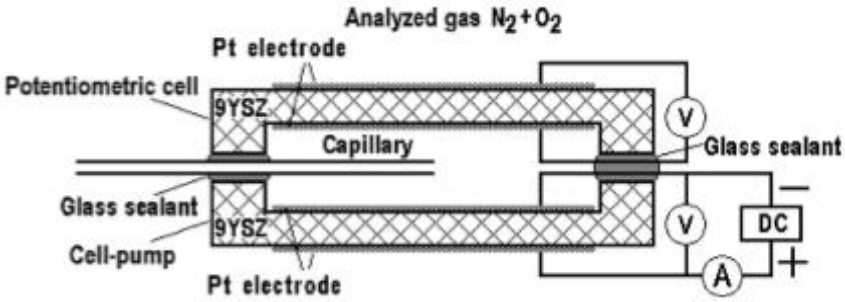

Figure 46: Scheme of a combined potentiometric/amperometric oxygen sensor [57].

The principle of operation of these sensors has already been discussed. This sensor can operate as both a potentiometric and amperometric sensor. As far as the amperometric mode, a DC voltage is applied to the electrodes of one of the cells to force the reduction of oxygen in the internal electrode. This way, oxygen is electrochemically pumped out of the sensor to the ambient gas. As the voltage increases, the concentration of oxygen inside the sensors decreases. At a certain voltage, the limiting current is observed. When the limiting current is observed, the concentration of oxygen inside the sensor is negligible. With the help of the potentiometric cell, it is possible to control the oxygen content inside the sensor. Summarizing, in this case, the potentiometric cell has the role of a control cell and uses as a reference the analyzed gas.

For the experimental part, the *EMF-V* and the limiting current-V dependence for different oxygen concentrations are measured simultaneously. In **Fig. 47c,** the measurements of *EMF* and current plotted against the applied voltage are displayed. Note that the concentration of oxygen, for the *EMF-V* and *I-V* plots in **Fig. 47c**, is 7.5%. It is observed that the limiting current region starts at about 400 mV of applied voltage (blue line). At this condition, the concentration of oxygen inside the sensor tends to zero. However, after about 1000mV the current gradually grows again, mainly because of the electrolytic decomposition of steam. At about 1300 mV, a sharp growth is observed. The latter is a result of the appearance of electronic conductivity in the YSZ electrolyte. Furthermore, it is observed that the *EMF-V* plot (green line) also presents a plateau region. The plateau here testifies that for a wide range of applied voltages (600-900mV), the

concentration of oxygen inside the sensor is constant. However, due to the decomposition of steam, there is a sharp rise in the *EMF* as well. At this point, the impact of molecular oxygen on *EMF* is negligible, so the observed *EMF* is mainly defined by the hydrogen and humidity in the N_2+H_2O+H_2 mixture.

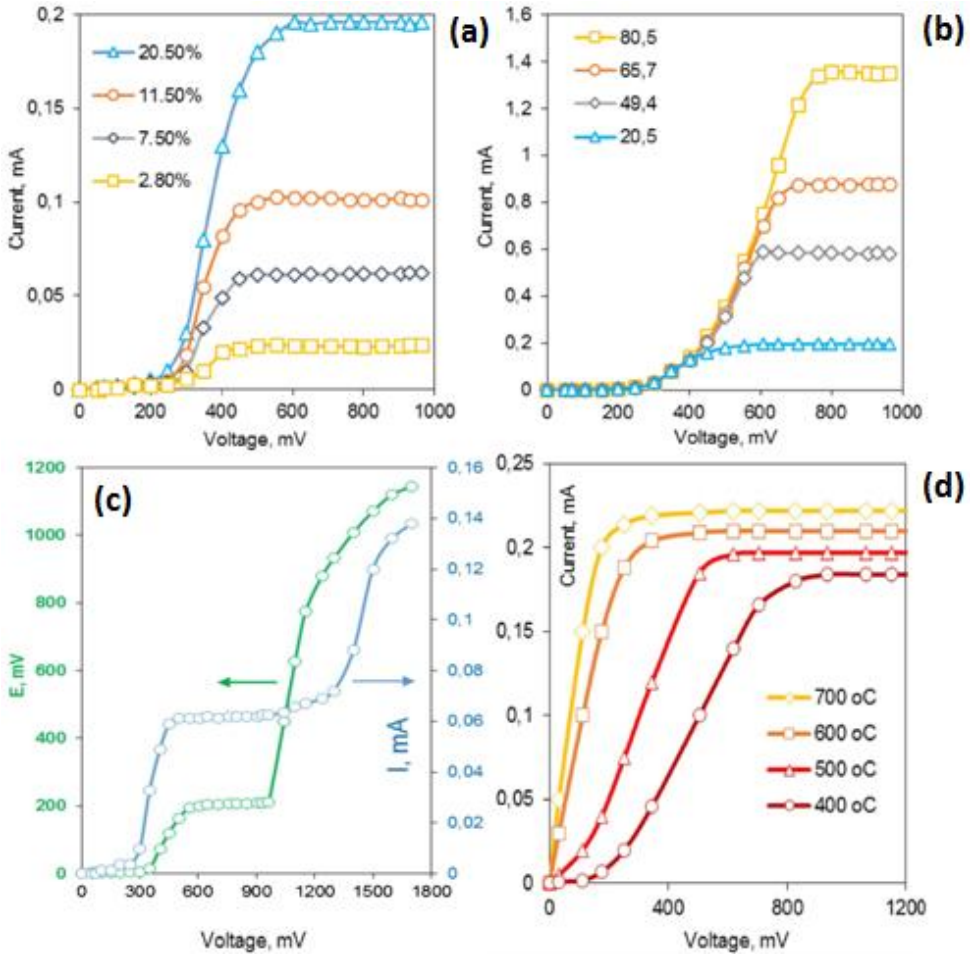

Figure 47: Current-voltage curves of the sensor at (a) low and (b) high oxygen's concentration at 500°C, (c) typical *EMF-V* and *I-V* characteristics at 500°C and oxygen's concentration of 7.5%, (d) current-voltage curves at different temperatures [57].

The current-voltage curves of the amperometric cell for different oxygen concentrations, between 2.8% and 80%, are presented in **Fig. 47a,b** at 500°C. As it can be seen in **Fig. 47a**, the limiting current region is reached at an applied voltage ranging between 400 and 600mV for low oxygen concentrations (2.8-20.5%). While, for higher oxygen concentrations (20.5-80%) it is reached at 600-800mV. Concluding, as the oxygen concentration inside the analyzed gas increases so does the applied voltage at which the limiting current is observed. Also, a significant growth in limiting current's value is observed as the oxygen's content

increases. Another important result is the dependence of the *I-V* curves with the temperature of operation.

In **Fig. 47d**, the *I-V* curves for different temperatures are plotted. The first two curves at 400 and 500°C have an S-shaped behavior due to the low activity of the Pt electrodes at these temperatures. As the temperature of operation increases, the electrode's activity increases as the polarization of the electrodes doesn't affect the *I-V* curves. Also, the measured limiting current is much higher and is reached at lower applied voltages at high temperatures (700°C) compared to low temperatures (400°C).

Fig. 48a shows the relation between the oxygen's concentration and the diffusion limiting current at the temperature of 500°C. As observed, it seems to present a non-linear behavior. However, this is because of the wide range of oxygen concentration (2.8-80%). It is suggested that the sensor can properly measure oxygen. For smaller ranges, such as (2.8-20%), the behavior is linear.

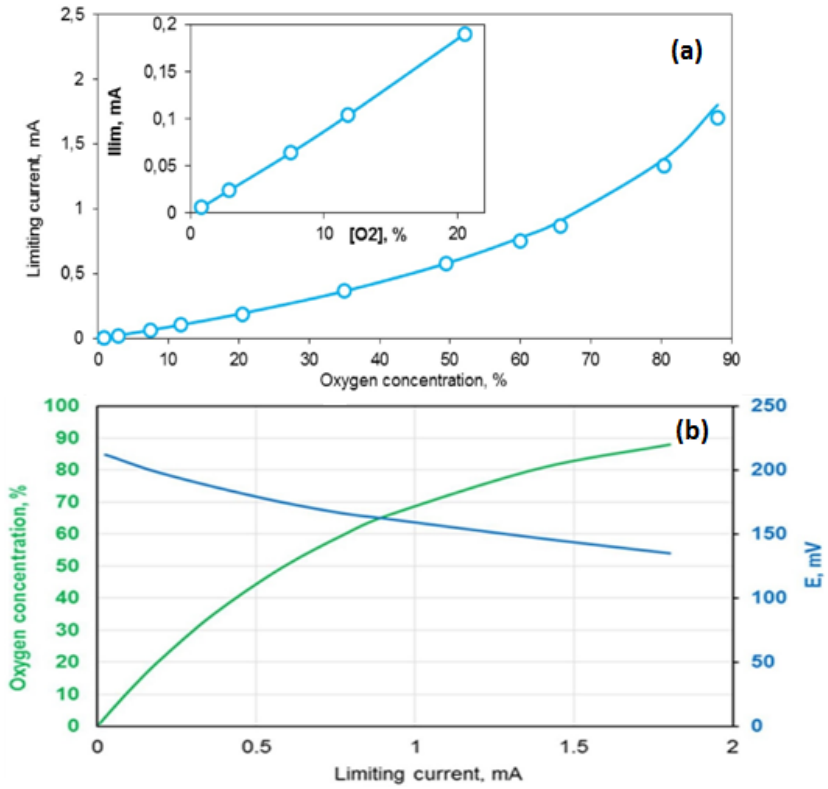

Figure 48: (a) Relation between limiting current and oxygen concentration at 500°C, (b) calibration curves at 500°C for the determination of oxygen's concentration through limiting current (green line) and dependence of the *EMF* on the limiting current (blue line) [57].

By measuring, simultaneously, the *EMF* and the limiting current for different oxygen concentrations and then plotting the oxygen concentration and the *EMF* against the limiting current, the diagram in **Fig. 48b** is obtained. Note that, if at a certain limiting current, the measured *EMF* value is different to that from the *EMF*-I_{lim} curve then the measured oxygen concentration is considered incorrect. However, considering the deviation from the correct value, two cases can be distinguished:

- First, the *EMF* value is lower compared to that of the calibration curve. This condition testifies that more than the expected oxygen reaches the electrode, either due to cracks in the electrolytes or the sealant. As a result, the measured oxygen concentration is higher than that in the analyzed gas.
- Second, the *EMF* value is higher compared to that of the calibration curve. This condition testifies that the characteristics of the metal capillary have changed. Corrosion or deposition of particles inside the capillary can change its inner diameter. As a result, the measured oxygen concentration is lower than that in the analyzed gas [57].

5.4.1.4 Resistive oxygen sensors

Resistor-type oxygen sensors are another type employed for the detection of oxygen in harsh environments. The resistor-type oxygen sensors are based on a semiconducting metal oxide electrolyte and are commonly used because they provide several advantages. The main advantages are the simple design and principle of operation of the sensor, the low cost and the miniaturization capability. At temperatures above 800 °C, the dominant conduction mechanism of restive oxygen sensors is the bulk conduction based on bulk defects. Generally, in metal oxides, bulk defects are associated with metal ion interstitial and vacancies, oxygen vacancies, holes and electrons. Semiconducting metals are divided into two categories based on the charge carriers, n-type conductors with electrons as charge carriers and p-type conductors with holes as charge carriers.

When exposed at high temperatures, the bulk defects species in metal oxide have high mobility, allowing the interface between the oxide and the targeted gas to reach equilibrium conditions. Due to the reactions between the gas species and the oxide, a change in the concentration of the charge carriers is observed. Therefore, the bulk conductivity of the metal

oxide depends on the concentration of the surrounding gas, and by measuring the changes, the concentration of the analyte gas is determined. During the operation of the resistor-type oxygen sensor, a lattice oxygen is generated (O_o^x) by the reaction of an oxygen vacancy ($V_o^{"}$) in the n-type semiconductor with two electrons and an oxygen molecule from the surrounding gas (O_2). The direction of this reaction depends on the oxygen's partial pressure.

$$O_o^x \rightarrow V_o^{"} + 2e^- + \frac{1}{2}O_2 \tag{5.46}$$

The electron conductivity in n-type semiconductor metal oxides is inversely proportional to the partial pressure of the oxygen. The relation between conductivity and partial pressure is expressed in equation (5.47).

$$\sigma = A \cdot \exp\left(-\frac{E_A}{k \cdot T}\right) \cdot P_{O_2}^{1/m} \tag{5.47}$$

In equation (5.47), σ is the electrical conductivity, E_A is the activation energy, A is a constant and m is a parameter that depends on the defects and the charge carriers. Depending on the conductor, its sign is either positive for p-type or negative for n-type conductors. Also, regarding its value, depending on the involved defects, it varies between 1/4 and 1/6. Generally, the sensitivity is inversely proportional to m and E_A, so it is desired for the selected semiconducting metal oxide to exhibit low values of E_A and m. Over the past decades, many different metal oxides have been studied, such as niobium pentoxide (Nb_2O_5), titanium dioxide (TiO_2), cerium oxide (CeO_2), gallium oxide (Ga_2O_3) and perovskite strontium titanate ($SrTiO_3$). However, only TiO_2 exhibit acceptable sensitivity for a wide range of oxygen partial pressure [52].

5.4.2 Humidity (H_2O steam) sensors

The first humidity sensor was developed by Iwahara et al. based on a $SrCe_{0.95}Yb_{0.05}O_{3-\delta}$ (SCY) electrolyte. Iwahara designed a Pt|SCY|Pt type galvanic cell that operates as a potentiometric humidity sensor. For the experimental part, this cell was tested in a wet air atmosphere at operating temperatures between 300-400°C. At one side of the sensor, humidity's partial pressure was swept from 0.008 to 0.135 atm, while on the opposite side,

humidity's partial pressure was kept constant. The dependence of the electrical potential difference was linear to humidity content at the sensing side.

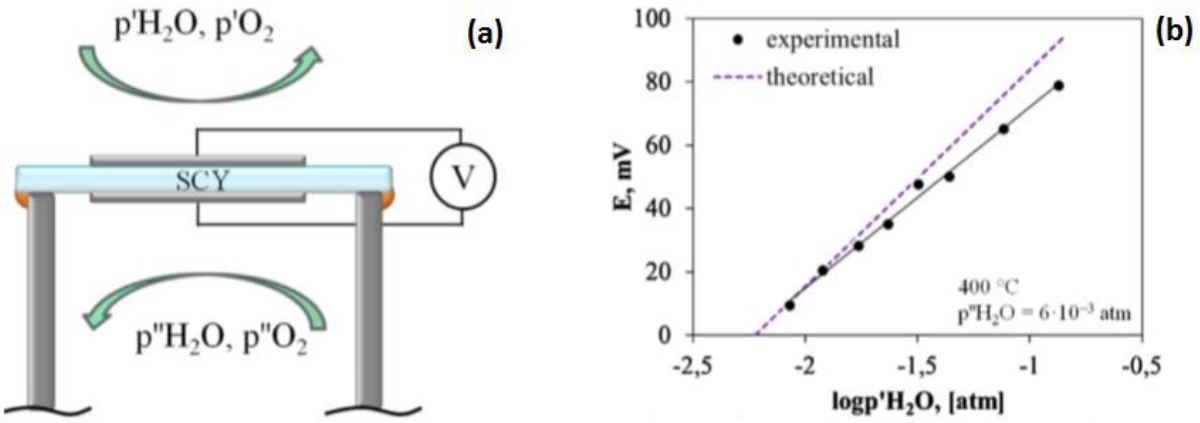

Figure 49: (a) Scheme of the humidity sensor fabricated by Iwahara et al., (b) theoretical and experimental E(mV)-log(p_{H2O}) plot at 400°C [20].

In **Fig. 49a,b**, the configuration of the sensor is presented, and in **Fig. 49b,** the measured *EMF* values plotted against the logarithmic value of humidity's partial pressure are shown. As observed, there is a deviation (up to 10%) from the theoretical values obtained from equation (5.48),

$$E = \frac{R \cdot T}{2 \cdot F} \ln\left(\frac{p'_{H_2}}{p''_{H_2}}\right) \tag{5.48}$$

There are several reasons involved in this inaccuracy. At first, a common problem is leakage through the cell or the SCY electrolyte. Additional leakage results in the mixing between the gases at each side of the electrolyte, therefore the signal generated from the potential difference is deteriorating. Furthermore, the presence of electronic conductivity in the solid electrolyte. The electronic conductivity in the SCY electrolyte, in the operating conditions, takes about 10% of the total conductivity. Last, equation (5.48) is the simplified form of equation (5.49),

$$E = \frac{R \cdot T}{2 \cdot F} \ln\left(\frac{p'_{H_2}}{p''_{H_2}} \cdot \left(\frac{p''_{O_2}}{p'_{O_2}}\right)^{1/2}\right) \tag{5.49}$$

To obtain equation (5,48) from (5.49), it is assumed that the oxygen's partial pressure at each side of the electrolyte is the same, $p''_{O_2} = p'_{O_2}$. However, for high H_2O partial pressure, this equality isn't satisfied, resulting in an error in the measured *EMF* value. Another humidity sensor was developed by Katahira et al. This sensor is based on two similar Pt|SCY|Pt type (pumping-sensing) cells glued together, with a high-temperature glass sealant, such that a chamber and a special channel are formed. The chamber inside the sensor and the outside of the sensor are connected through this special channel. The sensor's configuration is described in **Fig. 50**.

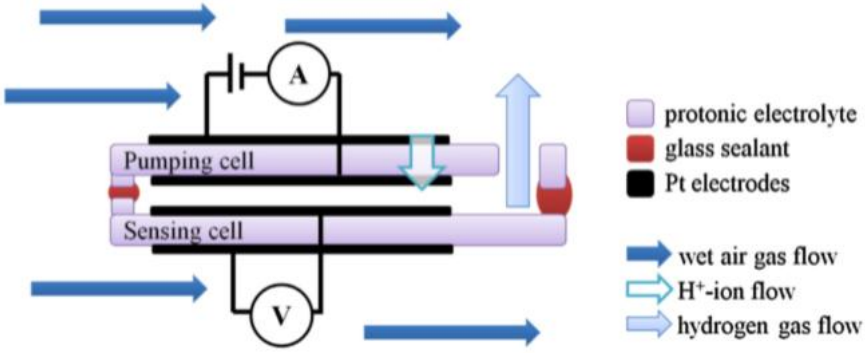

Figure 50: Configuration of the humidity sensor designed by Katahira et al [20].

When the sensor is placed in the wet air atmosphere, a voltage is applied to the pumping cell such that hydrogen in the form of ions flows from the wet air inside the sensor. This hydrogen is generated by the decomposition of the water vapor at the external electrode. The decomposition of water occurs according to the following reaction,

out: $$H_2O \rightarrow 2H^+ + \frac{1}{2}O_2 + 2e^- \qquad (5.50)$$

in: $$2H^+ + 2e^- \rightarrow H_2 \qquad (5.51)$$

The produced hydrogen is pumped inside the sensor, displacing nitrogen molecules and eventually forming a pure hydrogen atmosphere. Practically, this atmosphere inside the sensor can be utilized as a reference gas because the partial pressure of hydrogen inside is known and equal to p'_{H_2}=1 atm. Consequently, by measuring the voltage difference between the electrodes of the sensing cell, it is possible to calculate the hydrogen's partial pressure of the surrounding gas from equation (5.52). Knowing the hydrogen's partial pressures inside and outside of the sensor, one can measure humidity's content, according to equation (5.54).

$$E = \frac{R \cdot T}{2 \cdot F} \ln\left(\frac{p'_{H_2}}{p''_{H_2}} \right) \tag{5.52}$$

$$H_2O \xrightarrow{K} \frac{1}{2} O_2 + H_2 \tag{5.53}$$

$$E = \frac{R \cdot T}{2 \cdot F} \ln\left(\frac{p'_{H_2O} \cdot K}{p''_{H_2} \cdot p'^{\,1/2}_{O_2}} \right) \tag{5.54}$$

In equation (5.54), K is the equilibrium constant of the decomposition of water, reaction (5.53), and p'_{O_2} is the oxygen's partial pressure in the wet air atmosphere. Note that oxygen partial pressure in the atmosphere is 0.21 atm for low humidity values and 0.21·(1- p'_{H_2O}) atm for high humidity values.

The dependence of the potential difference (E) on the applied voltage and humidity content in the wet air atmosphere is presented in **Fig. 51a,b** [20].

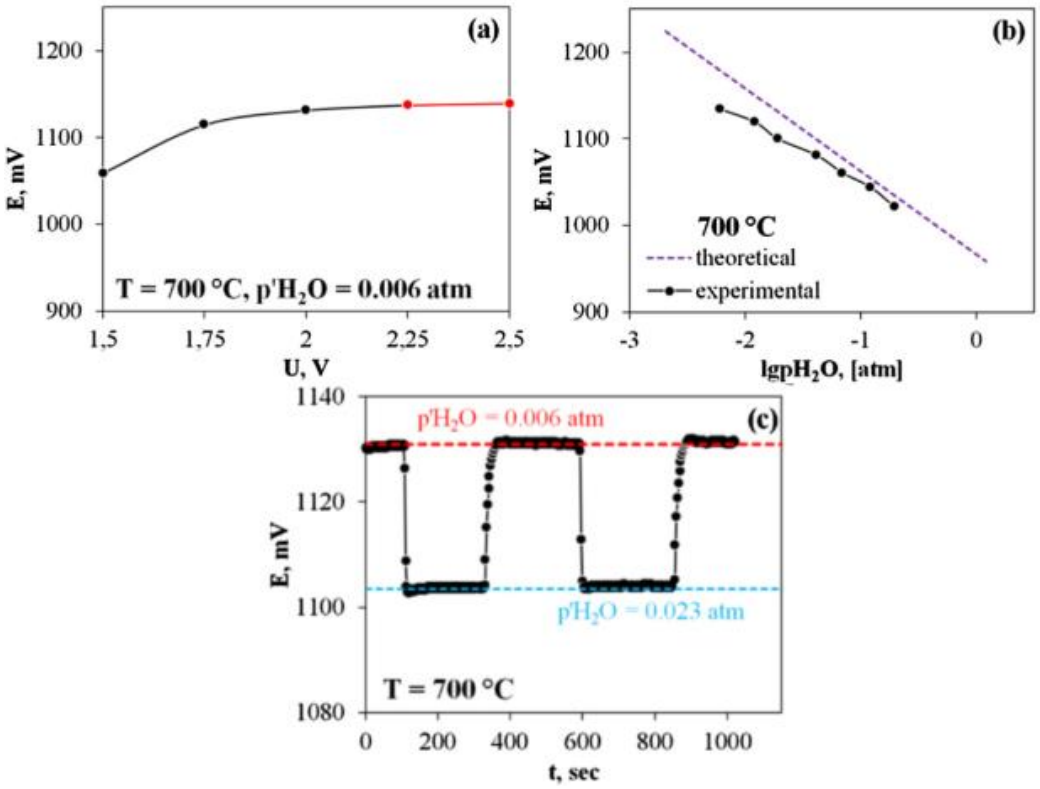

Figure 51: Electric potential as a function of applied voltage (a) and H_2O (b) vapor content at 700 °C, (c) E(mV)-t(sec) for cyclical changes in p'_{H2O} [20].

The red line in **Fig. 51a** indicates that steady-state conditions have been established inside the chamber and p'_{H_2}=1 atm. As seen in **Fig. 51b**, the experimental values are close to the theoretical ones. Another important result presented in **Fig. 51c** is that the t_{90} parameter of the sensor is equal to 30 seconds at 700°C. This parameter refers to the time that the sensor needs to reach 90% of the final value after a change in one of the system's parameters. This makes the sensor suitable for operation when a fast response is needed.

Another amperometric humidity sensor was fabricated by Gorbova et al. This sensor combines a proton-conducting $La_{0.9}Sr_{0.1}YO_{3-\delta}$ (LSY) electrolyte and an oxygen ion-conducting YSZ electrolyte. The two ceramic electrolytes are sealed together, with a high-temperature glass sealant, as shown in **Fig. 52c**, and an empty chamber is formed between them. Pt electrodes are deposited at each side of both electrolytes and a capillary is employed that connects the inner chamber with the surrounding environment. It is important to note that, for this sensor, the inner electrodes are connected, forming a common electrical circuit. For the experimental part, the sensor is heated in an oven and is fed with a mixture of H_2O+N_2 to imitate the operating conditions. For the operation of the sensor, a DC voltage is applied to the sensor in such a way that the minus sign corresponds to the external electrode of the LSY electrolyte and the plus sign at the external electrode of the YSZ electrolyte. This way, the decomposition of water takes place at the inner electrodes according to the reactions (5.55-5.58) until a pure nitrogen atmosphere is formed in the inner chamber, as presented in **Fig. 52a,b**. Reactions (5.55) and (5.56) occur at the YSZ's inner electrode,

$$H_2O + 2e^- \rightarrow 2O^{2-} + H_2 \tag{5.55}$$

or the as formed O_2 can react according to the reaction,

$$\frac{1}{2}O_2 + 2e^- \rightarrow O^{2-} \tag{5.56}$$

Reactions (5.57) and (5.58) occur at the LSY's inner electrode,

$$H_2O \rightarrow 2H^+ + 2e^- + \frac{1}{2}O_2 \tag{5.57}$$

or the as generated H_2 can react according to the reaction,

$$H_2 \rightarrow 2H^+ + 2e^- \tag{5.58}$$

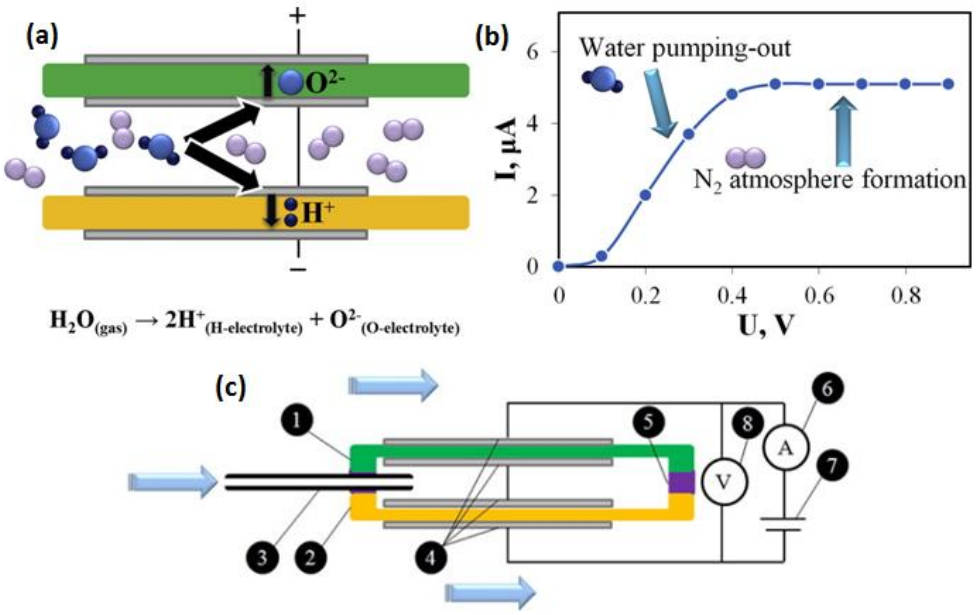

Figure 52: (a) reactions at the inner electrodes and (b) the formation of pure nitrogen atmosphere as the applied voltage increases, (c) (1) YSZ electrolyte, (2) LSY electrolyte, (3) capillary barrier, (4) Pt electrodes, (5) high-temperature glass sealant, (6) amperemeter, (7) DC source and (8) voltammeter [75].

As the water is pumped out of the sensor, due to the reaction (5.55-5.58), the water's diffusion flux through the capillary barrier increases. However, there is a point where the applied voltage is so high that the rate of the reaction is much higher than the diffusion flux and as a result the water's concentration inside the chamber is negligible. Under this condition, an unchanged current response is observed, known as limiting current. The limiting current is theoretically calculated according to the equation (5.59),

$$I_{\lim} = \frac{2 \cdot F \cdot D_{(H_2O)} \cdot S \cdot P}{R \cdot T \cdot L} p_{H_2O} \qquad (5.59)$$

As far as the experimental part, **Fig. 53a** presents the current-voltage curves for different initial H_2O partial pressures. As equation (5.59) suggests, the more the water's partial pressure at the surrounding gas the more will be the limiting current value. However, it is also observed that the current response follows the applied voltage until a certain voltage value. This value differs depending on the water partial pressure. For example, the plateau region is observed at 0.9 V when the p_{H20}=0.078 atm and at 0.4 when p_{H20}=0.004 atm. These curves refer to the 650°C temperature of operation. Furthermore, from equation (5.59) is expected that the relation between the limiting current and the water's partial pressure is linear.

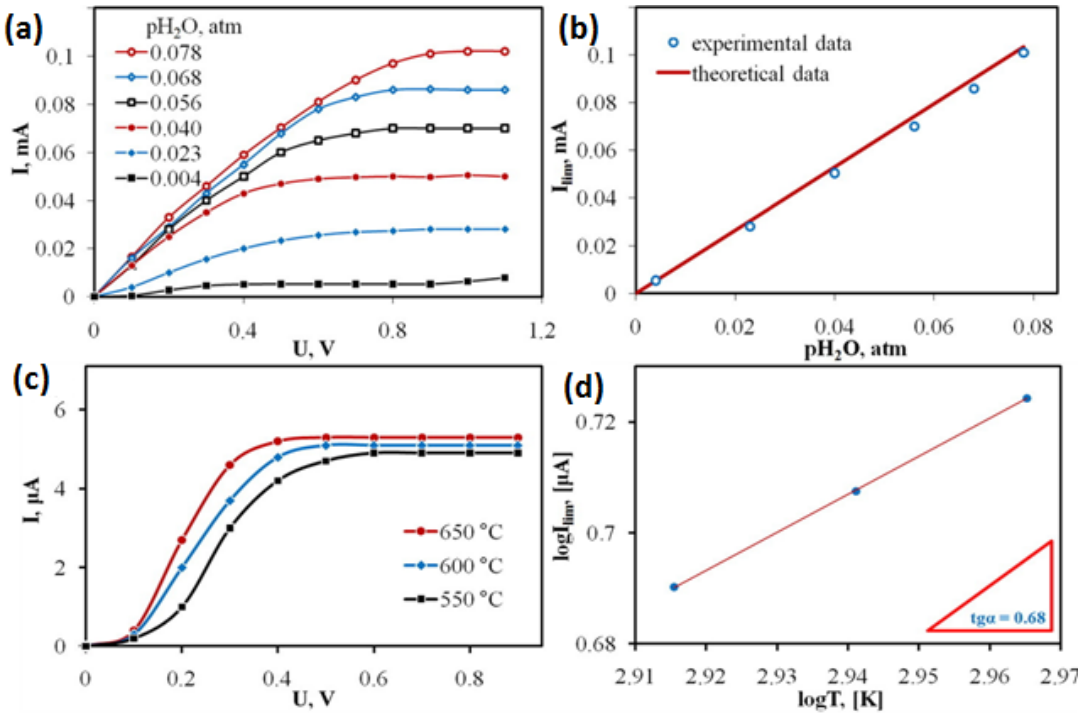

Figure 53: (a) current-voltage curves for different H_2O concentrations, (b) relation between the limiting current value and the H_2O concentration and comparison between the theoretical and experimental values, (c) volt-ampere curved at different temperature for the mixture of N_2+H_2O for p_{H2O}=0.0004 atm and (d) temperature dependence of limiting current [75].

As it is observed from **Fig. 53b,** this condition is satisfied. Also, **Fig. 53b** shows the comparison of the theoretical data (blue dots) obtained from the equation (5.59) and the experimental data (red line). The diffusion coefficient of water is calculated by equation (5.60) if the pressure and temperature of operation are known. D_o is the diffusion coefficient of H_2O measured at pressure P_o=1 atm and temperature T_o=0°C and n is considered equal to n=2 for real gases or n=3/2 for ideal gases.

$$D_{(H_2O)} = D_{o(H_2O)} \left(\frac{T}{T_o}\right)^n \left(\frac{P_o}{P}\right) \tag{5.60}$$

By combining equation (5.59) with the equation of water's diffusion coefficient (5.60), the equation (5.61) is obtained,

$$I_{\lim} = \frac{2 \cdot F \cdot D_{o(H_2O)} \cdot S \cdot P_o}{R \cdot L \cdot (T_o)^n} p_{H_2O} \cdot T^{n-1} \tag{5.61}$$

This equation is important because it suggests that $D_{o(H2O)}$ and n can be estimated from the experiment by the dependence of the limiting current on temperature, as shown in **Fig. 53c**. Modifying equation (5.61) with the aid of logarithms and by plotting $\log(\mathrm{I_{lim}})$ against $\log(\mathrm{T})$, those parameters can be extracted from the graph, as shown in **Fig. 53d**. Equation (5.61) is modified to equation (5.62),

$$\log(I_{\lim}) = (n-1)\cdot\log(T) + \log\left(\frac{2\cdot F\cdot S\cdot P_o\cdot D_{o(H_2O)}}{R\cdot L\cdot (T_o)^n}\, p_{H_2O}\right) \qquad (5.62)$$

Concluding, this sensor is suitable for the monitoring of humidity in a mixture of N_2+H_2O and temperature range of operation from 400 to 700°C. As the author suggests, the temperature's lower limit depends on the activity of the Pt electrodes and the upper limit is based on the increased oxygen conductivity of the YSZ electrolyte. The sensor can properly operate for p_{H2O} between the range of 0.001-0.1 atm. In this range, the limiting current dependence of the H_2O concentration is linear [75].

Chapter VI

Concluding remarks

Nowadays, electrochemical gas sensors are important for the control of pollutants from human activities. Carbon oxides, nitrogen oxides, sulfur oxides and hydrocarbons are some of the species that are harmful to the environment and humans. These pollutants are responsible for dangerous phenomena such as acid rain and smog or the poisoning of the soil and water and also dangerous to human health. The main types of electrochemical sensors classified based on their operation are potentiometric (equilibrium or non-equilibrium), amperometric, resistor-type and impedance-based sensors. Potentiometric gas sensors exhibit great selectivity and sensitivity and acceptable stability for a long time. The main and most important of their disadvantages is the need for a reference gas electrode. Reference-free sensors will be able for more precise measurements as their design will offer better placement flexibility. Researchers have reported that it is possible to replace the reference gas electrode with an internal reference, such as the metal/metal oxide systems. So far, these systems can't operate properly at temperatures above 600°C. Considering that operating temperatures can reach temperatures between 800-1000°C, future research is directed to a reference-free potentiometric sensor capable of withstanding the operating environment. Non-equilibrium or mixed potential potentiometric sensors are extensively used for the detection of reducing gases. These sensors malfunctioning in high

temperatures because, at temperatures above 600°C, the operating conditions tend to an equilibrium and the reaction rate increases. A future trend for these sensors is the fabrication of more suitable materials for such conditions. Resistive gas sensors offer low cost, simple design and scope for miniaturization. The main reason that limits their commercial application is the poor selectivity and long-term stability. Resulting in a need for materials suitable for use for a long period of time and capable of detecting the gases of interest in harsh environments. Another promising technology is amperometric gas sensors. Amperometric sensors can detect a wide variety of gases and due to the linear dependence between the current response and the gas concentration, they exhibit great precision even at high concentrations. However, the complex architecture of the sensor's cell and the diffusion barrier results in difficulties concerning the design of the sensor. Last, a new and less investigated technology are the impedancemetric sensors. They show promising results for the detection at low concentrations, but there is a need for complex signal processing equipment and auxiliary electronics.

In this work, several solid electrolytes for electrochemical gas sensors are reviewed. However, even if many materials with different ionic conductivities are presented, proton-conducting and oxide ion-conducting materials attracted the most attention. Many works are discussed where proton and oxide ion-conducting materials are employed, as solid electrolytes, in electrochemical gas sensors for dangerous gases. All of these sensors were designed for operation at intermediate or high temperatures. These sensors were fabricated with the help of the laboratory of alternative energy conversion systems at the University of Thessaly. The as-fabricated ceramic electrolytes are divided into two categories, based on oxide ion-conducting electrolytes and based on proton-conducting electrolytes.

Yttrium-stabilized Zirconia (YSZ) is the most effective electrolyte employed in many electrochemical sensors for the detection of combustible gasses (such as H_2, CH_4 and CO), nitrogen oxides (NO_x), ammonia (NH_3) and oxygen (O_2). As far as the reported sensors based on oxygen-anion conducting materials an electrochemical amperometric sensor based on YSZ electrolyte with Pt electrodes and a metal capillary was tested, in operation-like conditions (high temperature and nitrogen atmosphere), for its potential to detect combustible gases such as H_2, CH_4 and CO. According to the results, it is stated that for a

concentration range from 0 to 6% of combustible gas in the abovementioned atmosphere, the limiting current present a linear dependence on the H_2, CO, CH_4 content. Another amperometric sensor based on YSZ electrolyte, Pt electrodes and metallic capillary proved suitable for the detection of nitrous oxide (N_2O) in mixtures of nitrogen/oxygen/air + nitrous oxide. The limiting current response was linear for a wide range of N_2O concentration in the mixtures and at temperatures of operation close to 700^oC. Moreover, an NH_3 amperometric sensor based on YSZ electrolytes, Pt electrodes and a chromo-nickel diffusion barrier was tested for the detection of NH_3 in nitrogen atmospheres at 375-430^oC. This device is suitable for the detection of ammonia concentration between 0.1 and 5vol.% at 375-430^oC and it is capable of providing information about the diffusion coefficients and the electrochemical reaction that occurs at the inner electrodes. Last, as far as the YSZ based sensors, a combined oxygen sensor was reviewed. This sensor is able to operate at potentiometric and amperometric modes simultaneously, allowing the control of the sensor's stability and efficiency through the calibration curves [O_2]-I_{LIM} and *EMF*-I_{LIM}. Also, the sensor demonstrated great efficiency for an oxygen concentration range from 0.8 to 88% at 400-700^oC. **Table. 4** presents the abovementioned sensors based on ceramic oxide-ion conducting electrolyte.

Table 4: Electrochemical gas sensors based on oxygen anion-conducting materials.

Source	Date	Type	Temperature ^oC	Targeted gas	Electrolyte
[60]	2015	amperometric	450	H_2, CH_4, CO	9YSZ
[73]	2019	amperometric	700	N_2O	YSZ
[74]	2018	amperometric	375-430	NH_3	8YSZ
[57]	2020	Amperometric/potentiometric	400-700	O_2	9YSZ

On the other hand, regarding the proton-conducting materials, $BaCe_{0.9}Zr_{0.1}Y_{0.2}O_{3-\delta}$, $CaTi_{0.95}Sc_{0.05}O_3$, $CaZr_{0.9}Sc_{0.1}O_3$, $La_{0.9}Sr_{0.1}YO_{3-\delta}$ and $La_{0.95}Sr_{0.05}YO_3$ were synthesized for their potential application in electrochemical gas sensors for the detection of H_2, CO_2 and H_2O in a high-temperature nitrogen atmosphere. Concerning the proton-conducting materials, $BaCe_{0.9}Zr_{0.1}Y_{0.2}O_{3-\delta}$ is tested regarding its suitability for an electrochemical H_2 sensor operating under either potentiometric or amperometric mode. As it is stated, the combined

potentiometric-amperometric H_2 sensor is capable of detecting hydrogen (0.1-10 vol.%) at 450-550^oC. Furthermore, $La_{0.9}Sr_{0.1}YO_{3-\delta}$ is reported as a proton conductor and it is employed, in contact with YSZ electrolyte, in an amperometric hydrogen sensor. The sensor successfully detected even lower concentrations of hydrogen (0.1-3.3%) in a mixture of nitrogen at operating temperatures between 500-600^oC. Also, a similar cell, based on $La_{0.9}Sr_{0.1}YO_{3-\delta}$+YSZ electrolyte for the analysis of moisture in nitrogen atmospheres, is reviewed. This sensor is capable of detecting humidity at 400-700^oC. $La_{0.9}Sr_{0.1}YO_{3-\delta}$ is also employed in an amperometric CO_2 sensor. This sensor proved suitable for the detection of low CO_2 concentrations, ranging from 2 to 14 vol.% of CO_2, in a nitrogen atmosphere at 500-600^oC. Moreover, $La_{0.95}Sr_{0.05}YO_3$, $CaTi_{0.95}Sc_{0.05}O_3$ and $CaZr_{0.9}Sc_{0.1}O_3$ were tested for their proton-conducting properties. As it is stated $La_{0.95}Sr_{0.05}YO_{3-\delta}$ is suitable for amperometric H_2 sensors able to detect high concentration (10-98%) of hydrogen and $CaZr_{0.9}Sc_{0.1}O_3$ proved suitable for lower H_2 concentration (0.5-5%). However, as it is stated, $CaTi_{0.95}Sc_{0.05}O_3$ isn't suitable for application in hydrogen amperometric sensors, as it exhibits high electronic conductivity. **Table. 5** presents the above mentioned sensors based on ceramic proton-conducting electrolyte.

Table 5: Electrochemical gas sensors based on proton-conducting materials.

Source	Date	Type	Temperature ^oC	Targeted gas	Electrolyte
[61]	2016	amperometric	500-600	H_2	$La_{0.9}Sr_{0.1}YO_{3-\delta}$
[62]	2014	amperometric	850	H_2	$La_{0.95}Sr_{0.05}YO_3$ $CaZr_{0.9}Sc_{0.1}O_3$
[63]	2016	Amperometric/ potentiometric	450-550	H_2	$BaCe_{0.9}Zr_{0.1}Y_{0.2}O_{3-\delta}$
[75]	2017	amperometric	650	H_2O	$La_{0.9}Sr_{0.1}YO_{3-\delta}$+YSZ
[65]	2021	amperometric	500-600	CO_2	$La_{0.9}Sr_{0.1}YO_{3-\delta}$

Electrochemical gas sensors generate a signal from redox reactions between the gas and the sensor. During the sensor's operation, the targeted gas reacts at the surface between the sensing electrode and the electrolyte. Often, these reactions affect even the bulk phase of the materials. Due to these interactions the structure of the sensing material changes and through these changes a measurable electric signal is generated. Electrochemical sensors are already employed in many fields from industry to domestic

applications because they are reliable, fast, low cost and small devices. Especially, the development of high-temperature gas sensors based on solid electrolytes is expected to grow in the next years despite the various challenges. Summarizing, as far as the future research trends on solid electrolytes, two categories can be distinguished, studies about the mechanisms and sensor characteristics. Firstly, it is important to deeply understand the mechanisms that govern the sensing technologies and the relation between the sensing element and sensing properties of the materials. Until now, most of the materials have been developed empirically or following a trial and error-type method. That makes it obvious that there is a need to analyze the structure and the sensing properties of the so far effective materials in order to develop models and establish guidelines for predicting the most suitable materials for every sensor and gas. Secondly, the optimization of the synthesis of the employed materials, the architecture design of the sensor and the combination of sensing technologies can improve the effectiveness of future solid-state sensors.

References

1. Vayenas, C., S.I. Bebelis, I. Yentekakis, and S. Neophytides, *The C.R.C Handbook of solid state electrochemistry.* CRC, 1997: p. 445-480.
2. Funke, K., *Solid State Ionics: from Michael Faraday to green energy-the European dimension.* Sci Technol Adv Mater, 2013. **14**(4): p. 043502.
3. Möbius, H.-H., *On the history of solid electrolyte fuel cells.* Journal of solid state electrochemistry, 1997. **1**(1): p. 2-16.
4. Kiukkola, K. and C. Wagner, *Measurements on Galvanic Cells Involving Solid Electrolytes.* Journal of The Electrochemical Society, 1957. **104**(6): p. 379.
5. Kiukkola, K. and C. Wagner, *Galvanic Cells for the Determination of the Standard Molar Free Energy of Formation of Metal Halides, Oxides, and Sulfides at Elevated Temperatures.* Journal of The Electrochemical Society, 1957. **104**(5): p. 308.
6. Weissbart, J. and R. Ruka, *Oxygen Gauge.* Review of Scientific Instruments, 1961. **32**(5): p. 593-595.
7. West, A.R., *Solid Electrolytes.* Berichte der Bunsengesellschaft für physikalische Chemie, 1989. **93**(11): p. 1235-1241.
8. Medvedev, D., A. Brouzgou, A. Demin, and P. Tsiakaras, *Proton-Conducting Electrolytes for Solid Oxide Fuel Cell Applications*, in *Advances in Medium and High Temperature Solid Oxide Fuel Cell Technology*2017, Springer. p. 77-118.
9. Park, C.O., S.A. Akbar, and W. Weppner, *Ceramic electrolytes and electrochemical sensors.* Journal of Materials Science, 2003. **38**(23): p. 4639-4660.
10. Hui, S.R., J. Roller, S. Yick, X. Zhang, C. Deces-Petit, Y. Xie, R. Maric, and D. Ghosh, *A brief review of the ionic conductivity enhancement for selected oxide electrolytes.* Journal of Power Sources, 2007. **172**(2): p. 493-502.
11. VOUZAVALIS, A., *FABRICATION AND CHARACTERIZATION OF ELECTROCHEMICAL AMMONIA SENSORS*, 2018, University of Thessaly.
12. Smith, Q.B., *Impedance Spectroscopy Studies of Yttria Stabilized Zirconia Under Extreme Conditions.* 2016.
13. Zhuiykov, S., *Electrochemistry of zirconia gas sensors. CRC Press, Boca Raton, FL*2007.
14. Liu, T., X. Zhang, X. Wang, J. Yu, and L. Li, *A review of zirconia-based solid electrolytes.* Ionics, 2016. **22**(12): p. 2249-2262.
15. Skinner, S.J. and J.A. Kilner, *Oxygen ion conductors.* Materials Today, 2003. **6**(3): p. 30-37.

16. Ishihara, T., H. Matsuda, and Y. Takita, *Doped LaGaO3 perovskite type oxide as a new oxide ionic conductor.* Journal of the American chemical society, 1994. **116**(9): p. 3801-3803.
17. Ishihara, T., H. Matsuda, M.A. bin Bustam, and Y. Takita, *Oxide ion conductivity in doped Ga based perovskite type oxide.* Solid State Ionics, 1996. **86**: p. 197-201.
18. Ishihara, T., M. Honda, T. Shibayama, H. Minami, H. Nishiguchi, and Y. Takita, *Intermediate Temperature Solid Oxide Fuel Cells Using a New LaGaO3 Based Oxide Ion Conductor: I. Doped as a New Cathode Material.* Journal of The Electrochemical Society, 1998. **145**(9): p. 3177.
19. Bates, J.B., J. Wang, and N.J. Dudney, *Solid electrolytes: the beta aluminas.* Phys. Today;(United States), 1982. **35**(7).
20. Volkov, A., E. Gorbova, A. Vylkov, D. Medvedev, A. Demin, and P. Tsiakaras, *Design and applications of potentiometric sensors based on proton-conducting ceramic materials. A brief review.* Sensors and Actuators B: Chemical, 2017. **244**: p. 1004-1015.
21. Ebbing, D.D., S.D. Gammon, and R. Wentworth, *General chemistry*2005: Houghton Mifflin Boston.
22. Ciobanu, M., J.P. Wilburn, M.L. Krim, and D.E. Cliffel, *1 - Fundamentals*, in *Handbook of Electrochemistry*, C.G. Zoski, Editor 2007, Elsevier: Amsterdam. p. 3-29.
23. Ramachandran, R. and M. Nosonovsky, *Coupling of surface energy with electric potential makes superhydrophobic surfaces corrosion-resistant.* Phys. Chem. Chem. Phys., 2015. **17**.
24. He, W., W. Lv, and J.H. Dickerson, *Gas Diffusion Mechanisms and Models*, in *Gas Transport in Solid Oxide Fuel Cells*2014, Springer International Publishing: Cham. p. 9-17.
25. Nnamchi, P.S. and C.S. Obayi, *Chapter 4 - Electrochemical Characterization of Nanomaterials*, in *Characterization of Nanomaterials*, S. Mohan Bhagyaraj, O.S. Oluwafemi, N. Kalarikkal, and S. Thomas, Editors. 2018, Woodhead Publishing. p. 103-127.
26. Oxtoby, D.W., H.P. Gillis, and L.J. Butler, *Principles of modern chemistry*2015: Cengage learning.
27. Giorgi, L. and F. Leccese, *Fuel cells: technologies and applications.* The Open Fuel Cells Journal, 2013. **6**(1).
28. Morgan, T., *The hydrogen economy: A non-technical review*2006: UNEP/Earthprint.
29. Owens, B.B. and M. Munshi, *History of Solid State Batteries*, 1987, MINNESOTA UNIV MINNEAPOLIS CORROSION RESEARCH CENTER.
30. Palacín, M.R., *Recent advances in rechargeable battery materials: a chemist's perspective.* Chemical Society Reviews, 2009. **38**(9): p. 2565-2575.

31. Gulzar, U., S. Goriparti, E. Miele, T. Li, G. Maidecchi, A. Toma, F. De angelis, C. Capiglia, and R. Zaccaria, *Next-Generation Textiles: From Embedded Supercapacitors to Lithium Ion Batteries.* J. Mater. Chem. A, 2016. **4**: p. 16771-16800.

32. Lim, H.-D., J.-H. Park, H.-J. Shin, J. Jeong, J.T. Kim, K.-W. Nam, H.-G. Jung, and K.Y. Chung, *A review of challenges and issues concerning interfaces for all-solid-state batteries.* Energy Storage Materials, 2020. **25**: p. 224-250.

33. Mandapati, J. and K. Balasubramanian, *Simple Capacitors to Supercapacitors-An Overview.* Int. J. Electrochem. Sci, 2008. **3**: p. 1196-1217.

34. Das, S., A. dey, A. Biswas, and A. Mohanty, *A novel design of Super-Capacitor used to enhance solar-energy restoration of photo-voltaic cells*2014. 61-64.

35. P. S. Joshi, and D.S. Sutrave, "*Supercapacitor: Basics and Overview, Journal of information and Computional Science,Vol. 9 Issue 12, pp.* 609-625, 2019.

36. Schneuwly, A. and R. Gallay. *Properties and applications of supercapacitors from the state-of-the-art to future trends*. in *Proceeding PCIM*. 2000.

37. Brouzgou, A., E. Gorbova, Y. Wang, S. Jing, A. Seretis, Z. Liang, and P. Tsiakaras, *Nitrogen-doped 3D hierarchical ordered mesoporous carbon supported palladium electrocatalyst for the simultaneous detection of ascorbic acid, dopamine, and glucose.* Ionics, 2019. **25**(12): p. 6061-6070.

38. Elgrishi, N., K.J. Rountree, B.D. McCarthy, E.S. Rountree, T.T. Eisenhart, and J.L. Dempsey, *A Practical Beginner's Guide to Cyclic Voltammetry.* Journal of Chemical Education, 2017. **95**(2): p. 197-206.

39. Vidaković, T., M. Christov, and K. Sundmacher, *The use of CO stripping for in situ fuel cell catalyst characterization.* Electrochimica Acta, 2007. **52**(18): p. 5606-5613.

40. Franklin, R.K., S.M. Martin, T.D. Strong, and R.B. Brown, *Chemical and Biological Systems: Chemical Sensing Systems for Liquids*, in *Reference Module in Materials Science and Materials Engineering*2016, Elsevier.

41. Zoski, C.G., *Handbook of electrochemistry*2006: Elsevier.

42. Rodat, S., S. Sailler, F. Druart, P.X. Thivel, Y. Bultel, and P. Ozil, *EIS measurements in the diagnosis of the environment within a PEMFC stack.* Journal of Applied Electrochemistry, 2009. **40**(5): p. 911-920.

43. Instruments, G., *Basics of electrochemical impedance spectroscopy.* G. Instruments, Complex impedance in Corrosion, 2007: p. 1-30.

44. Allen, J.B. and R.F. Larry, *Electrochemical methods fundamentals and applications*2001: John Wiley & Sons.
45. Peiris, T.A.N., *Microwave-assisted processing of solid materials for sustainable energy related electronic and optoelectronic applications*, 2014.
46. Zhou, W., R. Apkarian, Z.L. Wang, and D. Joy, *Fundamentals of scanning electron microscopy (SEM)*, in *Scanning microscopy for nanotechnology*2006, Springer. p. 1-40.
47. Yahia, L.H. and L.K. Mireles, *4 - X-ray photoelectron spectroscopy (XPS) and time-of-flight secondary ion mass spectrometry (ToF SIMS)*, *Characterization of Polymeric Biomaterials*, 2017, Woodhead Publishing. p. 83-97.
48. Lin, P.-C., S. Lin, P.C. Wang, and R. Sridhar, *Techniques for physicochemical characterization of nanomaterials.* Biotechnology Advances, 2014. **32**(4): p. 711-726.
49. Capone, S., A. Forleo, L. Francioso, R. Rella, P. Siciliano, J. Spadavecchia, D. Presicce, and A. Taurino, *Solid state gas sensors: state of the art and future activities.* Journal of Optoelectronics and Advanced Materials, 2003. **5**(5): p. 1335-1348.
50. Demin, A., E. Gorbova, A. Brouzgou, A. Volkov, and P. Tsiakaras, *Chapter 6 - Sensors based on solid oxide electrolytes*, in *Solid Oxide-Based Electrochemical Devices*, M. Lo Faro, Editor 2020, Academic Press. p. 167-215.
51. Yunusa, Z., M.N. Hamidon, A. Kaiser, and Z. Awang, *Gas Sensors: A Review.* Sensors and Transducers, 2014. **168**: p. 61-75.
52. Liu, Y., J. Parisi, X. Sun, and Y. Lei, *Solid-state gas sensors for high temperature applications–a review.* Journal of Materials Chemistry A, 2014. **2**(26): p. 9919-9943.
53. López-Gándara, C., F.M. Ramos, and A. Cirera, *YSZ-Based Oxygen Sensors and the Use of Nanomaterials: A Review from Classical Models to Current Trends.* Journal of Sensors, 2009. **2009**: p. 1-15.
54. Jasiński, P., *Solid-state electrochemical gas sensors.* Materials Science Poland, 2006. **24**(1): p. 269-278.
55. Liu, T., X. Zhang, L. Yuan, and J. Yu, *A review of high-temperature electrochemical sensors based on stabilized zirconia.* Solid State Ionics, 2015. **283**: p. 91-102.
56. Mulmi, S. and V. Thangadurai, *Editors' Choice—Review—Solid-State Electrochemical Carbon Dioxide Sensors: Fundamentals, Materials and Applications.* Journal of The Electrochemical Society, 2020. **167**(3): p. 037567.
57. Kalyakin, A., A. Demin, E. Gorbova, A. Volkov, and P. Tsiakaras, *Combined amperometric-potentiometric oxygen sensor.* Sensors and Actuators B: Chemical, 2020. **313**: p. 127999.

58. Kalyakin, A., J. Lyagaeva, D. Medvedev, A. Volkov, A. Demin, and P. Tsiakaras, *Characterization of proton-conducting electrolyte based on La0. 9Sr0. 1YO3–δ and its application in a hydrogen amperometric sensor.* Sensors and Actuators B: Chemical, 2016. **225**: p. 446-452.

59. Haaland, D.M., *Internal-reference solid-electrolyte oxygen sensor.* Analytical Chemistry, 1977. **49**(12): p. 1813-1817.

60. Fadeyev, G., A. Kalyakin, E. Gorbova, A. Brouzgou, A. Demin, A. Volkov, and P. Tsiakaras, *A simple and low-cost amperometric sensor for measuring H2, CO, and CH4.* Sensors and Actuators B: Chemical, 2015. **221**: p. 879-883.

61. Kalyakin, A., J. Lyagaeva, D. Medvedev, A. Volkov, A. Demin, and P. Tsiakaras, *Characterization of proton-conducting electrolyte based on La0.9Sr0.1YO3–δ and its application in a hydrogen amperometric sensor.* Sensors and Actuators B: Chemical, 2016. **225**: p. 446-452.

62. Kalyakin, A., G. Fadeyev, A. Demin, E. Gorbova, A. Brouzgou, A. Volkov, and P. Tsiakaras, *Application of Solid oxide proton-conducting electrolytes for amperometric analysis of hydrogen in H2+N2+H2O gas mixtures.* Electrochimica Acta, 2014. **141**: p. 120-125.

63. Kalyakin, A., A. Volkov, J. Lyagaeva, D. Medvedev, A. Demin, and P. Tsiakaras, *Combined amperometric and potentiometric hydrogen sensors based on BaCe 0.7 Zr 0.1 Y 0.2 O 3−δ proton-conducting ceramic.* Sensors and Actuators B: Chemical, 2016. **231**: p. 175-182.

64. Fergus, J.W., *A review of electrolyte and electrode materials for high temperature electrochemical CO2 and SO2 gas sensors.* Sensors and Actuators B: Chemical, 2008. **134**(2): p. 1034-1041.

65. Kalyakin, A.S., D.A. Medvedev, and A.N. Volkov, *Electrochemical sensors based on proton-conducting electrolytes for determination of concentration and diffusion coefficient of CO2 in inert gases.* Chemical Engineering Science, 2021. **229**: p. 116046.

66. Liu, F., J. Wang, R. You, Z. Yang, J. He, C. Wang, A. Liu, Q. Wang, X. Yan, and P. Sun, *YSZ-based solid electrolyte type sensor utilizing ZnMoO4 sensing electrode for fast detection of ppb-level H2S.* Sensors and Actuators B: Chemical, 2020. **302**: p. 127205.

67. Yang, X., Y. Zhang, X. Hao, Y. Song, X. Liang, F. Liu, F. Liu, P. Sun, Y. Gao, and X. Yan, *Nafion-based amperometric H2S sensor using Pt-Rh/C sensing electrode.* Sensors and Actuators B: Chemical, 2018. **273**: p. 635-641.

68. Zhang, H., T. Zhong, R. Sun, X. Liang, and G. Lu, *Sub-ppm H 2 S sensor based on NASICON and CoCr 2− x Mn x O 4 sensing electrode.* RSC Advances, 2014. **4**(98): p. 55334-55340.

69. Miura, N., Y. Yan, G. Lu, and N. Yamazoe, *Sensing characteristics and mechanisms of hydrogen sulfide sensor using stabilized zirconia and oxide sensing electrode.* Sensors and Actuators B: Chemical, 1996. **34**(1-3): p. 367-372.

70. Guan, Y., C. Yin, X. Cheng, X. Liang, Q. Diao, H. Zhang, and G. Lu, *Sub-ppm H2S sensor based on YSZ and hollow balls NiMn2O4 sensing electrode.* Sensors and Actuators B: Chemical, 2014. **193**: p. 501-508.

71. Hao, X., C. Ma, X. Yang, T. Liu, B. Wang, F. Liu, X. Liang, C. Yang, H. Zhu, and G. Lu, *YSZ-based mixed potential H2S sensor using La2NiO4 sensing electrode.* Sensors and Actuators B: Chemical, 2018. **255**: p. 3033-3039.

72. Cooper, C.D. and F.C. Alley, *Air pollution control: A design approach*2010: Waveland Press.

73. Kalyakin, A., A. Volkov, A. Demin, E. Gorbova, and P. Tsiakaras, *Determination of nitrous oxide concentration using a solid-electrolyte amperometric sensor.* Sensors and Actuators B: Chemical, 2019. **297**: p. 126750.

74. Kalyakin, A., A. Volkov, A. Vylkov, E. Gorbova, D. Medvedev, A. Demin, and P. Tsiakaras, *An electrochemical method for the determination of concentration and diffusion coefficient of ammonia-nitrogen gas mixtures.* Journal of Electroanalytical Chemistry, 2018. **808**: p. 133-136.

75. Medvedev, D., A. Kalyakin, A. Volkov, A. Demin, and P. Tsiakaras, *Electrochemical moisture analysis by combining oxygen- and proton-conducting ceramic electrolytes.* Electrochemistry Communications, 2017. **76**: p. 55-58.